NOTICE

The quality of this microform is heavily dependent upon the quality of the original thesis submitted for microfilming. Every effort has been made to ensure the highest quality of reproduction possible.

If pages are missing, contact the university which granted the degree.

Some pages may have indistinct print especially if the original pages were typed with a poor typewriter ribbon or if the university sent us an inferior photocopy.

Reproduction in full or in part of this microform is governed by the Canadian Copyright Act, R.S.C. 1970, c. C-30, and subsequent amendments.

AVIS

La qualité de cette microforme dépend grandement de la qualité de la thèse soumise au microfilmage. Nous avons tout fait pour assurer une qualité supérieure de reproduction.

S'il manque des pages, veuillez communiquer avec l'université qui a conféré le grade.

La qualité d'impression de certaines pages peut laisser à désirer, surtout si les pages originales ont été dactylographiées à l'aide d'un ruban usé ou si l'université nous a fait parvenir une photocopie de qualité inférieure.

La reproduction, même partielle, de cette microforme est soumise à la Loi canadienne sur le droit d'auteur, SRC 1970, c. C-30, et ses amendements subséquents.

RS Codes and Linear Prediction Techniques for Land Mobile Satellite Channels

by

Chokri Trabelsi, B.A.Sc.

A thesis submitted to the

School of Graduate Studies and Research

in partial fulfilment of the requirements for the degree of

Master of Applied Science

Ottawa-Carleton Institute for Electrical Engineering

Department of Electrical Engineering

Faculty of Engineering

University of Ottawa

December 1990

ISBN 0-315-68080-6

UNIVERSITÉ D'OTTAWA
UNIVERSITY OF OTTAWA

Abstract

Reed-Solomon codes as nonbinary block codes with multiple burst-error-correcting capability are well suited for error control in fading channels. This thesis studies the effectiveness of Reed Solomon codes and provides a complete characterization of these codes for a class of land mobile satellite communication channels.

Earlier studies on the performance of RS codes in mobile satellite channels did not consider shadowing. Furthermore, they considered only the slow fading case. In our simulation the effect of shadowing is taken into consideration and a fast fading assumption is used with system fading bandwidths of 1 to 10 percent of the transmission rate. This range of normalized fading bandwidths corresponds to vehicle speeds from 15 to 60 mph at bit rate of 2400 bps and 4800 bps for L-band carrier frequency.

BER performance results show that RS codes can provide large improvement, however there is still 5 to 20 dB discrepancy between the performance in an AWGN channel and LMSAT channel. Therefore to obtain further improvement a novel receiver structure which employs fading prediction in conjunction with RS codes has been introduced and analyzed. With practical predictor lengths, simulated performance results show that the proposed technique greatly reduces the performance degradation caused by the fading channel.

I hereby declare that I am the sole author of this thesis.

I authorize The University of Ottawa to lend this thesis to other institutions or individuals for the purpose of scholarly research.

Chokri Trabelsi

I further authorize The University of Ottawa to reproduce this thesis by photocopying or by other means, in total or in part, at the request of other institutions or individuals for the purpose of scholarly research.

Chokri Trabelsi

To my family

To Ines

Acknowledgements

I wish to express my gratitude to Dr. A. Yongaçoğlu for his continuous encouragement and invaluable suggestions throughout the research. Thanks to Dr. John H. Lodge of CRC for providing us some reports on MSAT communications systems. Thanks to Mr. Chun Loo of CRC for providing us with his report on MSAT channel. Thanks to Mr. Dimitrios Makrakis for his helpful suggestions. A special thanks to Drs. El-Tanany and J Y Chouinard for reading this thesis and for their suggestions and encouragement to continue the research. I would like to express my sincere thanks to the Tunisian government for its scholarship program. I would also like to acknowledge the partial funding from NSERC and TRIO grants. My epitome thanks go to my family for their patience, sacrifice, and support during all those years of my studies.

Contents

List of Figures

List of Tables

Acronyms and Definitions

AFD:	Average Fade Duration
APS:	Adaptive Polarization Shaping
ARQ:	Automatic Repeat Request
AWGN:	Additive White Gaussian Noise
BER:	Bit Error Rate
BPSK:	Binary Phase Shift Keying
BOSS:	Block Oriented Systems Simulator
DMSK:	Differentially Detected Minimum Shift Keying
DPSK:	Differentially Detected Phase Shift Keying
FEC:	Forward Error Correction
GF:	Galois Field
GMSK:	Gaussian Minimum Shift Keying
LCR:	Level Crossing Rate
LMSAT:	Land Mobile Satellite
QPSK:	Quadrature Phase Shift Keying
RS:	Reed-Solomon
TCM:	Trellis Coded Modulation

Nomenclature

B : fading bandwidth

T^{-1} : transmission symbol rate

BT : normalized fading bandwidth

$\tilde{R}$: received phasor

$\tilde{r}$: complex channel gain

ψ: phase shift due to the combined effect of fading and shadowing

β: phase for PSK signal

$\tilde{A}$: complex channel gain

W: Rayleigh component

Z: line-of-sight component, $Z = e^U$.

μ_0: mean of the Gaussian process U

d_0: variance of the Gaussian process U

b_0: variance of the Rayleigh component

DT: time interval in seconds between signal samples for the simulation run

I_0: modified Bessel function of zeroth order

f_c: carrier frequency

V: vehicle speed

N_0: one-sided power spectral density

$N(R)$: level crossing rate

$n(R)$: expected crossing number at a signal level R

$N'(R)$: level crossing rate normalized to the doppler frequency

$\bar{t}(R)$: average fade duration

$\bar{t}'(R)$: average fade duration normalized to the doppler frequency

E_b: energy per information bit

E_c: energy per coded bit

K-factor: the direct-to-multipath signal power ratio

t: maximum number of correctable errors per code word

e: number of erasures in a code word

n: blocklength of a code word

k: number of information symbols in a code word

m: number of bits per code symbol

d_{min}: minimum distance of a code

L: order of the predictor

p_k: prediction coefficients

Chapter 1

Introduction

1.1 Introduction

The link between a satellite and a land mobile terminal is degraded by fading due to multipoint reflections and by shadowing due to obstacles between the satellite and the mobile unit. The receiver performance of communication systems operating in such fading environments is of importance for designing fading compensation methods such as error detection, error correction and ARQ schemes. The performance with small terminals and lower elevation angles is particulary bad. The required increase of signal power to achieve a sufficiently low BER can not be tolerated on a satellite link. Some of possible techniques to mitigate shadowing and fading are :

a) Forward error correction (FEC) with redundant codes;

b) Automatic repeat request (ARQ) techniques;

c) Diversity transmission with appropriate combining;

d) Adaptive polarization shaping (APS) to supress the reflected component.

Method (d) is under discussion for future standard terminals and voice transmission where no additional delay can be tolerated. Japanese experiments conducted by KDD concentrated on antennas using a technique called polarization shaping to reduce the multipath fading [44]. Diversity techniques require statistically indepen-

dent diversity paths. For mobile satellite channels, this rules out frequency diversity because of the large coherence bandwidth. Antenna (spatial) diversity is probably too complex for small and cheap terminals. Thus methods (a) and (b) seem to be most suitable for data transmission with small terminals. Especially FEC combined with ARQ offers many advantages. However, method (b) depends heavily on the access and protocol techniques on the forward and return channel, and its analysis needs further system specifications.

Various FEC coding schemes were investigated in the literature for different kinds of channels. Convolutional codes with Viterbi decoding and Reed-Solomon codes are strong candidates for land mobile satellite channels.

The bit error probability for convolutional coded transmission over fading channels is well known from the literature [30-38]. Most of these works report that convolutional codes are good candidates for land mobile satellite applications and provide a significant coding gain when they are used in an efficient manner. However, question may arise that do convolutional codes represent the most suitable codes for LMSAT applications. Does this class of codes represent the best choice which minimizes the mobile terminal complexity and cost while maintaining its flexibility ?

Hagenauer [35] reports that convolutional codes are not directly suited for fading channels, because Viterbi as well as sequential decoders are sensitive to burst errors. Interleaving could be used to transform bursts into statistically independent errors, then significant coding gain could be achieved. Also it was shown [30] that BCH block codes and convolutional codes require a higher degree of interleaving than comparable Reed-Solomon block codes. Therefore one may think of other codes which could substitute convolutional codes or could be concatenated together to provide highly reliable data transmission.

Reed-Solomon codes as nonbinary block codes with multiple burst-error-correcting capability are well suited for error control over fading channels. The objective of this thesis is to report on the effectiveness of Reed Solomon codes and provide a complete characterization of these codes for a class of land mobile satellite communication channels.

By exploiting the statistical characteristics of the multipath fading and shadowing, an effective coding/interleaving scheme is proposed. Simulated performance results show that the proposed coding/interleaving scheme provides large improvements in the BER performance. It is also found that erasure information improve the performance of the decoder significantly. However there is still a large discrepancy between the performance in an AWGN channel and an LMSAT channel. Therefore, to obtain further improvements, a novel receiver structure which employs fading prediction in conjunction with RS codes has been introduced and analyzed.

Earlier studies on the performance of RS codes in mobile satellite channels did not consider shadowing [30,35,37]. Furthermore, they considered only the slow fading case. In our simulation the effect of shadowing is taken into consideration and a fast fading assumption is used with system fading bandwidths of 1 to 10 percent of the transmission rate.

To take into account the effect of shadowing, the model used for the fading channels is based on the one described in [1-4]. Loo et al report that land mobile satellite communication channels, in the Canadian rural environment, can be modeled as a shadowed Rician fading process [1-4]. The main application of the model is for signal transmission studies in the Canadian MSAT program. In [38], the model was used with the assumption that the shadowing and the multipath components have identical fading spectra. However there could be some difference in the time variation of

the signal envelope if the shadowing component bandwidth is varied. This difference could be significant in the second order statistics of the signal envelope where the time variation is used. In our simulation the multipath fading bandwidth was taken several times the shadowing component bandwidth.

As stated above, we intend to apply modulation, coding and prediction strategies to improve the performance of digital land mobile satellite communication links. But before examining the performance of any modulation and coding techniques, it is essential to gain a basic understanding of the characteristics of the land mobile satellite fading channel.

1.2 Literature Review

Fading model

In the literature two important models are available to characterize the land mobile satellite channel. The first model [7] is the Rician fading, where the received multipath signal consists of the sum of a direct or line-of-sight component and a fading component due to reflections from the nearby scatterers. The direct component is received without distortion other than an attenuation due to free space loss and a doppler shift due to movement of the vehicle. The multipath component is Rayleigh distributed in amplitude and uniformly distributed in phase. The direct component and multipath components combined give a received envelope which has the Rician distribution [6].

The second model is based on the one described by C. Loo in References [1-4]. Loo et al report that land mobile satellite communication channels, in the Canadian rural environment, behave as a shadowed Rician fading process. In the mathematical model for this fading channel, the line-of-sight component is subjected to a lognormal

transformation due to shadowing, instead of being constant as in Rician model and the scatter path or multipath is Rayleigh distributed.

It has been shown that the Rician model is well suited for describing the land mobile satellite channel in a clear (non shadowing) environment [14]. But in a shadowed area the model is not very accurate since the line-of-sight is treated as a constant, where in reality this component could vary considerably, especially if the mobile goes through a densely wooded area. Therefore the line-of-sight component should be treated as a stochastic process.

In this thesis Loo's model is considered and BOSS was used to generate the lognormal shadowed Rician fading process to predict the performance of various modulation and coding techniques.

Modulation techniques

Several modulation strategies for transmitting data over a land mobile satellite channel have appeared in the literature. These techniques have attempted to deal with the time-varying nature of the mobile channel in a variety of ways.

(1) Those which employ noncoherent, constant envelope techniques in order to minimize the sensitivity to the time-varying phase and amplitude of the channel [11].

(2) Those which send a reference signal along with the data signal, allowing for coherent detection schemes to be used [23].

(3) Those which employ a modulation (and coding) strategy, which introduces time diversity into the transmitted signal.

Approaches that employ noncoherent constant-envelope (or nearly constant envelope) techniques include differentially detected phase shift keying (DPSK) [11], differentially detected minimum shift keying (DMSK), Gaussian minimum shift keying (GMSK) [47] and tamed frequency modulation (TFM) [48]. These techniques

can suffer significant performance losses over a fading channel. In fact, they typically exhibit an "irreducible error rate" that cannot be bettered at any signal-to-noise-ratio.

Approaches that send a reference signal and then perform coherent detection include the transparent tone-in-band technique (TTIB) [49] and the tone calibrated technique (TCT) [50]. While these techniques have advantage of coherent detection, the presence of a reference signal requires some bandwidth and power in addition to that required by the data signal alone. Furthermore, since the modulated signals do not posses a constant envelope, any nonlinearity in the transmitter's power amplifier transfer characteristic will result in greater signal distortion for these signals than for the signals of the previous category. It has been shown that these techniques do not exhibit an "irreducible error rate." In fact, for Rayleigh fading and high SNR's, their error rate is approximately inversely proportional to the SNR [51]. Still, SNR's in excess of 30 dB are required to achieve a bit error rate (BER) of 10^{-4} for Rayleigh fading. It has been shown [23] that TTIB has a potential advantage in that it is a likely candidate for the amplitude companded single side band (ACSSB) speech modem. The TTIB processing performs the equivalent of a carrier recovery and it is also capable of providing a signal that can be used for bit timing purposes [49]. Thus there is a potential for reducing the hardware complexity by using a coherent data modem in conjunction with the TTIB modem, rather then having two completely distinct modems for speech and data.

Error correcting techniques

Several approaches that introduce time diversity into the transmitted signal with coding techniques have been published. These techniques demonstrate dramatically better performance than techniques that do not employ time diversity. The most relevant work to our study are those given in [30-41].

The performance of a bandwidth efficient coding and modulation for a lognormal shadowed Rician channel has been studied in [38]. Trellis coded 8PSK (TC-8PSK) and the binary multi-h codes are the bandwidth efficient modulation formats considered. In [38] a fast fading channel assumption is used with system fading bandwidths of 5% to 10% of the baud rate and both techniques considered correct random errors, rather than burst errors. It has been shown in [38] that the light shadowed Rician channel with normalized fading bandwidth of 10% is a random error channel and for normalized fading bandwidth of 5% the channel seems to be in a transitional state containing both burst and random errors. For the Ungerboeck's 8PSK trellis code, it was found that for the coherent case, the coding gain is larger in the case of fading channel than occurs for the AWGN channel. This coding gain increases with the fading bandwidth and the degree of shadowing. For differentially detected 8PSK he found that the phase jitter due to fading process has a very significant effect on the system performance. This phase jitter increases with an increase in fading bandwidth. Finally he has shown that the multi-h signal set gives improved performance relative to trellis coded 8PSK around $P_e = 10^{-3}$. However multi-h signals require more complex receivers.

Modestino and Mui studied the performance of DPSK with convolutional codes on time varying fading channels [32,33]. These works consider the coding gain due to bandwidth expanding convolutional codes for BPSK and DBPSK signal formats. They consider codes to correct random errors, and Rician fading model is considered. They found that for normalized fading bandwidths equal and greater than 10%, coding with no interleaving could achieve significant improvement. When the normalized fading bandwidths equal to 1% or lower, the fading aspect of the channel is quasi static and hence has burst error nature thus giving no coding gain for the

random error correcting codes. Some degree of interleaving is required whenever the signaling rate is such that the normalized fading bandwidth is less than 1%.

Previous works on the performance of RS codes on fading channels have been concerned exclusively with Rician fading. As stated above, recent propagation studies indicate that the signal fading is lognormal shadowed Rician rather than Rician distributed. It is of some interest then to provide a complete characterization of RS codes performance on lognormal shadowed Rician channels. We consider the performance of RS codes when used in conjunction with coherent phase shift keyed modulation.

Erich Lutz studied the performance of RS codes over Rician channel with normalized fading bandwidth equals to 0.001 (static channel) to compare the simulation results with the analytical results where the fading is assumed to be slow (quasi static channel).

1.3 Thesis Organization

In Chapter 2, a complex baseband signal model to be used in our study is presented. We present the fading model, discuss how a computer-based module has been developed using a communication simulator software package BOSS (Block Oriented System Simulator). We first build the block diagram that generates the fading process using BOSS, then the cumulative density function of the received signal envelope is determined. Many trials were carried out with different values of our fading model parameters with the objective of fitting our results to those derived from measurements. As a final step in this chapter, the second order statistics of the generated signal envelope were studied and the average fade duration at a specified signal level for different normalized fading bandwidths is deduced.

In Chapter 3, BOSS is used to determine the performance of the uncoded system.

As a first step the performance of BPSK in an AWGN channel is determined to make sure of the reliability of the simulation results provided by BOSS. The system model to be used in our study to evaluate the performance of BPSK in an AWGN channel is described. With a matched filter receiver it is found that for the AWGN case BOSS provides very accurate results. As a second step, this system model is expanded to study the performance of BPSK over AWGN and lognormal shadowed Rician channels. The bit error probability as a function of bit energy-to-noise density ratio (Eb/No) for different degrees of shadowing is found and the fade margin for the three degrees of shadowing at probability of error of 10^{-3} is deduced.

In Chapter 4, the performance of various RS codes in the AWGN and lognormal shadowed Rician channel is investigated. We first compute the bit error probability for block coded transmission over a non-fading channel and compare the results with literature. Then the simulation of bit error probability is adapted to fading and shadowing channels. First, different RS codes with different blocklength is investigated for a fixed fading bandwidth. It results that large gains in required SNR can be achieved using RS block codes. Then the influence of fading bandwidth is studied. Finally techniques such as interleaving and erasure-decoding are applied to improve the bit error rate performance.

In Chapter 5, a receiver which uses a linear predictor to estimate the fading from the received signal is introduced and analyzed. First the principle of linear prediction is presented, then the decision law for the new receiver is derived. Finally the performance of linear prediction for the land mobile satellite channel with uncoded and coded systems are determined.

In Chapter 6, we summarize the results and give suggestions for further research.

In Appendix A, we give all BOSS modules which have been used in our study.

In Appendix B, a brief description of RS codes (encoding, decoding and error/erasure-decoding) and the interleaver/deinterleaver techniques are given.

In Appendix C, some information relevant to the simulation is given.

Chapter 2

System Model for Land Mobile Satellite Channel

2.1 Introduction

In this chapter, our interest is to characterize the land mobile satellite channel. This will permit us to estimate the performance of communications sytems with various modulations and coding schemes.

First the system model used in our simulation is described, and a mathematical model for signal transmission is given. Then we describe the propagation environment in which land mobile satellite systems must operate. Finally we discuss the most important fading models for the land mobile satellite channel as suggested in the literature [1-4] and [6].

The first model of interest is the Rician fading model where the received signal consists of the sum of a direct component which is received without distortion other than an attenuation due to free space loss and a doppler shift due to movement of the vehicle, and a multipath component which is Rayleigh distributed in amplitude and uniformly distributed in phase. The second model is based on the model described by C. Loo in references [1-4], which we will refer to as lognormal shadowed Rician fading

model. A brief description of the latter model is given; then using BOSS, the fading and shadowing process is simulated. Many trials with different values of the model parameters have been carried out with the objective of fitting the results from application of the model to those derived from measurements made by J.S.Butterworth and E.E. Matt and Loo's [4] on an emulated satellite path. Finally the second order statistics, the level crossing rate and the average fade duartion of the received signal envelope for the lognormal shadowed model is determined for different degrees of shadowing.

2.2 Complex Baseband Model

A block diagram of the satellite mobile system model that is used for the analysis and simulation is shown in Figure 2.1. In this section each of the blocks is briefly discussed.

The data source module generates a pseudo random binary sequence, the symbol generated at any given time is independent of all previous symbols, and both elements of the symbol alphabet are equally likely. The channel encoder transforms each k-symbol information sequence at its input into a n-symbol encoded sequence by using Reed-Solomon coding. The encoded data are reordered by the interleaver and transmitted over the channel. The interleaver module places the encoded data in a rectangular array of D rows and n columns. Each row of the array constitutes a code word of length n. An interleaver of degree D consists of D rows (D code words). The symbols are read out column-wise and transmitted over the channel. The PSK modulator modulates the input bit sequence into points in the complex plane. These point are (-1,0) and (1,0) for BPSK and (-1,1), (-1,-1), (1,-1) and (1,1) for QPSK.

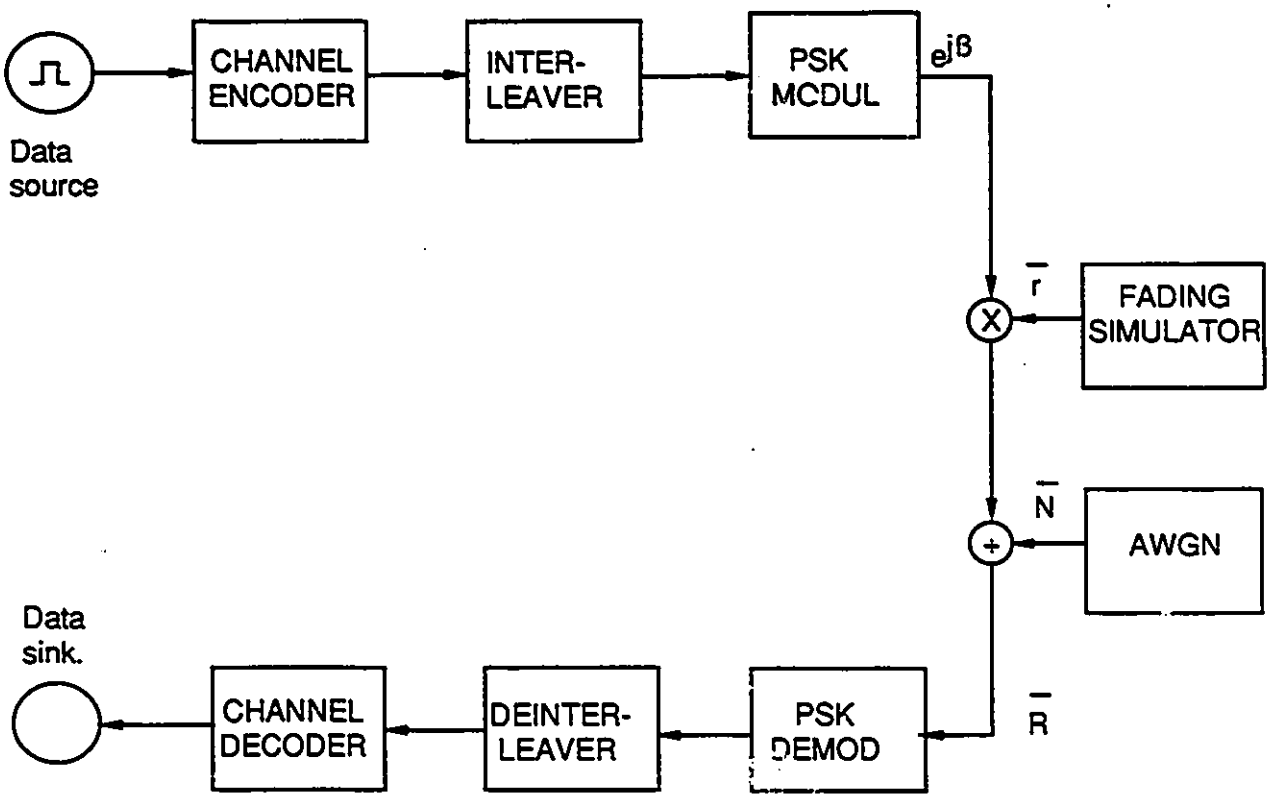

Figure 2.1: Baseband signal transmission model.

Besides fading, the transmitted signal is corrupted also by the additive white Gaussian noise. At the receiver, after demodulation, the deinterleaver puts the data in proper sequence and passes it to the decoder. As a result of the interleaving-deinterleaving, error bursts are spread out in time so that errors within a code word appear to be independent. The PSK demodulator is a matched filter demodulator for PSK. It integrates for each symbol interval, and then quantizes the output to the nearest PSK constellation point. After deinterleaving, the data is decoded before it is passed to the data sink. The channel decoder transforms the coded sequence at its input into an information sequence on its output using Reed-Solomon decoding. The decoding algorithm is the Berlekamp's iterated decoding algorithm [52].

The mathematical model for transmission can be written as follows:

$$\bar{R} = \bar{r}e^{j\beta} + \bar{N} \tag{2.1}$$

$$\bar{r} = \bar{z} + \bar{w} = r\, e^{j\psi} \tag{2.2}$$

where:

$\bar{R}$: is the received phasor,

β : phase for PSK,

$\bar{N}$: complex Additive Noise,

$\bar{r}$: complex channel gain,

ψ : Phase shift due to the combined effect of fading and shadowing,

$\bar{z}$: line-of-sight component: (channel gain),

$\bar{w}$: Multipath or scatter components: (channel gain).

In our simulation a normalized fading bandwidth in the range of 0.01 to 0.1 is considered for the following reason.

The future land mobile satellite system is being designed in such a way that a major portion of the message traffic will likely be handled with digital transmission with information rate of 2400 to 4800 bits per second. A spectrum allocation in L-band (1540-1660 MHz) is of interest for land mobile satellite applications. If we consider a vehicle speed in the range of 20 to 100 Km per hour the normalized fading bandwidth will be in the range of 0.006 to 0.064. Table 2.1 shows the normalized fading bandwidth for different vehicle speeds. In this table the fading bandwidth is given by

$$B = \frac{V}{c} f_c \tag{2.3}$$

where f_c is the carrier frequency, V is the vehicle speed and c is the speed of light. B_1 and B_2 in Table 2.1 correspond to 1540 MHz and 1660 MHz respectively.

Vehicle speed (Km/h)	B_1 (Hz)	B_2 (Hz)	B_1 T		B_2 T	
			$R = 4800bps$	$R = 2400bps$	$R = 4800bps$	$R = 2400bps$
20	28.3	30.7	0.006	0.012	0.0065	0.013
30	42.75	46.1	0.009	0.018	0.0095	0.019
40	57	61.4	0.012	0.024	0.013	0.026
50	71.25	76.8	0.0145	0.029	0.016	0.032
60	85.5	92.17	0.0175	0.035	0.019	0.038
70	99.75	107.5	0.021	0.042	0.0225	0.045
80	114	122.9	0.024	0.048	0.025	0.051
90	128.25	138.25	0.0265	0.053	0.029	0.058
100	142.5	153.6	0.03	0.06	0.032	0.064

Table 2.1: Normalized fading bandwidths as a function of vehicle speed and transmission rate for L-Band (1540-1660 MHz).

2.3 Mobile Satellite Propagation Model

Figure 2.2 shows the propagation environment in a land mobile satellite communications system. The mobile receiver is equipped with a low gain antenna that collects three electromagnetic rays. The rays collected by the vehicle antenna include a direct path, R_0, a diffuse path, R_1, and a ground-reflected path, R_2. In contrast to a mobile satellite, conventional satellite-communication earth terminals equipped with high-gain antennas can completely reject the last two components, collecting only R_0.

We may model the input signal as the sum of three vectors consisting of the direct wave, the ground reflection and a diffuse one, i.e.,

$$\bar{r} = \bar{z} + \bar{g} + \bar{w} \tag{2.4}$$

where $\bar{r}$, $\bar{z}$, $\bar{g}$ and $\bar{w}$ denote the input, direct component, ground reflection, and diffuse components, respectively.

Due to shadowing, the direct component is subjected to a lognormal transformation [4]. Analyses as well as experiments have shown that the diffuse component arrives at an elevation angle of about zero degree and that the wave amplitude is statistically described by a Rayleigh distribution [9].

The diffuse component has a two-sided bandwidth of $2V/\lambda$, where V and λ denote the speed of the vehicle and the carrier wavelength, respectively.

Relative to the diffuse component, the changes in the ground reflection are very slow. Furthermore, since the ground reflection arrives at a negative elevation angle, the antenna substantially attenuates this reflection. Hence the input signal can be effectively modeled as the sum of only two vectors, the direct and diffuse components.

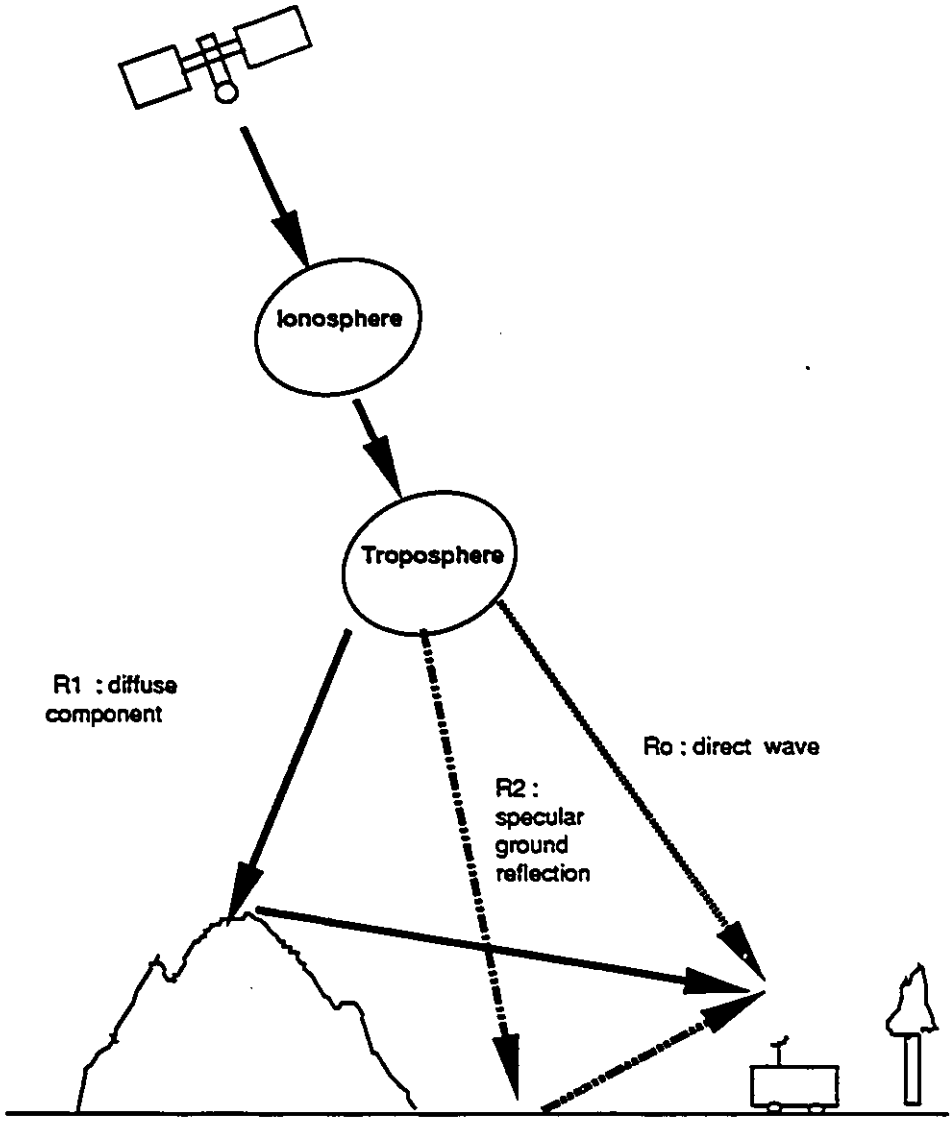

Figure 2.2: Propagation model for land mobile satellite channels.

2.4 Rician Fading Model

Figure 2.3 shows the block diagram used in our simulations for generating the Rician fading process.

The independent source processes $s_1(t)$ and $s_2(t)$ are regarded as white gaussian random generators with zero mean and variance σ^2.

The average powers of X(t) and Y(t) are given by :

$$d = N_0 \ B \tag{2.5}$$

where N_0 and B represent the one-sided power spectral density of the gaussian random generator and the filter bandwidth respectively.

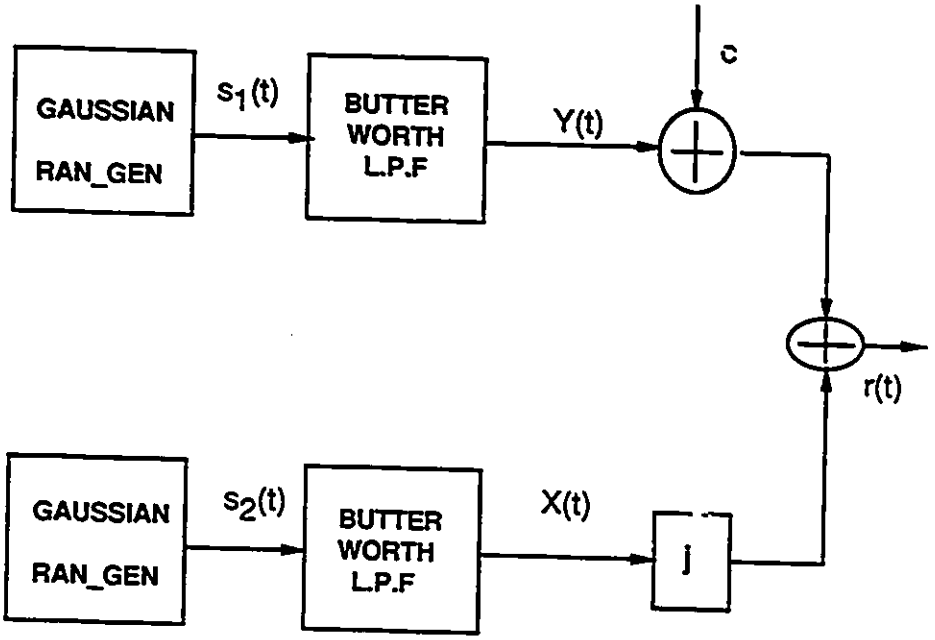

Figure 2.3: Block diagram for generating a Rician fading process.

The severity of fading is determined by the direct-to-multipath signal power ratio

known as K-factor and defined as :

$$K = \frac{c^2}{2d}, \tag{2.6}$$

where c is the constant value of the direct component and d is the variance of the quadrature and in-phase channel. Using (2.5) the K-factor could be rewritten as:

$$K = \frac{c^2}{2\,N_0\,B} \tag{2.7}$$

The fading amplitude $r(t)$ is a Rician process with a probability density function of

$$P(r) = \frac{r}{d}\; e^{(-\frac{r^2+c^2}{2d})}\; I_0\,(\frac{rc}{d}) \tag{2.8}$$

2.5 Lognormal Shadowed Rician Fading Model

2.5.1 Probability Density Function

The mathematical derivations required to describe the model are given in the literatur : [1-4], the major steps of derivation are included here for the sake of completeness.

Consider the sum of a lognormally distributed random phasor and a Rayleigh phasor

$$re^{j\psi} = ze^{j\phi_0} + we^{j\phi}\;;\;\; z, w > 0 \tag{2.9}$$

where the phases ϕ_0 and ϕ are uniformly distributed between 0 and 2π, z is lognormally distributed, and w has Rayleigh distribution. If z is temporarily kept constant, then the conditional probability density function of r is simply that of a Rician vector.

$$P(r|z) = \frac{r}{b_0}\; e^{[-(r^2+z^2)/2b_0]}\; I_0(\frac{rz}{b_0}) \tag{2.10}$$

where $2b_0$ represents the variance of the Rayleigh component and $I_0(.)$ is the modified Bessel function of zeroth order. Applying the theorem of the total probability, one

obtains

$$P(r) = \frac{r}{b_0} \int_0^{\infty} e^{[-(r^2+z^2)/2b_0]} \; I_0(\frac{rz}{b_0}) \; P(z)dz \tag{2.11}$$

It has been assumed that P(z) is lognormal, given by :

$$P(z) = \frac{1}{z\sqrt{2\pi d_0}} \; e^{[-(lnz-\mu_0)^2/2d_0]} \tag{2.12}$$

where d_0 and μ_0 are the variance and mean of the normal distribution. Thus substituting (2.12) into (2.11), one obtains :

$$P(r) = \frac{r}{b_0\sqrt{2\pi d_0}} \int_0^{\infty} \frac{1}{z} \; e^{[-(lnz-\mu_0)^2/2d_0-(r^2+z^2)/2b_0]} \; I_0(\frac{rz}{b_0})dz \tag{2.13}$$

It has been shown [5] that the probability density function of the received signal phase ψ due to the combined effect of fading and shadowing is approximately Gaussian. Thus

$$P(\psi) = \frac{1}{\sqrt{2\pi}\sigma} \; e^{[-(\psi-\eta)^2/2\sigma^2]} \tag{2.14}$$

where η and σ are the mean and the standard deviation of the received signal phase.

This completes the mathematical description required to obtain expressions for the probability density function due to combined effect of Rician fading and lognormal shadowing.

Now our interest is to simulate this model to generate the received signal envelope. As mentioned earlier, the diffuse component $\bar{w}$ is modeled by a Rayleigh distribution envelope and uniformly distributed phase, therefore $\bar{w}$ can be written as :

$$\bar{w} = X + jY \tag{2.15}$$

where X and Y are two Gaussian random variables with zero mean and equal variances. $\bar{w}$ can be rewritten as:

$$\bar{w} = \sqrt{X^2+Y^2} \; e^{j\phi} \tag{2.16}$$

where $\sqrt{X^2+Y^2}$ is Rayleigh distributed and ϕ is uniformly distributed between 0 and 2π. On the other hand, it is straightforward to show that if U is a Gaussian random variable with mean μ_0 and variance d_0, $z = e^U$ is lognormally distributed.

Based on these mathematical derivations, the model given in Figure 2.4 is constructed to generate the lognormally shadowed Rician fading process. The independent source processes $s_1(t)$, $s_2(t)$ and $s_3(t)$ in Figure 2.4 are regarded as Gaussian processes with zero mean and variances ${\sigma_1}^2$, ${\sigma_2}^2$ and ${\sigma_3}^2$ respectively. The low pass filters are used to control the dynamics of the fading.

It is suggested that a third-order-Butterworth fading spectrum yields the best results when comparing with experimental results in [4].

2.5.2 Fading Model Parameters

In our simulation, the following parameters are used for the generation of the fading and shadowing process.

- ${\sigma_1}^2$, ${\sigma_2}^2$ and ${\sigma_3}^2$ are the variances of the gaussian random processes $s_1(t)$, $s_2(t)$ and $s_3(t)$ respectively. The value of these parameters were chosen in such a way to provide the values of the fading model parameters, b_0 and d_0 suggested in [1-4].

- μ_0: is the mean of the gaussian process $U(t)$.

- STOP-TIME: is the time duration of the simulation run in seconds. STOP-TIME is set large enough to get good estimates of the quantities of interest. If, for example, the simulation is being run to estimate a bit error probability of 10^{-3} when the bit error rate is 2400 bps, a value of 50 seconds for STOP-TIME should be chosen to get accurate results. (120000 bits are generated which are

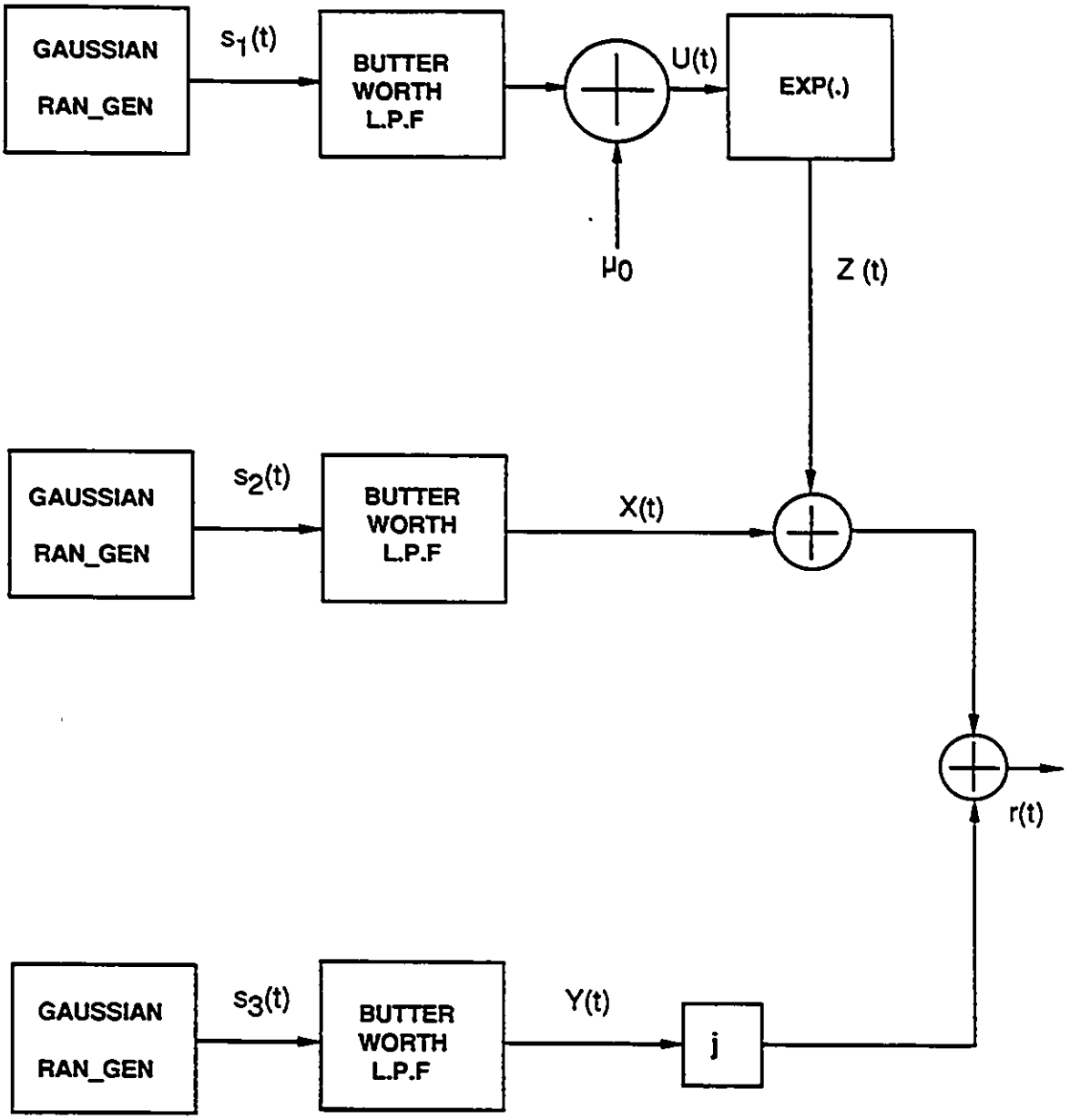

Figure 2.4: Block diagram for generating a lognormal shadowed Rician fading process.

120 times 10^3 bits).

- DT: is the time interval in seconds between signal samples for the simulation run, the simulation clock runs from time=0 to time=STOP TIME seconds in steps of DT seconds. DT must be small enough to avoid undue aliasing for the signals being sampled. Ideally, $\frac{1}{DT}$ should be greater than twice the highest frequency present in the signals to be sampled, but many waveforms have infinite bandwidth (e.g., an ideal bit stream), and so DT is made small enough that the aliased power falling into the simulation bandwidth is small compared to the noise power in the same bandwidth.

  It has been verified that eight samples in the period of a rectangular waveform is enough for the samples to accurately characterize the waveform for the purpose of simulation. It is also typical for DT to be set equal to a power of two. This is done so that the internal, binary representation of DT will be the same as the entered value. In our simulation this parameter changes with the value of the bit rate.

- m: is the order of the low pass filter.

- f_{m1}, f_{m2} and f_{m3} are the 3 dB cut-off frequencies of the low pass filters 1, 2 and 3 respectively. Since the quadrature and in-phase components of the Rayleigh component are similar, identical filters ($H(f)$) are used to filter $s_2(t)$ and $s_3(t)$, thus f_{m2}=f_{m3}. The choice of f_{m2} depends on the normalized fading bandwidth desired. For instance, for BT = 2.5% and a bit rate of 2400 bps the value of this parameter should be 60 Hz. On the other hand shadowing varies more slowly than fading [18], in our simulation we found that our results for the cumulative density function of the received signal envelope fits very well with

the experimental results when the fading process varies 20 times faster than the shadowing process. For this reason f_{m1} was chosen as 3 Hz when f_{m2}= 60 Hz.

Figure 2.4 shows the fundamental set up for generating the lognormal shadowed Rician fading process. The independent source processes, $s_1(t)$, $s_2(t)$ and $s_3(t)$ are regarded as Gaussian noise. After filtering we have three zero-mean gaussian processes with noise equivalent bandwidths corresponding to the filter bandwidths,i.e.,

$$B = \int_0^\infty |H(f)|^2 \, df \tag{2.17}$$

The variance of the random process $U(t)$ is given by :

$$\sigma_U^2 = d_0 = N_{01} \, B_1 \tag{2.18}$$

and the average power of $X(t)$ and $Y(t)$ is given by

$$\sigma_X^2 = N_{02} \, B_2 \tag{2.19}$$

$$\sigma_Y^2 = N_{03} \, B_3 \tag{2.20}$$

where N_{01}, N_{02} and N_{03}, represent the one-sided power spectral densities of the gaussian random generators 1, 2 and 3 respectively. B_1, B_2 and B_3 represent the bandwidths of the filters 1, 2 and 3 respectively.

As mentioned before, the quadrature and in-phase components of the scatter component are similar. For this reason, in our simulation ${\sigma_2}^2 = {\sigma_3}^2$ and $f_{m2} = f_{m3}$, thus

$$\sigma_X^2 = \sigma_Y^2 = b_0 = N_{02} \, B_2 \tag{2.21}$$

For the Butterworth filter which is used to control the dynamics of the fading we have

$$|H(f_i)|^2 = \frac{1}{1 + (\frac{f}{f_{mi}})^{2m}} \quad \text{for } i = 1, 2 \tag{2.22}$$

where f_{mi} is the 3 dB cut-off frequency of the Butterworth low pass filters in Figure 2.4. Substituting this into (3.9) we find

$$B_1 = \frac{\pi f_{m1}}{2m\ sin(\pi/2m)} \tag{2.23}$$

$$B_2 = \frac{\pi f_{m2}}{2m\ sin(\pi/2m)} \tag{2.24}$$

Therefore b_0 and d_0 can be written as a function of all our model parameters.

$$b_0 = \frac{\pi N_{02} f_{m2}}{2m\ sin(\pi/2m)} \tag{2.25}$$

and

$$d_0 = \frac{\pi N_{01} f_{m1}}{2m\ sin(\pi/2m)} \tag{2.26}$$

Since in our study a third-order-Butterworth was chosen, i.e., $m = 3$ therefore the filter bandwidth can be rewritten as

$$B_1 = \frac{\pi f_{m1}}{3} \approx f_{m1} \tag{2.27}$$

$$B_2 = \frac{\pi f_{m2}}{3} \approx f_{m2} \tag{2.28}$$

Many trials have been carried out with different values of ${\sigma_1}^2$, ${\sigma_2}^2$, f_{m1}, f_{m2} and μ_0 with the objective of fitting our results to those derived from measurements made by J.S. Butterworth and E.E. Matt and Loo's [4] on a simulated satellite path.

During these measurements a helicopter was flown at a fixed elevation angle of 15 degree with respect to the receiver. The measurement site was a rural area with about 35 percent tree cover. Light shadowing was generally experienced when travelling through sparsely wooded areas, and heavy shadowing was experienced when travelling through densely wooded areas. Comparing with other sets of experimental data obtained by the same group, the sets of data we have chosen represent the worst case for heavy shadowing and the best case for light shadowing. Loo shows [5] that the

received signal level for 99 percent of the time in a suburban area is better than heavy shadowing in a rural area, thus depending on the multipath component, the received signal on the suburban area could approach to average shadowing in a rural area.

After many trials the parameters chosen and the corresponding values of b_0 and d_0 are given in Table 2.2.

Parameters	Light	Average	Heavy
STOP TIME (sec)	100	100	100
DT (sec)	1.22E-4	1.22E-4	1.22E-4
σ_1^2	114.2	285.6	488
σ_2^2	8.97	6.9	3.94
Filter order m	3	3	3
f_{m1} (Hz)	3	3	3
$f_{m2} = f_{m3}$ (Hz)	60	60	60
b_0	0.157	0.12	0.069
μ_0	0.028	-0.289	-3.91
d_0	0.11	0.28	0.7

Table 2.2: Shadowed Rician fading simulation model parameters.

2.5.3 Simulation Results

By computer simulations using BOSS, we obtained the cumulative probability distribution of the amplitude of the shadowed Rician fading channel for light, average and heavy shadowing shown in Figure 2.5, 2.6, and 2.7 respectively. The model

in Figure 2.4 was used to generate these results. It is found that our results closely agree with Loo's results [1-4].

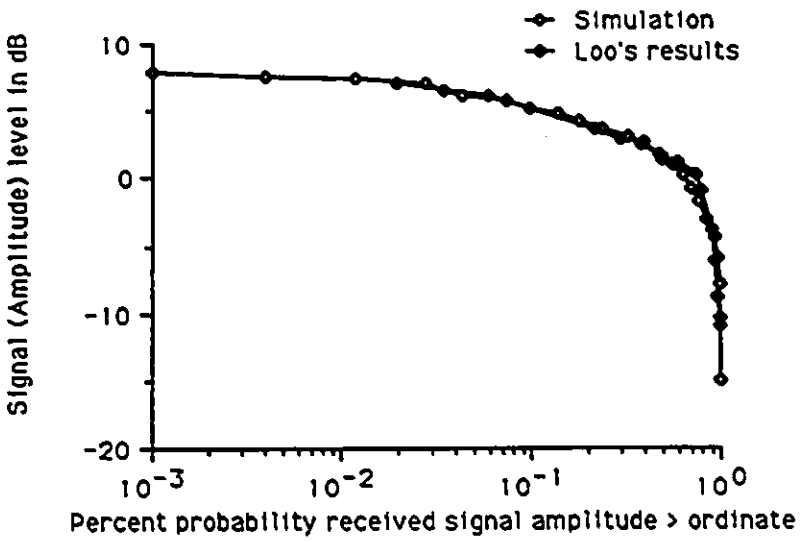

Figure 2.5: Comparison of the amplitude cumulative probability distributions between the experimental and simulated results for light shadowing.

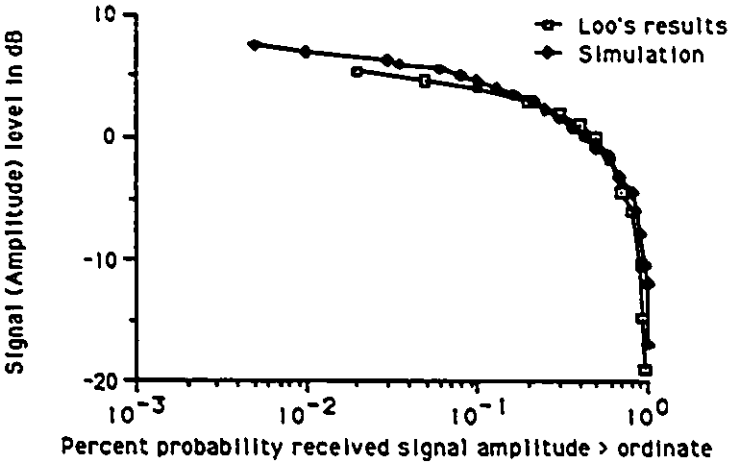

Figure 2.6: Comparison of the amplitude cumulative probability distributions between the experimental and simulated results for average shadowing.

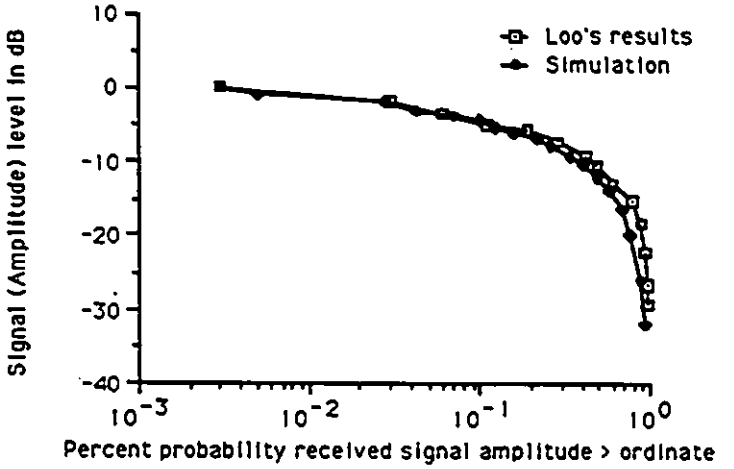

Figure 2.7: Comparison of the amplitude cumulative probability distributions between the experimental and simulated results for heavy shadowing.

2.6 Second Order Statistics of the Fading Process

Our interest in this section is to find the second order statistics, the level crossing rate (LCR), and the average fade duration (AFD) of the received signal envelope from the simulated data samples. The results of the LCR and AFD will provide information which will be useful in determining the error correction techniques to be used for land mobile satellite communication system.

2.6.1 Level Crossing Rate

The level crossing rate is considered as a second order statistic, since it is time depended and is also affected by the speed of a mobile-radio vehicle. The LCR of the mobile-radio signal provides additional information which when combined with other statistical data enables the designer to make intelligent decisions.

Rice [42] has shown that for any wide sense stationary random process, the expected number at which the envelope crosses a specified signal level R with positive slope in time T is given by

$$n(R) = T \int_0^\infty \dot{r} \; P(R, \dot{r}) \, d\dot{r} \tag{2.29}$$

where $\dot{r}$ is the rate of change of the signal envelope, defined as

$$\dot{r} = \frac{dr(t)}{dt} \tag{2.30}$$

and $P(R, \dot{r})$ is the joint probability density function of $\dot{r}$ and r, at $r = R$. The total number of expected crossings per second, the level crosing rate, is defined as:

$$N(R) = \frac{n(R)}{T} = \int_0^\infty \dot{r} P(R, \dot{r}) \, d\dot{r} \tag{2.31}$$

In the following discussion the level crossing rate is normalized to the maximum

doppler shift frequency, f_m, to make results independent of the vehicle speed thus:

$$N'(R) = \frac{N(R)}{f_m} \tag{2.32}$$

2.6.2 Fade Duration

The duration of signal fade determines the probable number of signaling bits that will be lost during the fade. The duration of the signal fade is affected by several factors among which the primary factor is the travel speed of the mobile-radio vehicle. The relation between the average fade duration and the expected number of crossings at a particular level R per second can be stated as : r is below R

$$N(R) = \frac{P(r < R)}{\bar{t}(R)} \tag{2.33}$$

From (3.30), the average duration of fades below the level R can be calculated as :

$$\bar{t}(R) = \frac{P(r < R)}{N(R)} \tag{2.34}$$

and the normalized average fade duration is

$$\bar{t}'(R) = \frac{P(r < R)}{N'(R)} = \frac{P(r < R) f_m}{N(R)} \tag{2.35}$$

This equation shows that the cumulative probability distribution, the LCR and the AFD are interrelated. If two of them are known, the third one can be determined.

Figure 2.8 illustrates how a simulated data sample is used to find the number of crossing at different signal envelope levels. First, a line is drawn at a specified level across the data sample under study. Either the positive-slope or negative-slope crossings are counted, but not both. The level-crossing rate is given by :

$$N(R_i) = \frac{n(R_i)}{T} \tag{2.36}$$

and the average fade duration is deduced by using :

$$\bar{t}(R_i) = \frac{P(r < R_i)}{N(R_i)} \tag{2.37}$$

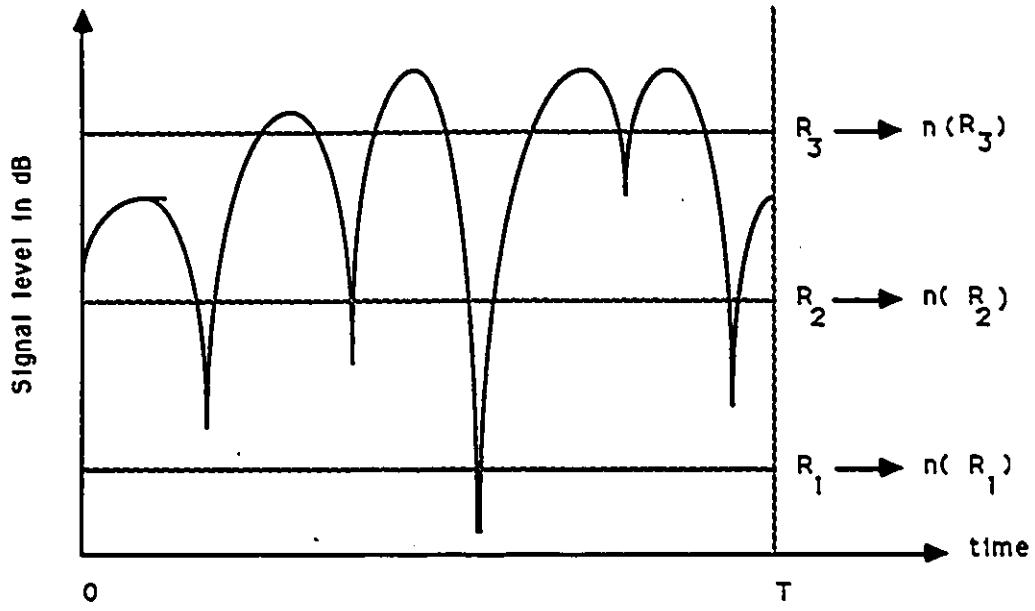

Figure 2.8: A graphic illustration of determining the LCR.

2.6.3 Simulation Results

Figure 2.9 through 2.14 show different results for the second order statistics of the simulated signal envelope. Figure 2.9 and 2.10 represent the normalized LCR and AFD for light shadowing, Figure 2.11 and 2.12 represent the normalized LCR and AFD for average shadowing and Figure 2.13 and 2.14 represent the normalized LCR and AFD for heavy shadowing.

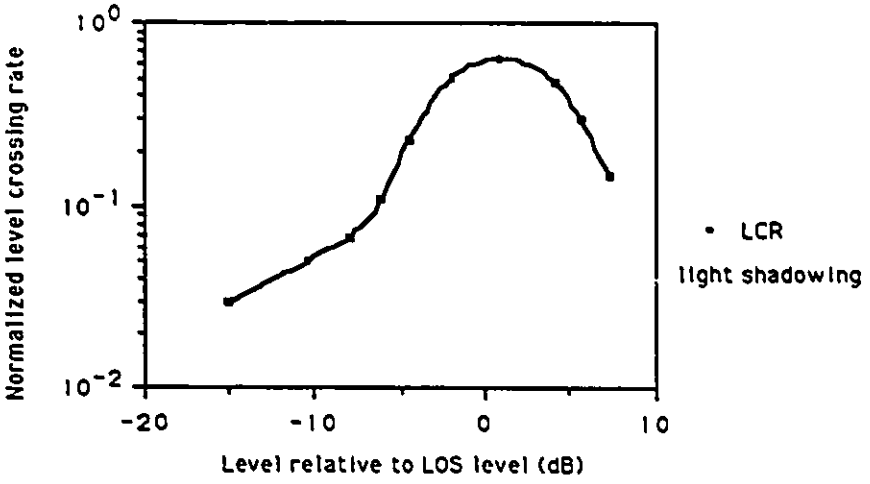

Figure 2.9: Level crossing rate for light shadowing.

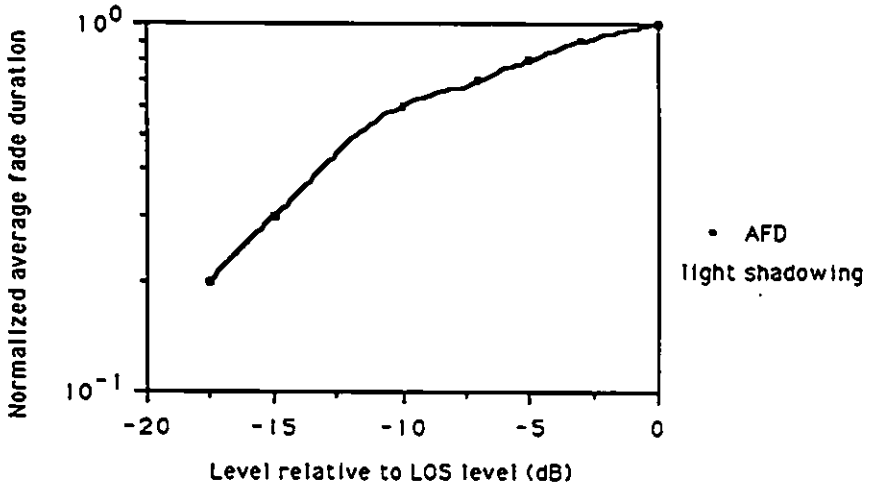

Figure 2.10: Average fade duration for light shadowing.

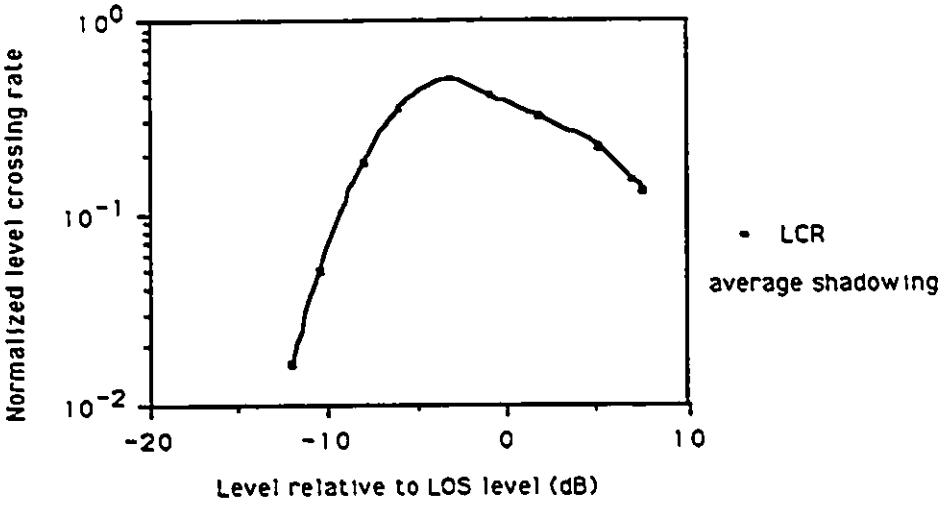

Figure 2.11: Level crossing rate for average shadowing.

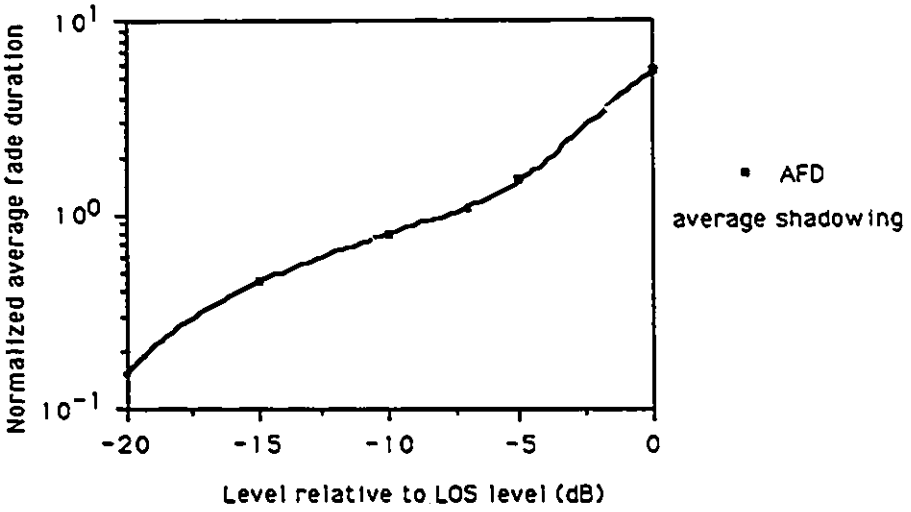

Figure 2.12: Average fade duration for average shadowing.

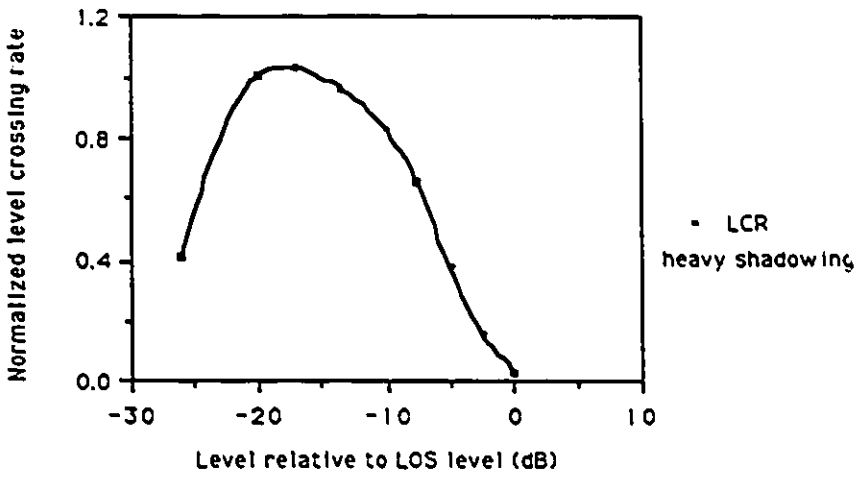

Figure 2.13: Level crossing rate for heavy shadowing.

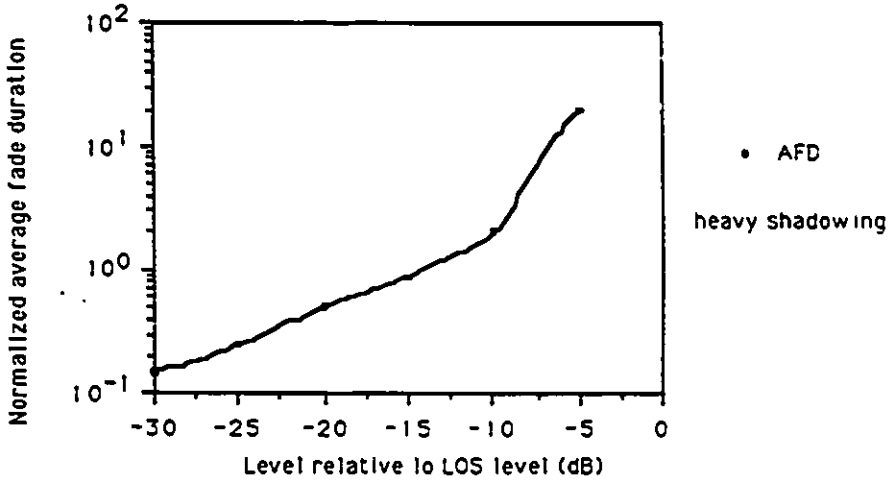

Figure 2.14: Average fade duration for heavy shadowing.

In what follows a normalized fading bandwidth of 1% to 5% is considered. This range corresponds to vehicle speeds from 20 to 90 Km/h at bit rate 2400 bps for L-band carrier frequency. If we consider that a received signal level relative to a clear line-of-sight level less than -10 dB corresponds to a channel in off-state which corresponds to 50% bit error rate, then a burst of errors occurs and lasts for the time the received signal level is below -10 dB. Using Figure 2.9 through 2.14, the average fade duration at a signal level of -10 dB, for different normalized fading bandwidths and degrees of shadowing was found and summarized in Table 2.3 through Table 2.5.

BT	B (Hz)	R (bps)	AFD (msec)	error burst length
1%	24	2400	25	60
2%	48	2400	12.5	30
5%	120	2400	5	12

Table 2.3: AFD at a signal level of -10 dB for light shadowing.

BT	B (Hz)	R (bps)	AFD (msec)	error burst length
1%	24	2400	33	80
2%	48	2400	16	40
5%	120	2400	6.6	16

Table 2.4: AFD at a signal level of -10 dB for average shadowing.

BT	B (Hz)	R (bps)	AFD (msec)	error burst length
1%	24	2400	83	200
2%	48	2400	41.6	100
5%	120	2400	16.6	40

Table 2.5: AFD at a signal level of -10 dB for heavy shadowing.

From these tables we note that the length of error bursts increases as the shadowing becomes more pronounced, therefore one has to consider this when designing the coding/interleaving scheme. For heavy shadowing with 2% BT, an effective coding/interleaving scheme should overcome bursts of 100 erroneous bits. In Chapter 4 we will show how to use these results to design the coding/interleaving scheme.

2.7 Conclusions

From the results presented in this chapter, the following conclusions can be drawn.

- The cumulative density function of the received signal envelope was determined and it is found that our results conform with the experimental results, therefore the model could be used to estimate the performance of various modulation and coding/interleaving schemes.

- The result of the AFD shows that the length of the burst of errors increases as shadowing becomes more pronouced and the normalized fading bandwidth becomes smaller. Therefore one should consider this when designing the coding/interleaving schemes

Chapter 3

Uncoded System Performance

3.1 Introduction

Our objective is to analyse the performance of RS codes in LMSAT channel, and propose an effective coding/interleaving techniques. However before proceeding with the analysis of coded system performance in a lognormal shadowed Rician fading channel, it is useful to consider the resulting bit error probability performance for uncoded BPSK.

In this chapter a computer simulation method is given to evaluate the probability of error of a receiver that detects the PSK data in a lognormally shadowed fading environment and with additive white gaussian noise (AWGN). The receiver filter considered is a matched filter. The channel model described in the previous section is used to estimate the performance of BPSK over the lognormal shadowed Rician fading and AWGN channel.

As a first step the system model for signal transmission to be used in our study to evaluate the error performance of BPSK in an AWGN is described. Therefore the reliability of this system to be used to evaluate the performance of BPSK over the lognormal shadowed Rician fading is deduced.

3.2 BPSK in an AWGN channel

The simulation model used to evaluate the error performance of BPSK in an AWGN channel is given in Figure 3.1. A detailed description of different modules used in this simulation model is shown in Appendix A.

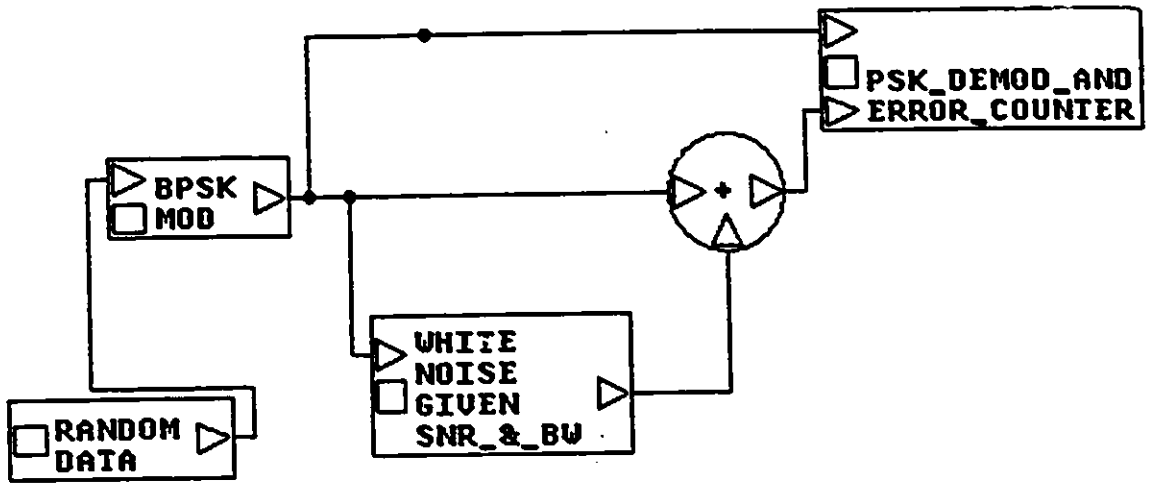

Figure 3.1: System model for BPSK in an AWGN channel.

The transmitted PSK signal can be written as :

$$s(t) = Re\ \{\sqrt{2S}\ a(t)\ e^{(j2\pi f_c t)}\} \tag{3.1}$$

where S is the average power and f_c is the carrier frequency.

The modulating function $a(t)$ has the following form :

$$a(t) = e^{(j\beta(t))} \tag{3.2}$$

in which

$$\beta(t) = \frac{\pi}{2}\ (1 - g(t)) \tag{3.3}$$

The function $g(t)$ is a sequence of M square pulses, each of duration T and with an amplitude of $+1$ or -1 corresponding to the information bits "1" and "0" respectively.

After this brief description of the simulation model, a comparison between the theoretical and simulated bit error rate of BPSK in an AWGN channel is drawn. The theoretical bit error rate of BPSK over the the AWGN channel is drawn using the formula :

$$P_e = Q\ (\sqrt{\frac{2E_b}{N_o}}) \tag{3.4}$$

where $Q(x)$ is the Q function defined as :

$$Q(x) = \frac{1}{\sqrt{2\pi}}\ \int_x^\infty\ e^{-t^2/2}\,dt \tag{3.5}$$

Figure 3.2 shows that the results of our system model simulation for the AWGN channel agree with the theoretical results computed from (3.5). Therefore this system model could be used to evaluate the performance of BPSK over the lognormal shadowed Rician fading and AWGN channel.

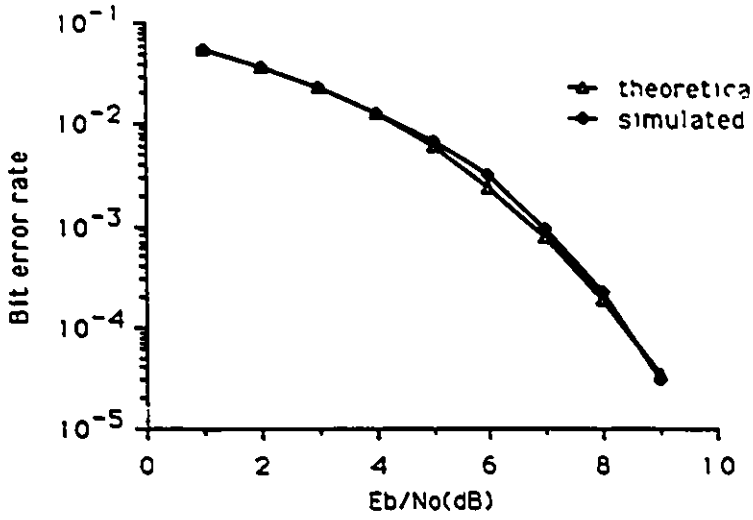

Figure 3.2: BPSK in an AWGN channel.

3.3 BPSK Over Lognormal Shadowed Rician Fading Channel

The system used for evaluation of the error performance of BPSK over the AWGN and lognormal shadowed Rician fading channel is shown in Figure 3.3. In this system only the magnitude of the fading process is considered, which means that the probability of error found is the probability of error due to amplitude fading. Thus the assumption is that the receiver perfectly tracks the phase shifts due to fading as well as other system phase uncertainties. This represents ideal performance as only the amplitude of fading process leads to performance losses.

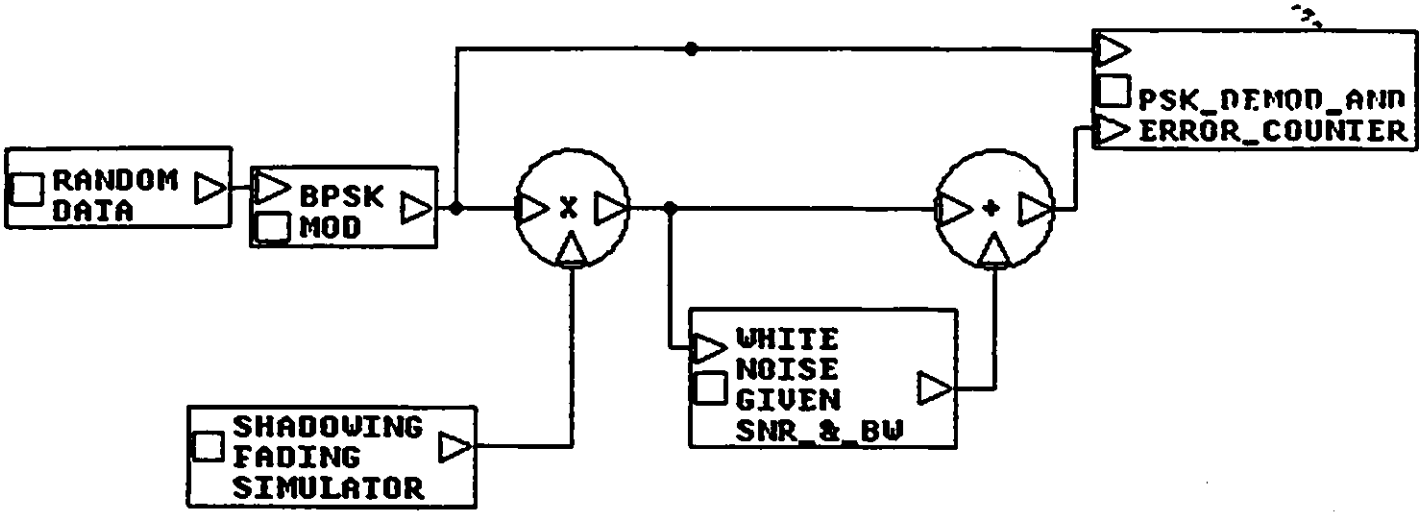

Figure 3.3: System model for BPSK over AWGN and lognormal shadowed Rician fading channel.

The results of our simulation for both the AWGN and fading channel are given in Figure 3.4 through 3.6 . The three fading scenarios considered are the light, average and heavy shadowing as described previously.

We will focus our attention on an error probability of 10^{-3} as this is the target BER in speech applications. For the three degrees of shadowing the SNR penalties, which are substantial when compared to AWGN case, are shown in Table 3.1.

Degree of shadowing	SNR penalties (dB)	
	$P_e = 10^{-2}$	$P_e = 10^{-3}$
Light shadowing	4.5	6.5
Average shadowing	6.7	9.8
Heavy shadowing	15.9	21

Table 3.1: SNR degradation due to fading and shadowing for BPSK.

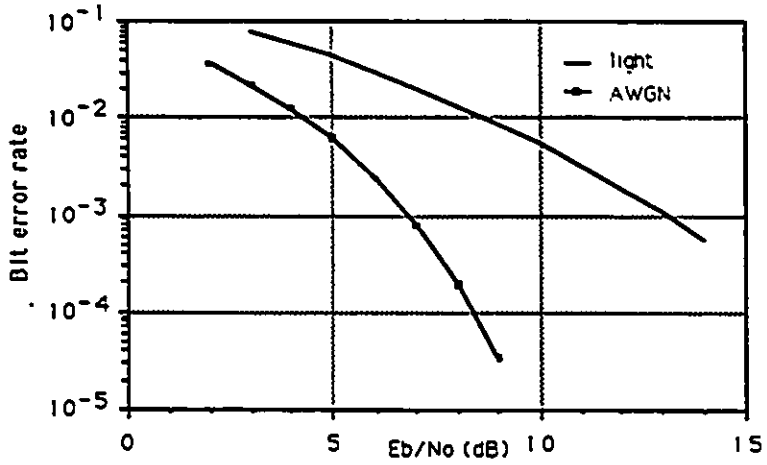

Figure 3.4: Performance of coherent PSK with light shadowing.

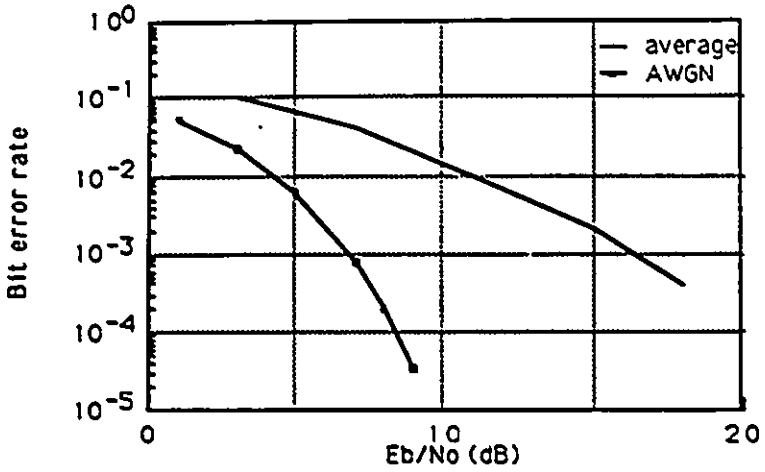

Figure 3.5: Performance of coherent PSK with average shadowing.

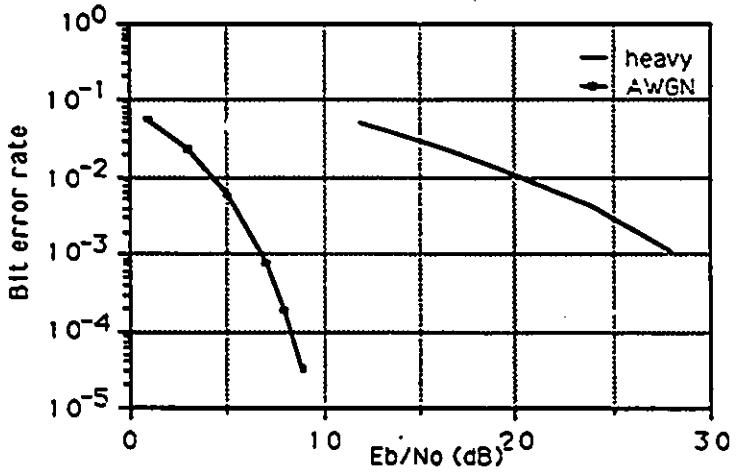

Figure 3.6: Performance of coherent PSK with heavy shadowing.

It has been shown [39] that the light shadowed Rician channel resembles the Rician channel having a K-factor of approximately 5 dB. Figure 3.7 shows the BER for ideal coherent BPSK in a lognormal shadowed Rician fading channel and a Rician fading channel with different K-factors.

We should point out that in our simulation all BER curves were given as function of the mean bit energy-to-noise ratio, $\frac{E_b}{N_o}$, defined mathematically as:

$$\frac{E_b}{N_o} = \frac{E'_b}{N_o} \; E(r^2) \tag{3.6}$$

where $\frac{E'_b}{N_o}$ represents the bit energy-to-noise density ratio in the absence of fading and shadowing. The term $E(r^2)$ is simply the average power of the received signal envelope. In the literature some people [30] consider that $E(r^2)$ is equal to one so that the mean bit enrgy-to-noise ratio is not affected by the fading. But in our case we did not consider this because the fading and shadowing processes, r, were simulated according to some experimental data.

From Figure 3.7 we can deduce that the light shadowed fading channel could be approximated by a Rician channel with a $K-$factor in the range of 5 to 8 dB at BER of 10^{-2} to 10^{-4}. The average shadowed Rician channel could be approximated by the Rician channel with a $K-$factor in the range of 0 to 5 dB.

It has been shown [31], [38] and [58] that the BER performance for PSK on heavy shadowed fading channel is slightly worse than the performance of PSK on a Rayleigh fading channel. This agrees with the results we found. This could be explained by the fact that in an LMSAT channel the direct component is the most important component of the received signal, while the multipath component is relatively weak. Therefore, intuitively one can say that if the direct component is very weak we can expect that the BER performance will be very bad, which is the case for the heavy shadowed channel. In contrast to the LMSAT case, the direct component in a terres-

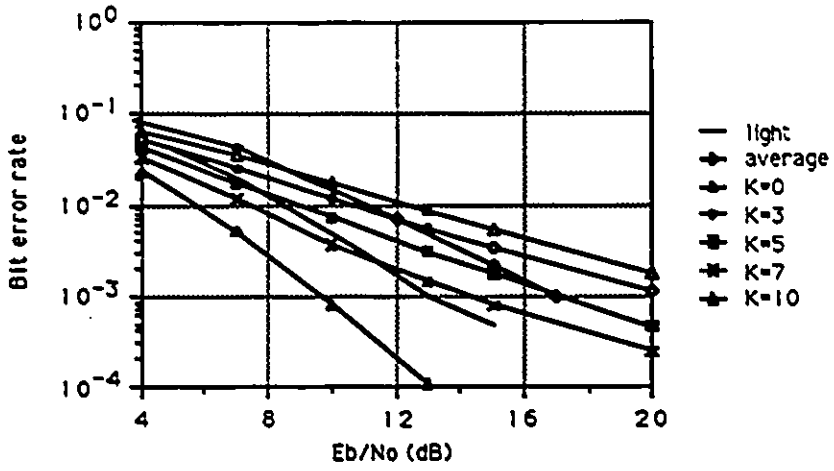

Figure 3.7: BER as a function of the mean bit energy-to-noise ratio for BPSK on a Rician and shadowed Rician fading channel.

trial mobile-radio signal is almost absent especially in urban areas, thus the mobile radio-signal is mainly constituted of multipath components where most of the energy is confined. This interpretation leads us to the conclusion that we have to distinguish between the multipath component of the LMSAT signal and the multipath component of the mobile-radio signal, although both of them were assumed to be Rayleigh but with different strengths. To understand further this point we should compute the average power of the generated shadowed fading process and see how this is varying with the degree of shadowing.

As mentioned before the average power of the scatter component is given by $2b_0$. For the lognormal component, z, the following computations are necessary to find out the average power. The mean of z is given by:

$$E(z) = \int_{-\infty}^{\infty} z\, P(z)\, dz \tag{3.7}$$

where P(z) is given by equation (2.12). Evaluation of the integral yields

$$E(z) = \exp(\mu_0 + d_0/2) \tag{3.8}$$

The average power of the lognormal component is given by:

$$E(z^2) = \int_{-\infty}^{\infty} z^2 \, P(z) \, dz = \exp(2\mu_0 + 2d_0) \tag{3.9}$$

The variance of the lognormal component can be obtained by:

$$\begin{aligned} \sigma_Z^2 &= E(z^2) - [E(z)]^2 \\ &= \exp(2\mu_0 + d_0) \, [\exp(d_0) - 1] \end{aligned} \tag{3.10}$$

The total average power of the received signal envelope is given by

$$\begin{aligned} E(r^2) &= E(w^2) + E(z^2) \\ &= 2b_0 + \exp(2\mu_0 + 2d_0) \end{aligned} \tag{3.11}$$

For heavy shadowing, with the parameters given in Table 2.2 we deduce that

$$E(z^2) = 0.0016 \tag{3.12}$$

This mean that the direct component is almost absent, therefore the average power of the received signal envelope is almost equal to the average power of the multipath component. Thus

$$E(r^2) \simeq E(w^2) = 2b_0 \simeq 0.14. \tag{3.13}$$

which means that the received signal is mainly constituted of the multipath component. From equation (3.13) one also can say that the received signal in heavy shadowed channel is very weak, even worse than the received signal in land mobile-radio channel in urban area, this is also confirmed by a comparison of the cumulative

density function of the received signal envelope in heavy shadowed (Figure 2.7) and the cumulative density function of the received signal envelope on a Rayleigh channel [9].

Finally we can say that if we keep the same parameters for the lognormal component and we change the value of $2b_0$, the BER performance will change correspondingly. For example if take $2b_0 = 1$ instead of 0.14 the BER performance will approach the BER performance over Rayleigh channel. But in our case for heavy shadowing $2b_0$ should be 0.14 because this is the value that fits to the experimental data.

3.4 Conclusions

The bit errorrate performance curves for uncoded BPSK show that:

- The fade margin required to compensate for the effect of fading and shadowing increases with the degree of shadowing.
- Some kind of multipath compensation technique is required to improve the bit error rate performance.

Chapter 4

Coded System Performance

4.1 Introduction

The bit error rate performance curves for uncoded binary phase shift keying and the second order statistics described in Chapter 2 and 3 show that some kind of multipath compensation technique is required to improve the performance.

In this chapter we focus on applying FEC to compensate the effect of fading. RS codes as non binary block codes with multiple burst-error correcting capability are well suited for error control in land mobile satellite channels.

First we determine the RS code performance with PSK transmission in an AWGN channel, then compare the results with those given in Reference [30]. Secondly the performance of RS codes over lognormal shadowed Rician fading channel is determined for different degrees of shadowing under the conditions of perfect coherence. The assumption is that the receiver perfectly tracks the phase shifts due to fading and shadowing as well as any other system phase uncertainty. This represents ideal performance as only the amplitude of the fading and shadowing process leads to performance losses.

By using the second order statistics obtained in Chapter 2, an effective coding/interleaving scheme is suggested to overcome the longest burst of errors to improve

the system performance while maintaining the receiver simplicity. Finally the benefit of using the erasure decoding is also investigated.

4.2 Performance of RS Codes in an AWGN Channel

In this section the performance of different RS codes in an AWGN channel is determined and the effect of blocklengths on the bit error rate is investigated.

It has been shown [30] that for RS codes with BPSK transmission over Rician channel, an optimum code rate of 0.55 exists at bit error rate of 10^{-5}. To study the influence of blocklengths on the bit error rate a fixed code rate of about 0.55 is assumed and the performance of (15,9), (31,17), (63,35), (127,71) and (255,153) RS codes is studied. Figure 4.1 shows bit error rate as a function of bit energy-to-noise density ratio ($\frac{E_b}{N_o}$) for different blocklengths for BPSK transmission in an AWGN channel. From this figure we can deduce that the coding gain increases with the blocklengths and the increase of this coding gain becomes less at large blocklengths, therefore RS codes with blocklengths exceeding 63 symbols is not advantageous. These results are in a good agreement with the analytical results found in [30].

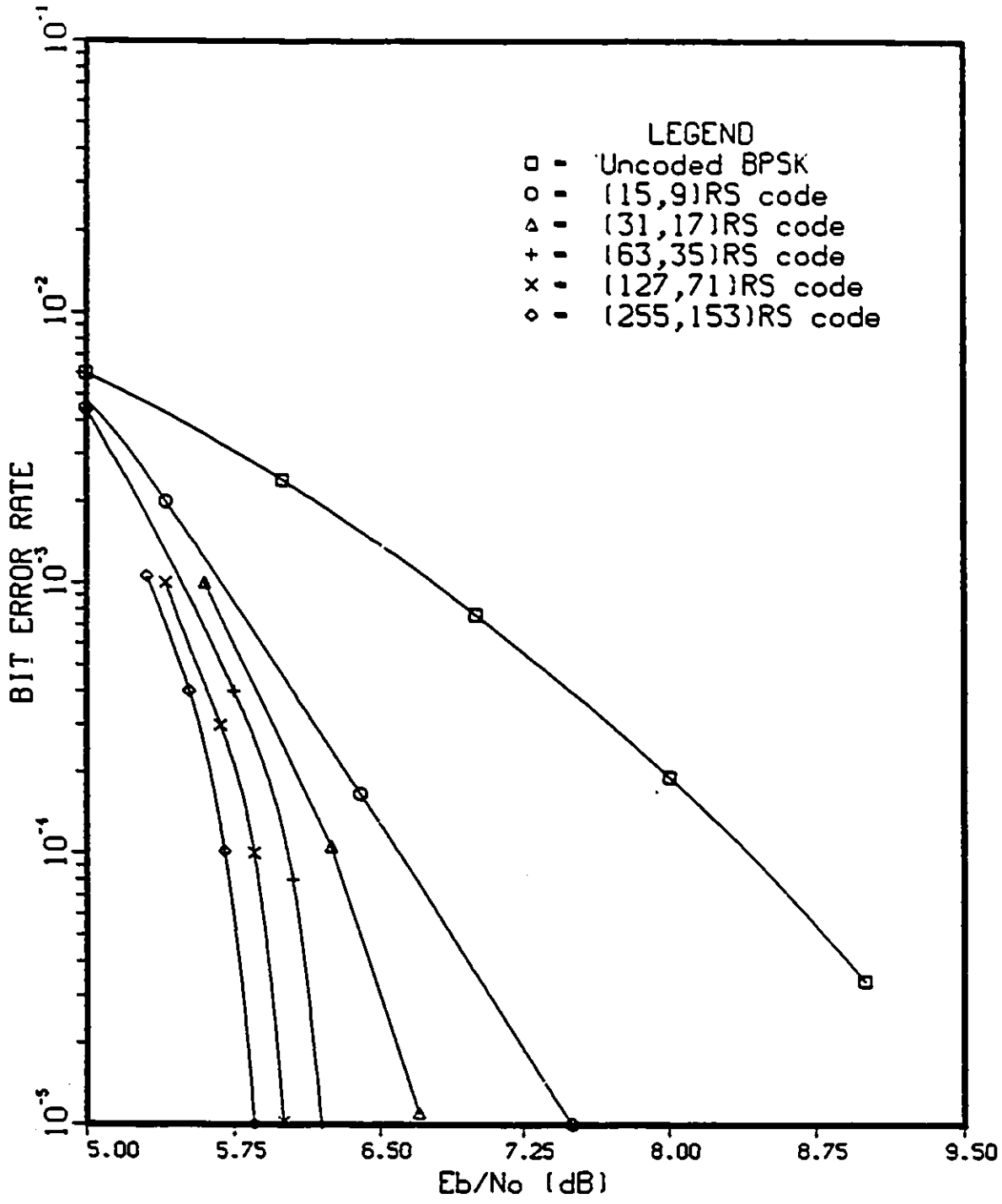

Figure 4.1: Performance of RS codes of rate 0.55 and different blocklengths in an AWGN channel.

4.3 RS Codes with BPSK Transmission over Lognormal Shadowed Rician Channel

In this section our interest is to provide a complete characterization of the performance of RS codes on a lognormal shadowed Rician fading channel. First the effect of blocklength on bit error rate for light, average and heavy shadowing for a fixed normalized fading bandwidth is studied. Secondly, the influence of fading bandwidth on bit error rate for the three degree of shadowing is investigated. Then having the background knowledge of the second order statistics, a block interleaver-deinterleaver is designed to be used with RS coding to spread out the burst of errors. The influence of interleaving on bit error rate for different normalized fading bandwidths is given. Finally, the erasure information is passed to the decoder to investigate the usefulness of error-erasure decoding in the lognormal shadowed Rician channel.

The system model used to evaluate the bit error rate for different RS codes with BPSK transmission over lognormal shadowed Rician and AWGN channel is given in Figure 4.2

In this system model, the REED-SOLOMON ENCODER module encodes information bits on its input generated by the module PN-SEQUENCE GENERATOR to coded bits on its output using RS coding. The RS codes can correct any number of coded symbol errors up to $\frac{(n-k)}{2}$. Notice that this is symbol errors and not bit errors, a symbol is made of $Log_2\,(n+1)$ consecutive bits. The encoder block changes the bit rate, the output bit rate is $\frac{n}{k}$ times the input bit rate.

REED-SOLOMON DECODER module decodes coded bits on its input to information bits on its output using RS coding. The decoding algorithm is the Berlekamp's iterated decoding algorithm [52].

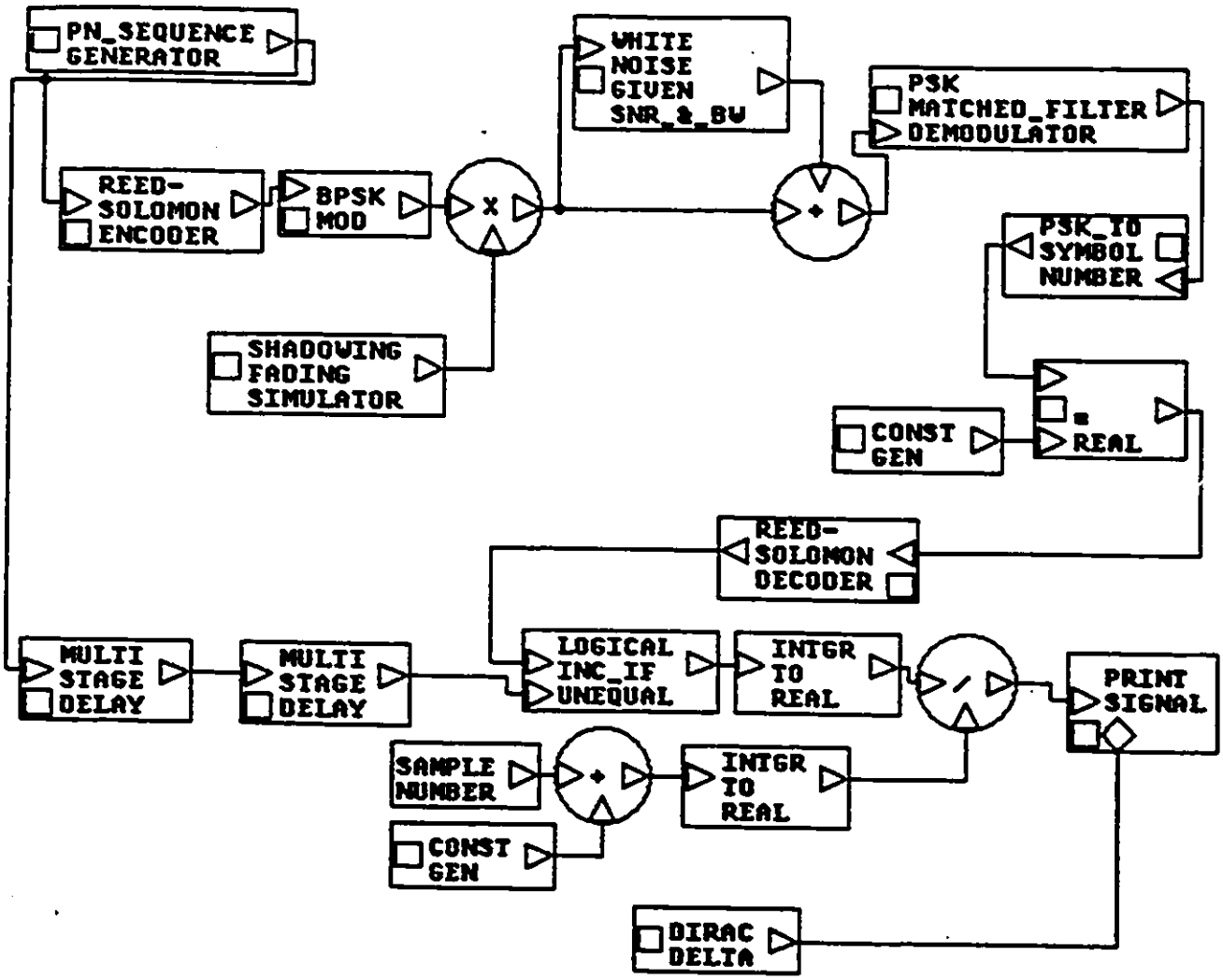

Figure 4.2: System model used to determine the performance of RS codes over a fading and shadowing channel.

4.3.1 Influence of Blocklength on Bit Error Rate

To investigate the influence of blocklength on bit error rate, a code rate of approximately 0.55 is assumed and the (15,9), (31,17) and (63,35) RS codes are chosen.

The results of our simulation for both AWGN and a fading channel are given in Figure 4.3 through 4.5. The three fading scenarios considered are light, average and heavy shadowing. From Figure 4.3 we note that, as in the Gaussian case, the coding gain in fading channel increases when longer codes are used. Moreover the coding gain is larger in the case of a fading channel than an AWGN channel. As the shadowing becomes more pronounced (or heavier), the coding gain increases.

We summarize the coding gains in Table 4.1 for an error probability of 10^{-3}.

RS Codes	Channel Model	Coding Gain (dB)
(15,9)	AWGN	1.1
(31,17)		1.2
(63,35)		1.3
(15,9)	Light shadowing	1.6
(31,17)		2.5
(63,35)		3
(15,9)	Average shadowing	2.6
(31,17)		3.8
(63,35)		4.6
(15,9)	Heavy shadowing	8.4
(31,17)		9.7
(63,35)		10.9

Table 4.1: Coding gain of different RS codes with BPSK transmission at a bit error rate of 10^{-3} and a normalized fading bandwidth of 5%.

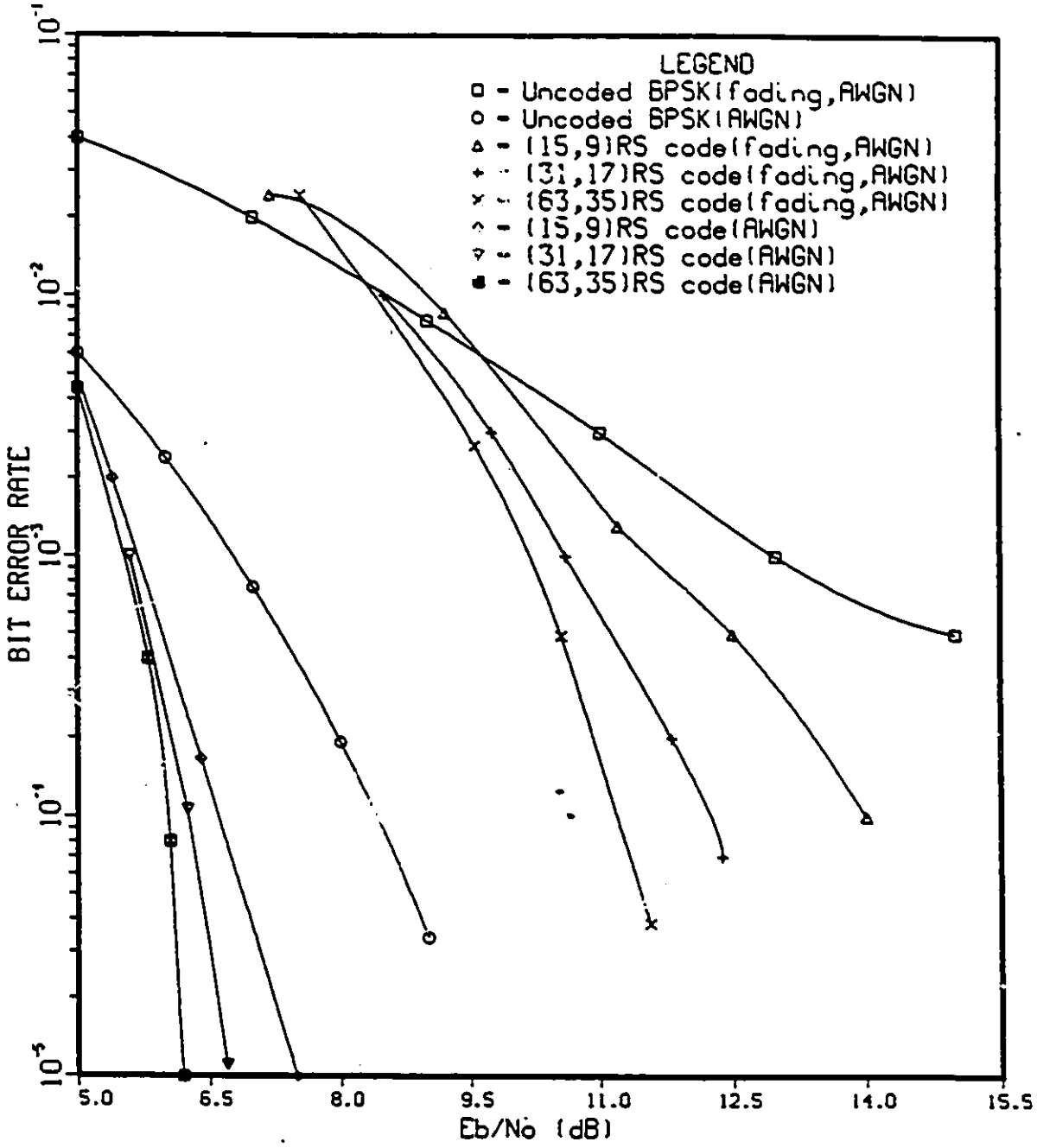

Figure 4.3: Performance of RS codes of rate 0.55 and different blocklengths with light shadowing and normalized fading bandwidth of 5%.

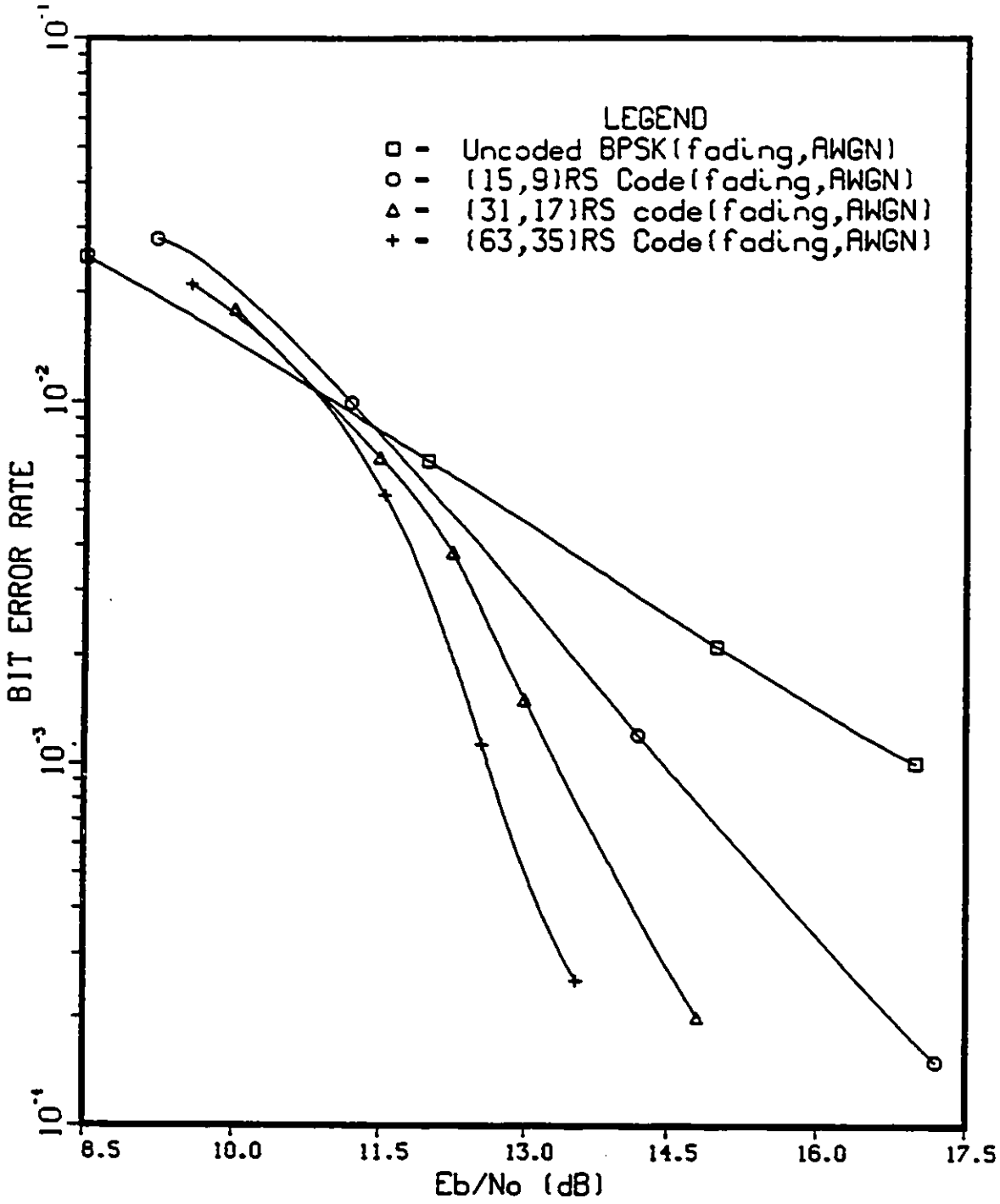

Figure 4.4: Performance of RS codes of rate 0.55 and different blocklengths with average shadowing and normalized fading bandwidth of 5%.

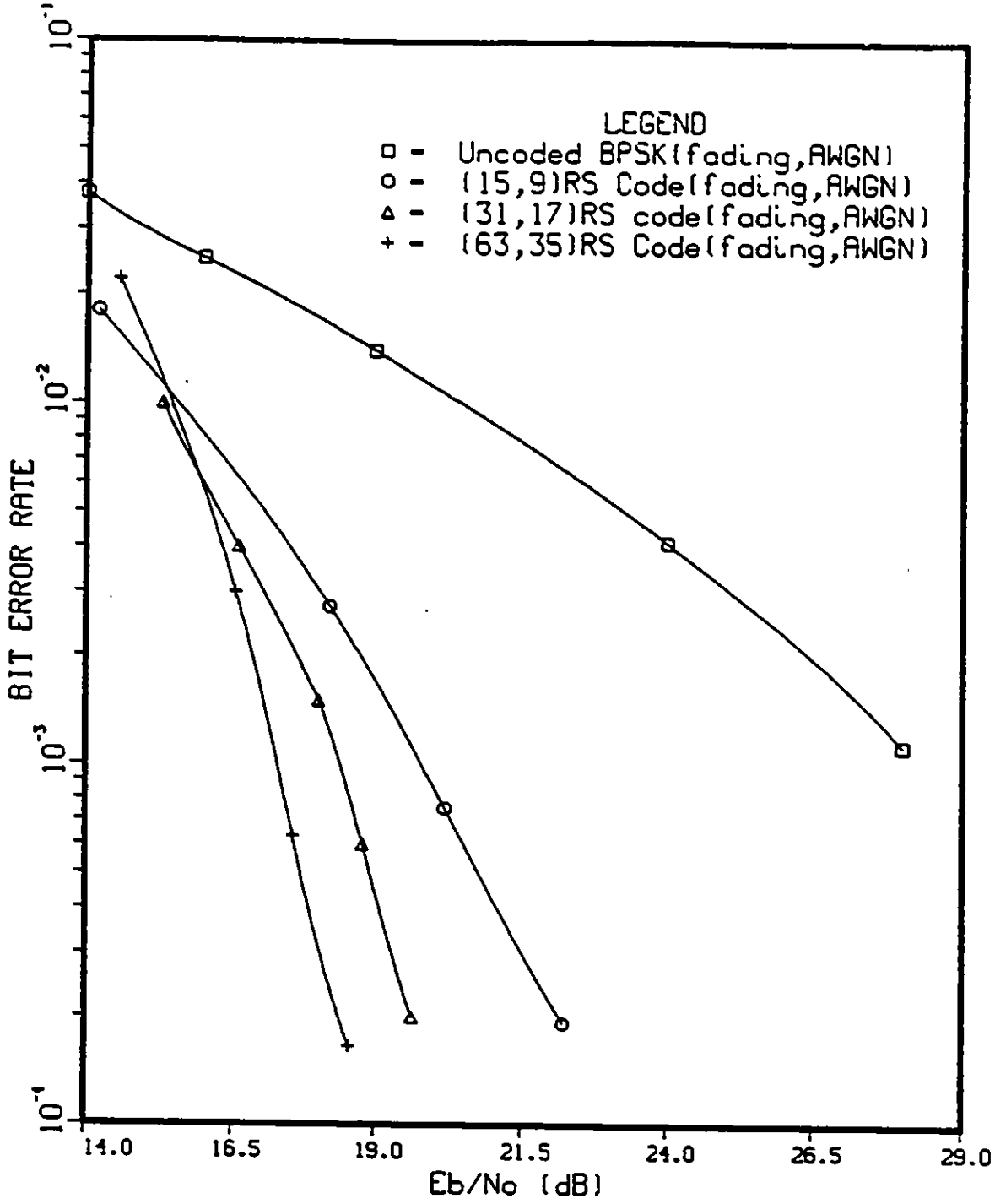

Figure 4.5: Performance of RS codes of rate 0.55 and different blocklengths with heavy shadowing and normalized fading bandwidth of 5%.

4.3.2 Influence of Fading Bandwidth

As mentioned before the normalized fading bandwidth BT varies from 1% to 10% for the mobile satellite applications. In our simulation two cases are studied. $BT = 1\%$ and $BT = 5\%$ for (63,35) RS code with light, average and heavy shadowing.

Figure 4.6 through 4.8 show bit error rate for (63,35) RS code for BPSK transmission over the lognormal shadowed Rician fading channel with 1% and 5% normalized fading bandwidth for the three degrees of shadowing.

From these figures we deduce that the performance becomes worse when the normalized fading bandwidth becomes smaller. As expected, the coding gain increases with increasing fading bandwidth. This increase could be explained by the fact that as bandwidth decreases, channel memory increases and the channel becomes more of a burst error channel. At bit error rate of 10^{-3} there is a 1.4 dB difference on the performance between $BT = 1\%$ and $BT = 5\%$ for light shadowing. This difference is a little higher for the average and heavy shadowing cases because the channel is more bursty. It is about 1.65 dB for average shadowing and 2 dB for heavy shadowing.

At this point we can say that in this range of normalized fading bandwidth which is the most common range for MSAT applications, the RS codes perform very well. Degradation on the error performance due to fading bandwidth change could be compensated by using interleaving which is an effective method for dealing with burst error channels that interleave the coded data in such a way that the bursty channel is transformed into a channel having independent errors.

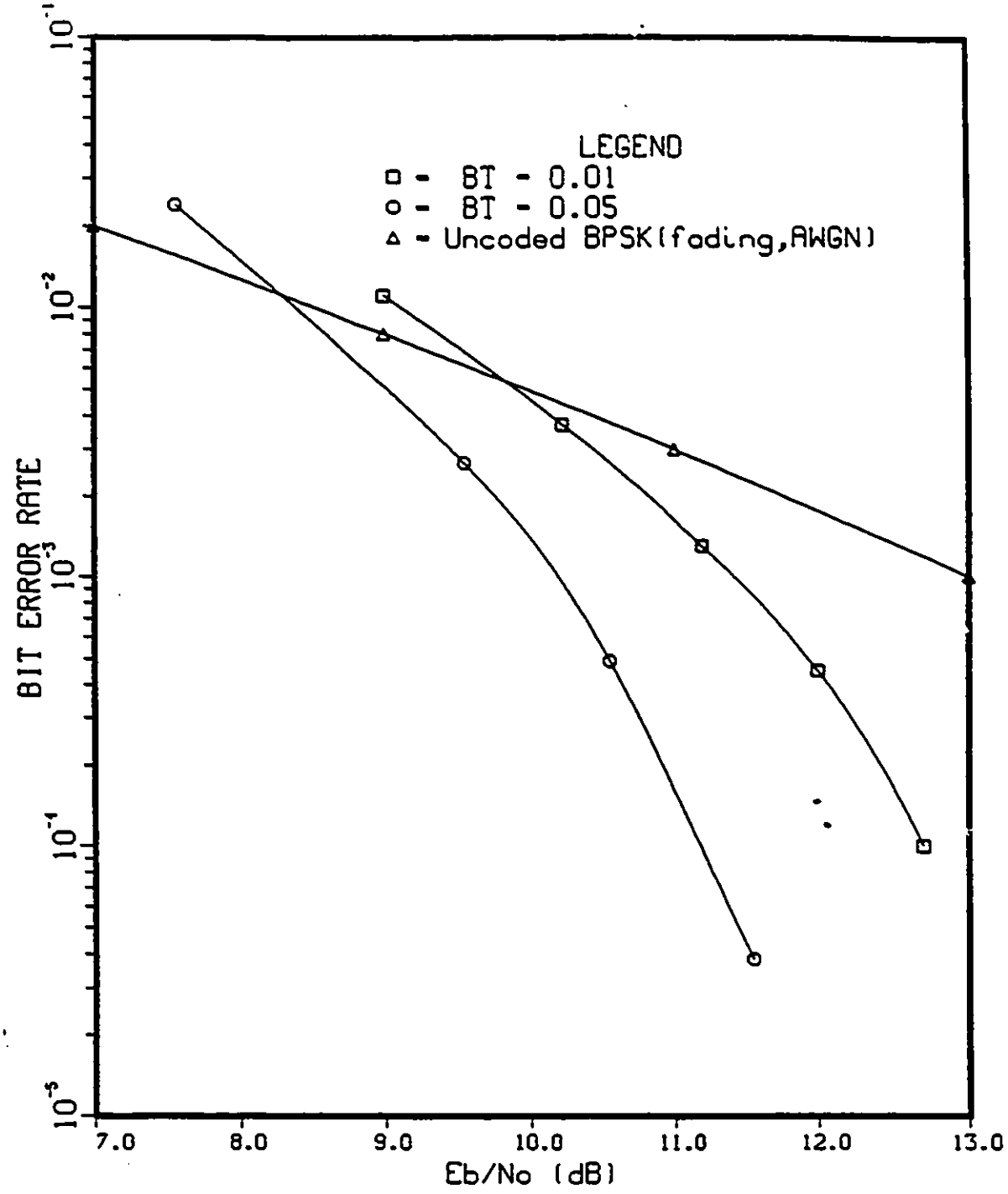

Figure 4.6: Performance of (63.35) RS code with different normalized bandwidth for light shadowing.

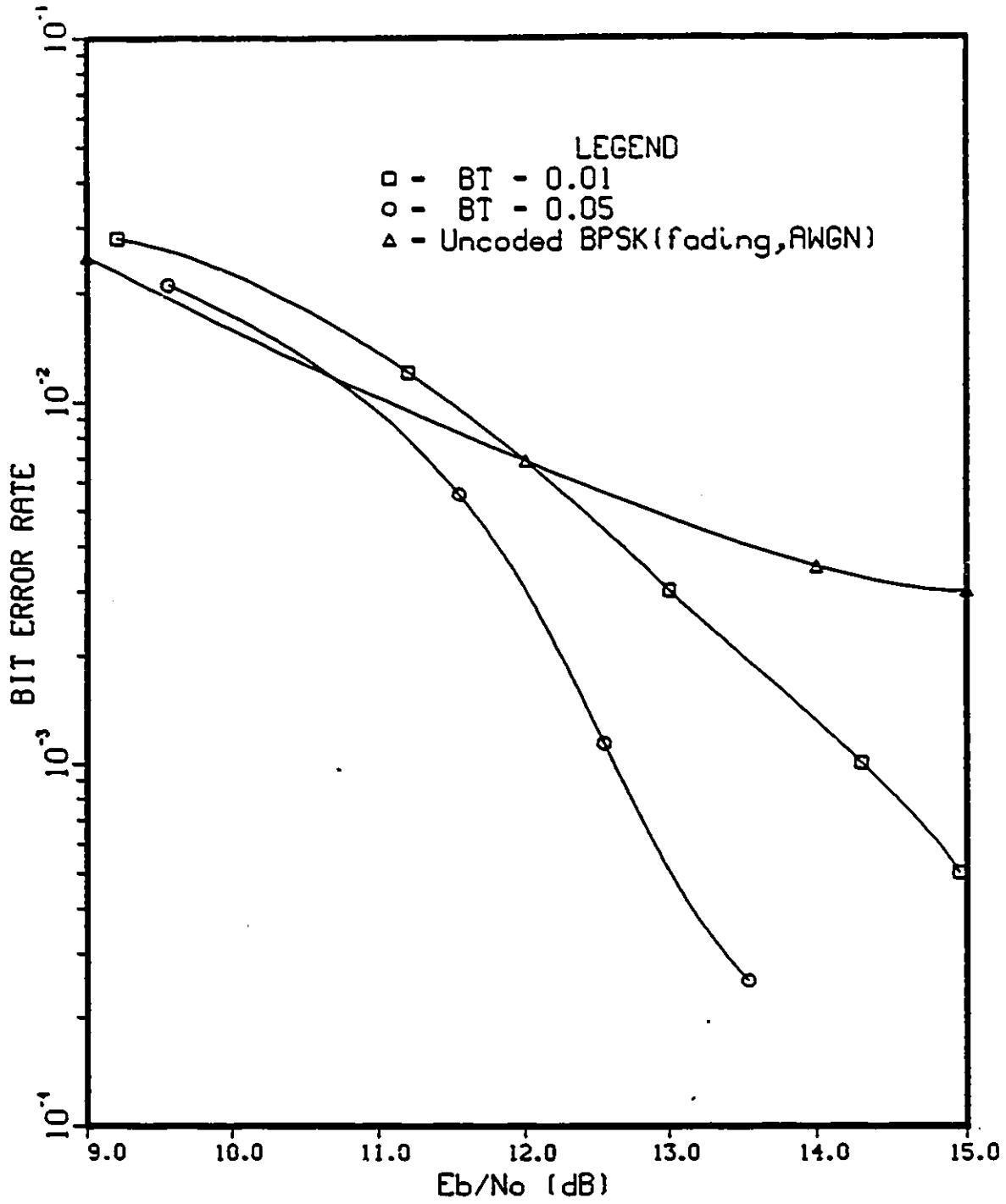

Figure 4.7: Performance of (63.35) RS code with different normalized bandwidth for average shadowing.

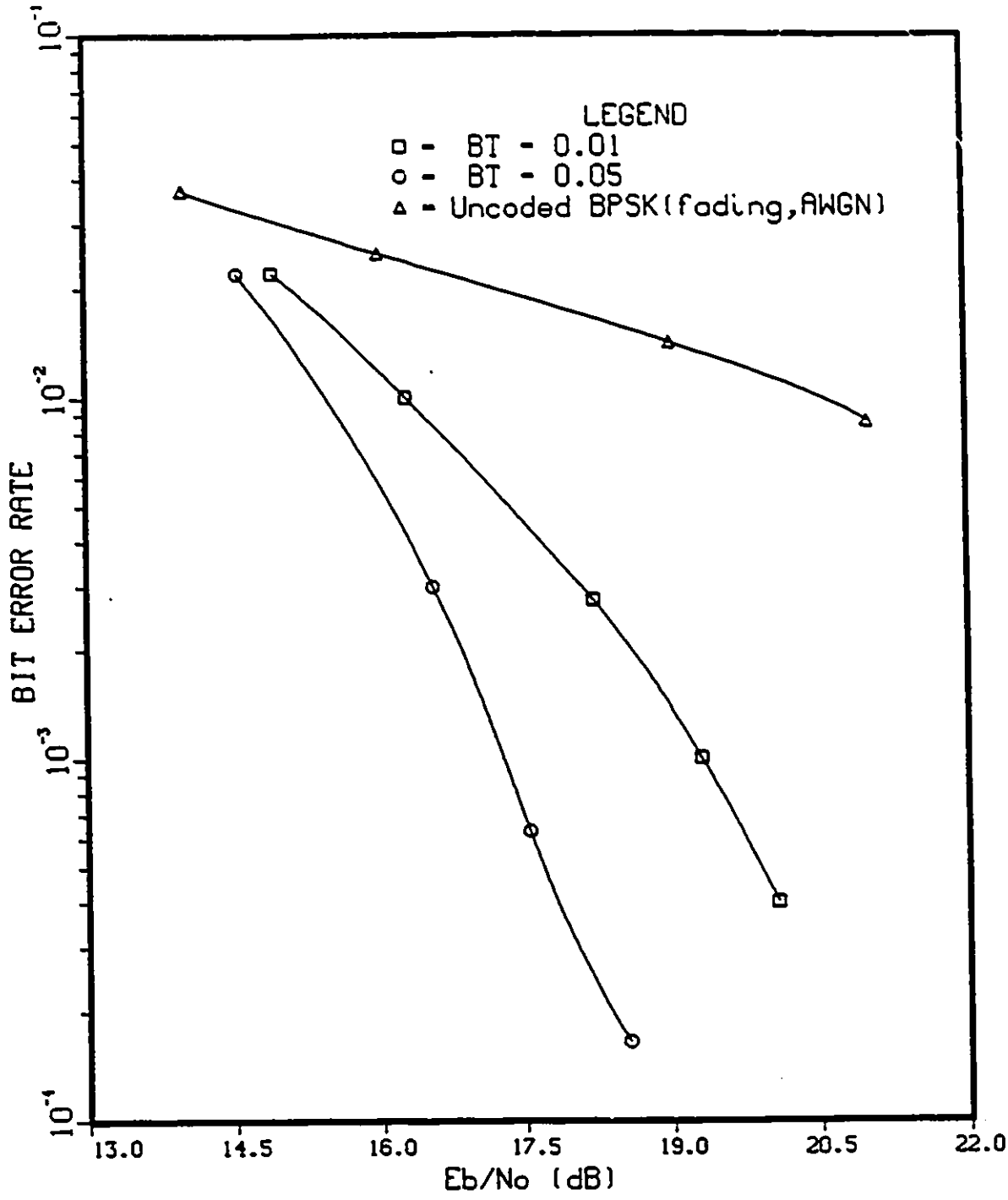

Figure 4.8: Performance of (63,35) RS code with different normalized bandwidth for heavy shadowing.

4.3.3 Influence of Interleaving

As demonstrated in the previous subsection, the performance degrades as the normalized fading bandwidth becomes smaller. One way to combat slow fading is to use interleaving. In this subsection we study the effect of interleaving on the system performance. The case of heavy shadowing is considered since it represents the worst case where there is much room for improvement.

The interleaver divides symbol sequences into blocks corresponding to a two-dimensional array, and to read symbols in by rows and out by columns as illustrated in Figure 4.9. The deinterleaver stores the data in the same rectangular array format, but it is read out row-wise, one code word at a time. As a result of this reordering of the data during transmission, a burst of errors of length $l = D \times b$ is broken up into D bursts of length b. Thus, an (n, k) code that can handle burst errors of length $b \leq (n-k)/2$ can be combined with interleaver of degree D to create an interleaved $(D \times n, D \times k)$ block code that can handle bursts of length $D \times b$.

Table 4.2 shows different RS codes and their error-correcting capabilities.

RS Codes	Code Rate	Erroneous symbols could be corrected	Maximum erroneous bits could be corrected
(15,9)	0.6	3	12
(15,7)	0.46	4	16
(31,25)	0.8	3	15
(31,21)	0.67	5	25
(31,17)	0.55	7	35
(63,41)	0.65	11	66
(63,35)	0.55	14	84
(127,71)	0.55	28	196
(255,153)	0.6	51	408

Table 4.2: Different RS codes and their error-correcting capabilities.

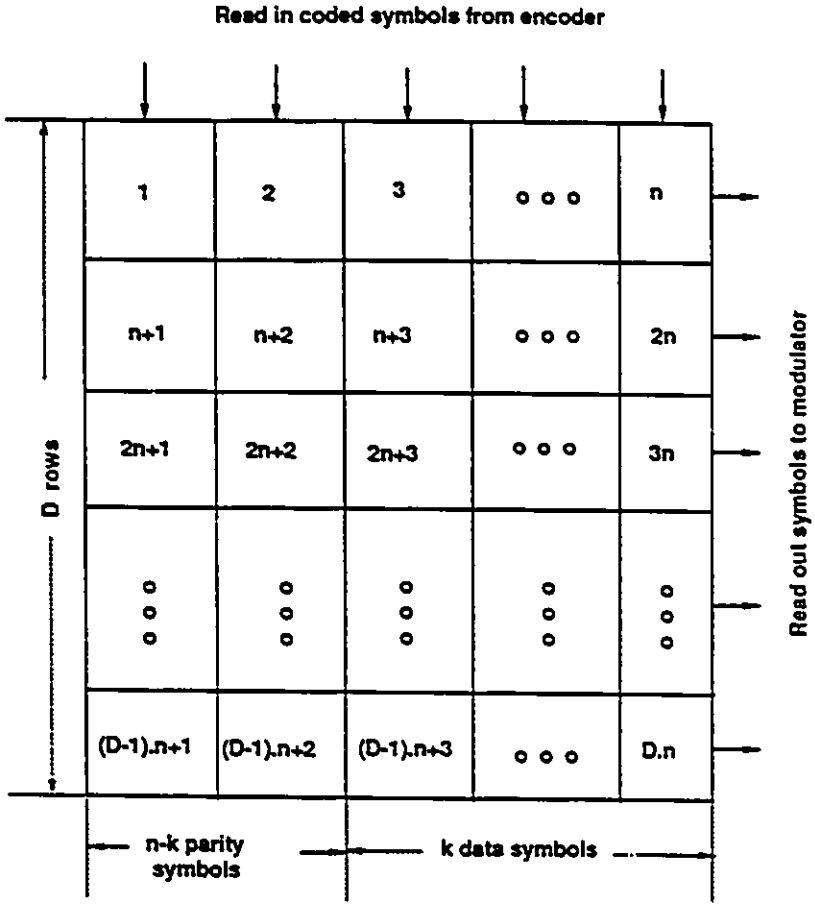

Figure 4.9: A block interleaver for coded data.

In Chapter 2 we have shown that the AFD at a signal level of -10 dB could have a value as high as 83 msec which correspond to 200 erroneous bits at a bit rate of 2400 bps (see Table 2.3, 2.4 and 2.5), therefore from Table 4.2 and Tables 2.3, 2.4 and 2.5 we can deduce that RS codes with blocklengths of 15 are not effective over such fading channels since their error correcting capability is not significant. If this code has to be used, high degree of interleaving should be applied. For example if the (15,9) RS code is used interleaving degree of at least 17 should be used to have an acceptable performance especially in the heavy shadowing case, where the burst length is large. But interleaving with high degree is not preferred since it introduces delay to the system, and the delay is an important factor to be considered where the propagation delay is large and any additional delay may not be tolerable. A longer code could be used to provide a better burst error-correcting capability and to reduce the degree of interleaving necessary.

The (31,17) RS code could be used with interleaving degree greater than 6 since it can correct a burst of length 210 bits or less. The (63,35) RS code could be used with interleaving degree greater than 3 since it corrects a burst of length 252 bits. The (127,71) RS code could be used with an interleaving degree greater than 2 since it can correct a burst of length 392 bits. The (255,153) RS code is a powerful code, it can correct a burst of length 408 bits or less without interleaving.

Finally we can conclude that the longer the code, the better performance we will have and less degree of interleaving is required. But with a long code the decoding delay will be considerable, and more importantly the complexity increases, therefore there is a trade-off between the blocklength and the interleaving degree. The (31,17) RS code with an interleaving degree of 6 or higher could be a good choice.

Figure 4.10 and 4.11 show the effect of interleaving on bit error rate for heavy

shadowing for $BT = 1\%$ and 5% respectively. From these figures we notice that the interleaving technique improve the system performance significantly.

Table 4.3 summarizes the improvement we obtain by using interleaving at a probability of error of 10^{-3} for 1% and 5% normalized fading bandwidths and different degrees of interleaving.

The choice of the degree of interleaving depends on the transmission rate, the speed of the vehicle and the carrier frequency. For a given transmission rate and carrier frequency, the burst is longer for slower speed, therefore the degree of interleaving required is more important at speed of 20 km/h than a speed of 90 km/h. Generally, as the normalized fading bandwidth is directly proportional to the vehicle speed, if a vehicle is travelling through a region of foliage blockage at a slow speed then the burst of errors is expected to last longer than when it is travelling at a lower speed. This explains why the degree of interleaving 6 provide better performance for a normalized fading bandwidth of 5% than 1%. These results show also for a degree of interleaving greater than 10 the improvement on error performance is more important for the 1% case rather than the 5% case since the channel is more bursty.

$BT = 1\%$		$BT = 5\%$	
D	Improvement (dB)	D	Improvement (dB)
6	1.7	4	1.7
10	2.9	6	2.45
16	3.56	10	2.83

Table 4.3: Improvement due to different degree of interleaving at BER of 10^{-3} for a (31,17) RS code with BPSK over heavy shadowing channel and different normalized fading bandwidth, BT.

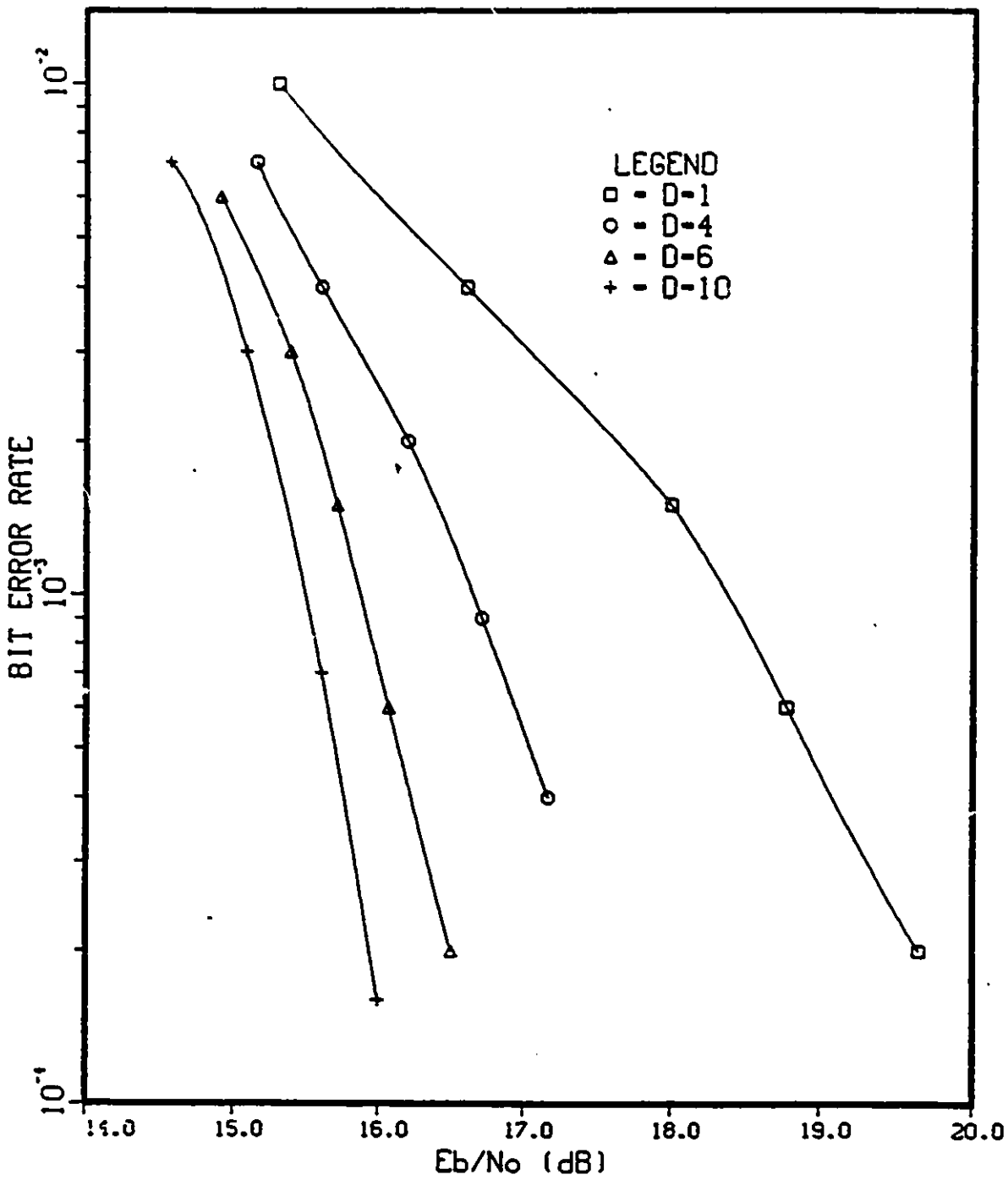

Figure 4.10: Performance of a (31,17) RS code with different degrees of interleaving for heavy shadowing and normalized fading bandwidth of 1%.

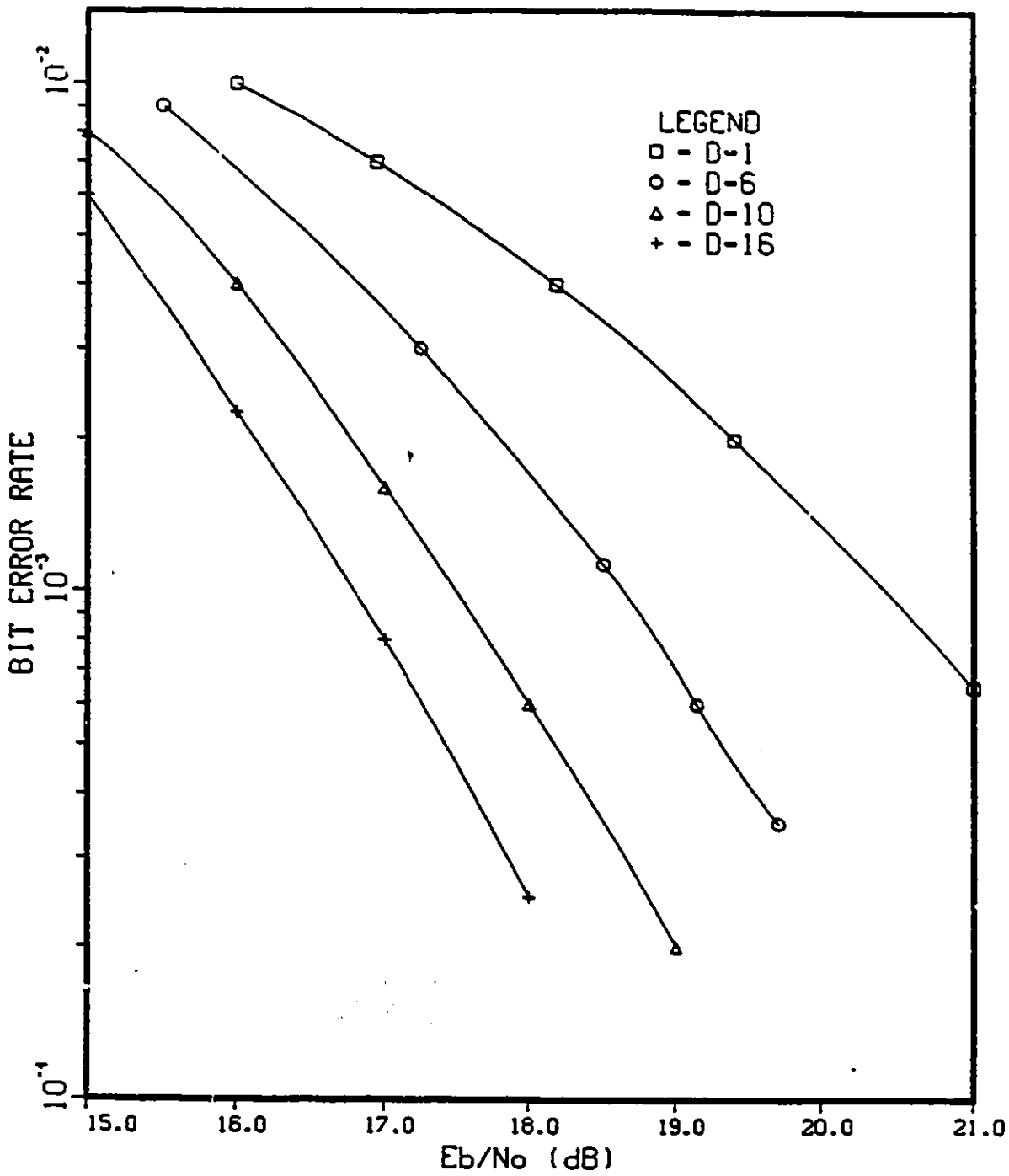

Figure 4.11: Performance of a (31,17) RS code with different degrees of interleaving for heavy shadowing and normalized fading bandwidth of 5%.

4.3.4 Performance with Erasure-Decoding

In this subsection we intend to investigate the effectiveness of erasure-decoding in a lognormal shadowed Rician channel. The erasure information is passed to the decoder. This information enables the decoder to distinguish between reliable and unreliable symbols.

The maximum-distance property of RS codes allows the correction of up to t errors and e erasures [37], as long as the relation

$$e + 2t \leq d - 1 \tag{4.1}$$

holds. In (4.1) d represents the minimum distance of the code. For maximum distance codes, d is determined by the number of parity symbols in a code word

$$d - 1 = n - k \tag{4.2}$$

Figure 4.12 shows the bit error rate of (15,9) RS code for the heavy shadowing with and without error erasure-decoding. From this figure we see that the erasure decoding is effective for the heavy shadowing, and provides an additional coding gain of 1.9 dB at probability of error of 10^{-3}.

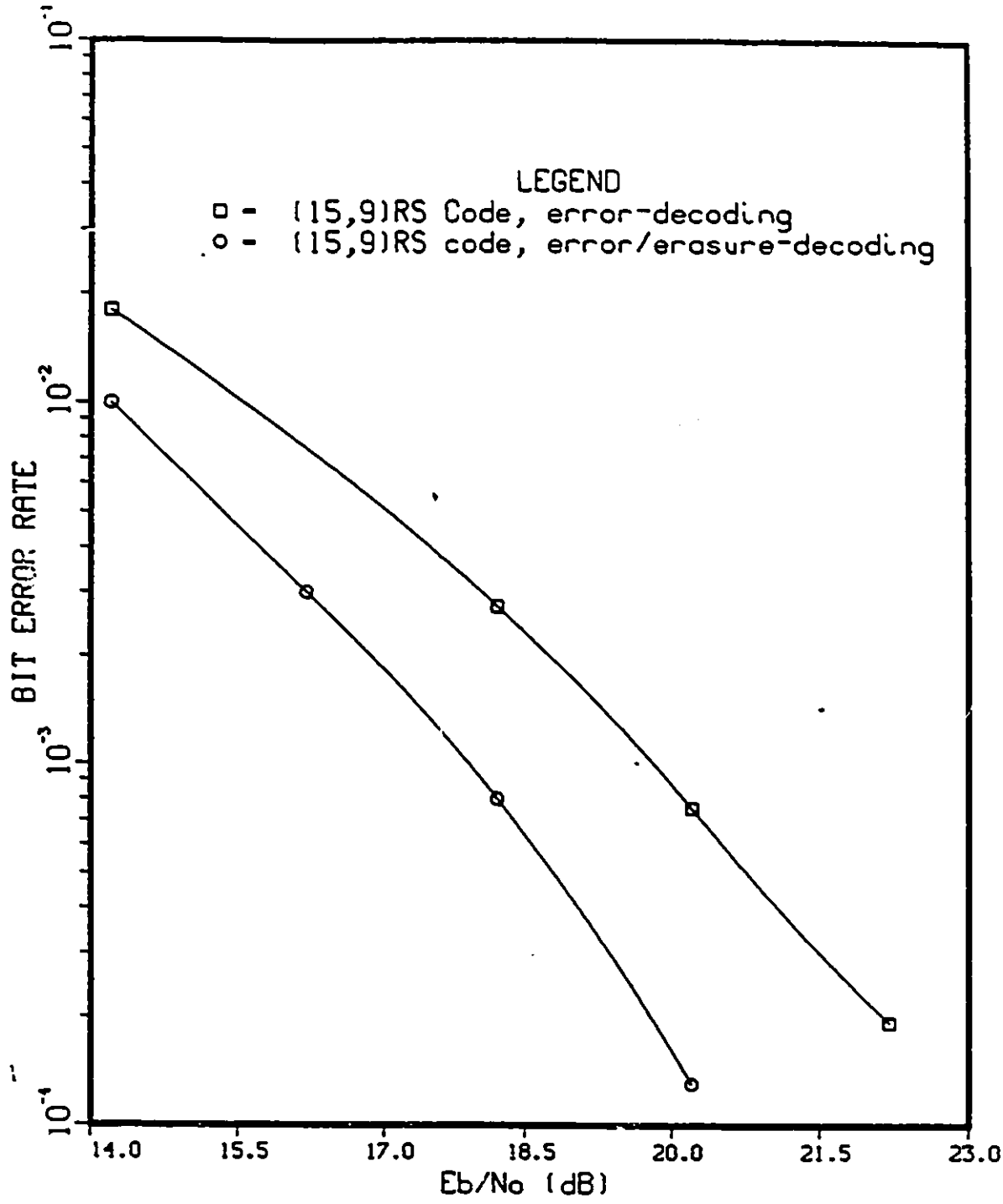

Figure 4.12: Performance of (15,9) RS code with error/erasure-decoding for heavy shadowing and a normalized fading bandwidth of 5%.

4.4 Conclusions

From the results presented in this section, the following conclusions can be drawn.

- The bit error rate performance curves for RS codes in an AWGN channel show that the coding gain increases with the blocklengths and the increase of this coding gain becomes less at large blocklengths, therefore RS codes with blocklengths exceeding 63 symbols do not justify the associated complexity.

- The bit error rate performance curves for RS codes in a lognormal shadowed Rician channel show that :

  1) Coding gain in fading and shadowing channel increases when longer codes are used.

  2) The coding gain increases as shadowing becomes more pronounced. At BER of 10^{-3}, the (63,35) RS code provide a coding gain of 3 dB for light shadowing and 10.9 dB for the heavy shadowing case.

- The bit error rate performance of RS codes over fading and shadowing channel degrades when the fading bandwidth becomes smaller. This decrease could be explained by the fact that as bandwidth decreases, channel memory increases and the channel becomes more like a bursty error channel. In this case long RS codes or interleaving should be applied to combat slow fading.

- The degree of interleaving required increases when the fading bandwidth becomes smaller. At $BT = 1\%$ an interleaver of degree six provide almost the same improvement as an interleaver of degree four for $BT = 5\%$. However for a high degree of interleaving, the improvement on error performance is more important for small fading bandwidth.

- Erasure decoding improves the system performance significantly. An additional coding gain of 1.9 dB is achieved at BER of $10^{-3}$for heavy shadowing channel.

A summary of our results is given in Table 4.4 and 4.5.

RS Codes	Channel Model	Normalized Fading Bandwidth	Fade Margin (dB)	Coding Gain (dB)
Uncoded BPSK	Light shadowing	NA	6.5	NA
(15,9)	Light shadowing	5%	4.9	1.6
(31,17)	Light shadowing	5%	4	2.5
(63,35)	Light shadowing	5%	3.5	3
(63,35)	Light shadowing	1%	4.9	1.6
Uncoded BPSK	Average shadowing	NA	9.8	NA
(15,9)	Average shadowing	5%	7.2	2.6
(31,17)	Average shadowing	5%	6	3.8
(63,35)	Average shadowing	5%	5.2	4.6
(63,35)	Average shadowing	1%	6.85	2.95
Uncoded BPSK	Heavy shadowing	NA	21	NA
(15,9)	Heavy shadowing	5%	12.6	8.4
(31,17)	Heavy shadowing	5%	11.3	9.7
(63,35)	Heavy shadowing	5%	10.1	10.9
(63,35)	Heavy shadowing	1%	12.1	8.9

Table 4.4: Fade margin and coding gain at BER of 10^{-3} for different RS codes.

RS Codes	Interleaving degree D	Normalized Fading Bandwidth	Fade Margin (dB)	Coding Gain (dB)
Uncoded BPSK	NA	NA	21	NA
(31,17)	4	5%	9.6	11.4
(31,17)	6	5%	8.85	12.15
(31,17)	6	1%	9.6	11.4
(31,17)	10	5%	8.47	12.53
(31,17)	10	1%	8.4	12.6
(31,17)	16	1%	7.74	13.26

Table 4.5: Fade margin and coding gain at BER of 10^{-3} for heavy shadowing and different degrees of interleaving.

Chapter 5

Fading Prediction in Conjunction with RS Codes over LMSAT Channel.

5.1 Introduction

In Chapter 3 we saw that the performance of PSK systems in LMSAT channels is very poor. As discussed in Chapter 4, FEC coding can provide large improvements. However there is still a 5 to 20 dB discrepancy between the performance in an AWGN channel and a Rician or lognormally shadowed Rician channel. Therefore to obtain further improvements various techniques can be employed. In this chapter we study the application of prediction techniques to achieve additional improvements.

First the principle of linear prediction is presented, then the decision law for the new receiver which uses linear prediction to estimate the fading from the received signal is derived. Using this decision law the performance of an uncoded system using linear prediction was simulated for LMSAT channel. Since our objective in this chapter is to prove the effectiveness of the proposed fading prediction technique therefore it is computationally more convenient to assume a Rician channel rather than a lognormally shadowed Rician channel. Results were obtained for predictors

optimized at various SNRs. The effect of error propagation were also observed in each simulation by producing a BER curve with and without error propagation. Error propagation was eliminated by passing the correct transmitted symbols from the modulator to the demodulator.

Finally a proposed technique which employ fading prediction in conjunction with RS coding to reduce the BER performance degradation due to error propagation was investigated.

In Chapter 4 the performance of RS codes was determined for only the amplitude of fading, whereas in this chapter the performance of the proposed fading prediction technique is found for the combined effect of amplitude and phase variation caused by fading. With practical predictor lengths, simulated performance results show a lower error floor for a receiver which utilizes fading prediction than the conventional one.

5.2 Linear Predictor Design Equations

Given the past samples of some observed signal $\{y_{i-1}, y_{i-2}, ..., y_{i-L}\}$, where $y_i = x_i + n_i$, a linear predictor estimates the value of the present sample x_i.

A predictor of order L is given by :

$$\hat{x}_i = \sum_{k=1}^{L} p_k \, y_{i-k} \tag{5.1}$$

where p_k represent the prediction coefficients. The orthogonality principle for MMSE states that [19]

$$E\{(x_i - \hat{x}_i)\, y_j^*\} = 0 \quad , \; i - L \leq j \leq i - 1 \tag{5.2}$$

This implies that

$$E\{x_i \, y_j^*\} = E\{\hat{x}_i \, y_j^*\}, \tag{5.3}$$

and assuming $E\{x_i\, n_j\} = 0$, we have

$$E\{x_i\, y_j^*\} = E\{x_i x_j^*\} = R^x_{j-i} \tag{5.4}$$

and

$$\begin{aligned} E\{\hat{x}_i\, y_j^*\} &= \sum_{k=1}^{L} E\{y_{i-k}\, y_j^*\}\, p_k \\ &= \sum_{k=1}^{L} (R^x_{j-i+k} + R^n_{j-i+k})\, p_k \end{aligned} \tag{5.5}$$

where $R^x_{j-i+k} = E\{x_{i-k} x_j^*\}$ and $R^n_{j-i+k} = E\{n_{i-k} n_j^*\}$. Substituting (5.5) and (5.4) into (5.3), produces the set of L linear equations,

$$R^x_{j-i} = \sum_{k=1}^{L} (R^x_{j-i+k} + R^n_{j-i+k})\, p_k \tag{5.6}$$

If all processes are wide sense stationary (WSS), then the MMSE predictor at a given time, i, is the MMSE predictor for all i. Hence i may be removed from the above equations to get

$$R^x_j = \sum_{k=1}^{L} (R^x_{k-j} + R^n_{k-j})\, p_k \quad , \; 1 \le j \le L \tag{5.7}$$

5.3 Autocorrelation of the Fading Process

As discussed in Chapter 2 the fading component can be modeled as a complex summation of two independent gaussian noise processes $f^I(t)$ and $f^Q(t)$, i.e.,

$$f(t) = f^I(t) + j f^Q(t) \tag{5.8}$$

$f^I(t)$ and $f^Q(t)$ result after passing the two white Gaussian noise process $n_f^I(t)$ and $n_f^Q(t)$ respectively through two identical low-pass filter $H(f)$. By varying the mean of $f^I(t)$, one may choose between Rayleigh and Rician fading characteristics. Since

identical filters $H(f)$ are used to filter the noise processes, then $f^I(t)$ and $f^Q(t)$ have the same autocorrelation function. Furthermore, the symmetry of $H(f)$ guarantees that the in-phase and quadrature fading process are independent and we have

$$R^f(\tau) = E\{f^I(t)\ f^I(t-\tau)\} = E\{f^Q(t)\ f^Q(t-\tau)\} \tag{5.9}$$

and

$$R^f(\tau) = \int_{-\infty}^{\infty} |H(f)|^2\ e^{j2\pi f\tau}\ df \tag{5.10}$$

since $H(f)$ is a symmetric transfer function, $R^f(\tau)$ becomes

$$R^f(\tau) = 2\ \int_0^{\infty} |H(f)|^2\ \cos(2\pi f\tau)\ df \tag{5.11}$$

for $\tau = kT$, the discrete fading autocorrelation function is given by

$$R_k^f = 2\ \int_0^{\infty} |H(f)|^2\ \cos(2\pi fkT)\ df \tag{5.12}$$

5.4 Calculation of the Fading Prediction Coefficients

There are two different methods which can be used for the computation of the prediction coefficients.

The first method is a direct calculation of these coefficients through a matrix inversion [19].

The second one is based on a recursive approach in which the prediction coefficients of a particular order are calculated from the prediction coefficients of the previous order. This method is known in the literature as Levinson algorithm [19].

In order to compute the prediction coefficients, it is computationally convenient to assume a rectangular fading channel. In this case, the transfer function of the

fading filter $H(f)$ is given by:

$$|H(f)|^2 = \begin{cases} \frac{1}{2B} & \text{for } |f| \leq B \\ 0 & \text{otherwise.} \end{cases} \tag{5.13}$$

Then the autocorrelation function is given by:

$$R_k^f = \frac{\sin(2\pi kBT)}{2\pi kBT} \tag{5.14}$$

It is clear from (5.14) that $R_k^f = R_{-k}^f$. In order to calculate the L-th order prediction coefficients, the following set of equations have to be considered

$$R_k^f = \sum_{i=1}^{L} (R_{i-k}^f + R_{i-k}^n)\, p_i \ , \ 1 \leq k \leq L \tag{5.15}$$

In a more compact form these equations are described by the following matrix equation :

$$\bar{R}_k^f \, \bar{P}_k = \bar{R}_k^f \tag{5.16}$$

with $\tilde{R}_k^f$ a $[k \times k]$ matrix, $\bar{P}_k$ a $[k \times 1]$ matrix and $\bar{R}_k^f$ a $[k \times 1]$ matrix which are given by

$$\tilde{R}_k^f = \begin{pmatrix} R_0^f + R_0^n & R_1^f & \cdots & R_{L-1}^f \\ R_{-1}^f & R_0^f + R_0^n & \cdots & R_{L-2}^f \\ \cdot & \cdot & & \cdot \\ \cdot & \cdot & & \cdot \\ \cdot & \cdot & & \cdot \\ R_{-L+1}^f & R_{-L+2}^f & \cdots & R_0^f + R_0^n \end{pmatrix} \tag{5.17}$$

$$\bar{P}_k = \begin{bmatrix} p_1 \\ p_2 \\ \cdot \\ \cdot \\ \cdot \\ p_L \end{bmatrix} \tag{5.18}$$

and

$$\bar{R}_k^f = \begin{bmatrix} R_1^f \\ R_2^f \\ \cdot \\ \cdot \\ \cdot \\ R_L^f \end{bmatrix} \tag{5.19}$$

The prediction coefficients then can be found by first inverting the matrix $\tilde{R}_k^f$ and then solving the following matrix equation

$$\bar{P}_k = (\tilde{R}_k^f)^{-1} \bar{R}_k^f \tag{5.20}$$

In our simulation, it is assumed that $BT = 0.1$, thus by using (5.14) the following values of the autocorrelation terms can be calculated as

$$R_0^f = 1 \qquad R_1^f = 0.9355 \quad R_2^f = 0.7568$$

$$R_3^f = 0.5045 \quad R_4^f = 0.2338 \quad R_5^f = 0$$

The value of R_0^n was taken as $N_0/2$, where N_0 is the one-sided power specral density of the white Gaussian noise. Finally by substituting the above values into (5.20) and for a fi ed SNR the prediction coefficients could be deduced. In Table 5.1, different prediction coefficients for different SNR were given for a third order prediction.

	$SNR \ll 1$	SNR=30dB	SNR=20dB	SNR=15dB	SNR=10dB
p_1	2.7402	2.4589	1.6378	1.297	1.062
p_2	-2.7122	-2.1882	-0.6797	-0.1114	0.138
p_3	0.968	0.6903	-0.0987	-0.367	-0.408

Table 5.1: Prediction coefficients for different SNR, $L = 3$ and $BT = 0.1$.

5.5 Decision Law

The BPSK signal over a Rician channel could be written as :

$$y_k = (1 + f_k)\, a_k + n_k \tag{5.21}$$

where f_k represents the fading process, n_k is the white Gaussian noise and a_k is either +1 or -1 depending upon the information bit.

Equation (5.21) could be rewritten as :

$$s_k = \frac{y_k}{a_k} - 1 = f_k + \frac{n_k}{a_k} \tag{5.22}$$

where s_k represents the fading and noise sample to be predicted.

The derivation of the decision rule is based on a well-known probabilistic theorem. The probability density function (pdf) of s_k given $s_{k-1}, s_{k-2}, ..., s_0$ has the following form:

$$P(s_k|s_{k-1}, s_{k-2}, ..., s_0) = \frac{1}{\sqrt{2\pi\epsilon^2}} \exp[\frac{-(s_k - \hat{s}_k)^2}{2\epsilon^2}] \tag{5.23}$$

where ϵ^2 is the minimum mean square prediction error and $\hat{s}_k$ represents the prediction of s_k based on $s_{k-1}, s_{k-2}, ..., s_{k-L}$ and can be expressed as

$$\hat{s}_k = \sum_{j=1}^{L} p_j\, s_{k-j} \tag{5.24}$$

Let us denote the estimated information bit at the output of the receiver by $\hat{a}_k$. Our aim is to estimate the symbol a_k, based on the sample y_k, the fading and noise estimates, $\hat{s}_{k-1}, \hat{s}_{k-2}, ..., \hat{s}_{k-L}$. By using the maximum likelihood ratio test (MLRT) the decision law can be formulated as

$$\frac{P(y_k|s_{k-1}, s_{k-2}, ..., s_0, a_k = 1)}{P(y_k|s_{k-1}, s_{k-2}, ..., s_0, a_k = -1)} \underset{\hat{a}_k=-1}{\overset{\hat{a}_k=1}{\gtrless}} 1 \tag{5.25}$$

Using (5.23), (5.24) and (5.25) the decision law can be reduced to

$$y_k(1 + \hat{s}_k) \underset{\hat{a}_k=-1}{\overset{\hat{a}_k=1}{\gtrless}} 0 \tag{5.26}$$

5.6 Performance Evaluation Results

The performance of a receiver which uses fading prediction with BPSK signal has been simulated for Rician channel. The results were obtained for predictors optimized at each SNR. The effect of error propagation were also observed by producing the BER curves with and without error propagation.

5.6.1 Uncoded System Performance with Linear Prediction

Figure 5.1 shows the performance of BPSK with linear prediction for Rician channel with $K = 5$ dB. In this case the predictor is optimized at each SNR (i.e., different prediction coefficients were used at each point on the BER curve) and a predictor length of 3 was considered. This graph show that as the SNR increases the BER of BPSK with fading prediction continues to decrease while the conventional BPSK (without prediction) approaches to its irreducible error rate. Another observation from Figure 5.1 is that the error propagation is a major problem of this technique.

Figure 5.2 shows the performance of BPSK with linear prediction for Rician channel with $K = 5$ dB using a predictor optimized at a SNR of 10 dB. This figure shows that a higher irreducible error rate was achieved than the previous case where the predictor was optimized at each SNR. The effects of error propagation was also significant in this case.

Figure 5.3 shows the performance of BPSK with linear prediction (without error propagation) for Rician channel with different K-factors, using a predictor optimized at each SNR. This figure shows that with increasing channel misbehavior the improvement provided by the fading prediction increases. This means that the fading prediction technique is especially powerful when the channel exhibits deep fading.

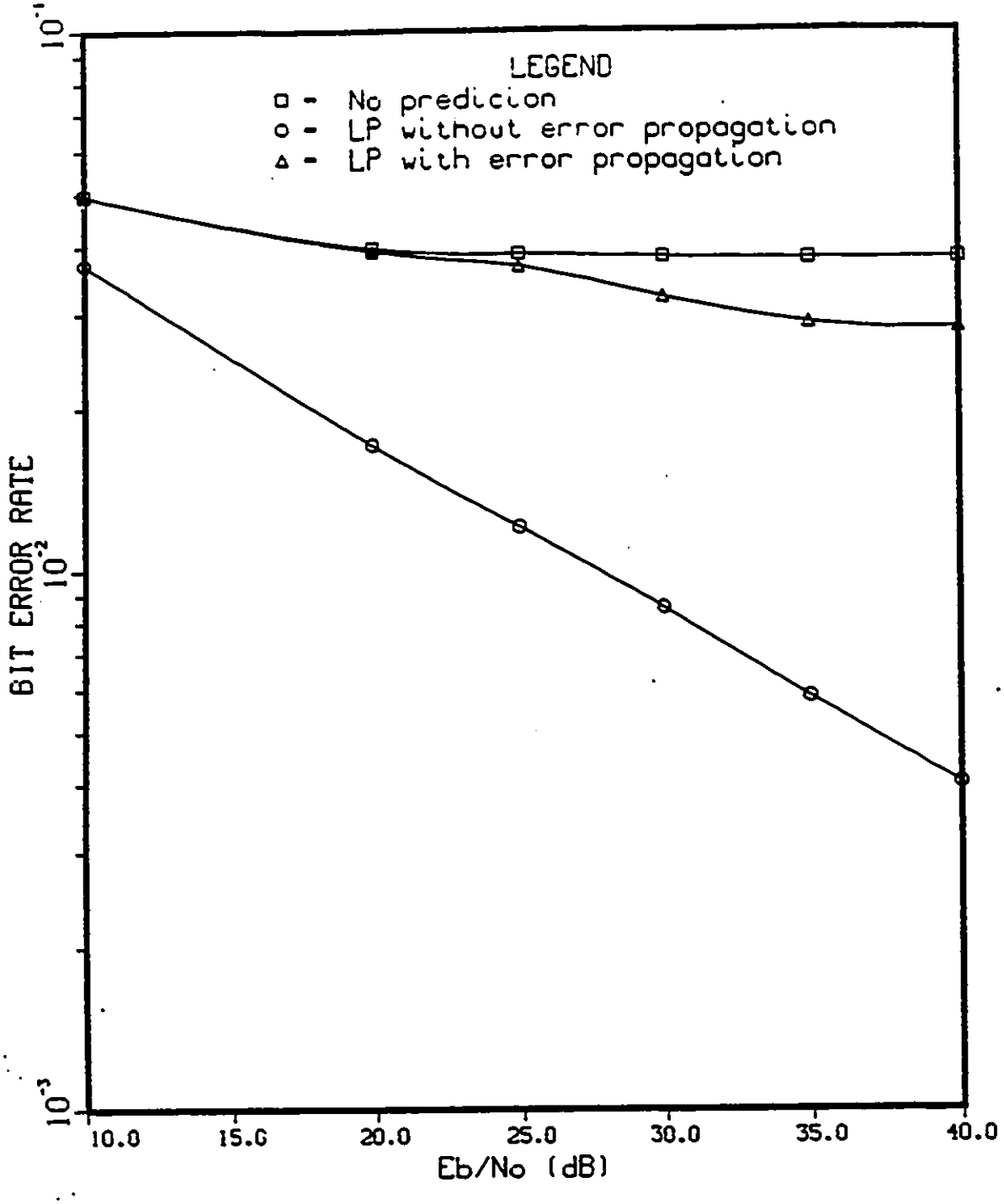

Figure 5.1: BER performance of BPSK with linear prediction over Rician channel with K =5 dB and a predictor optimized at each SNR.

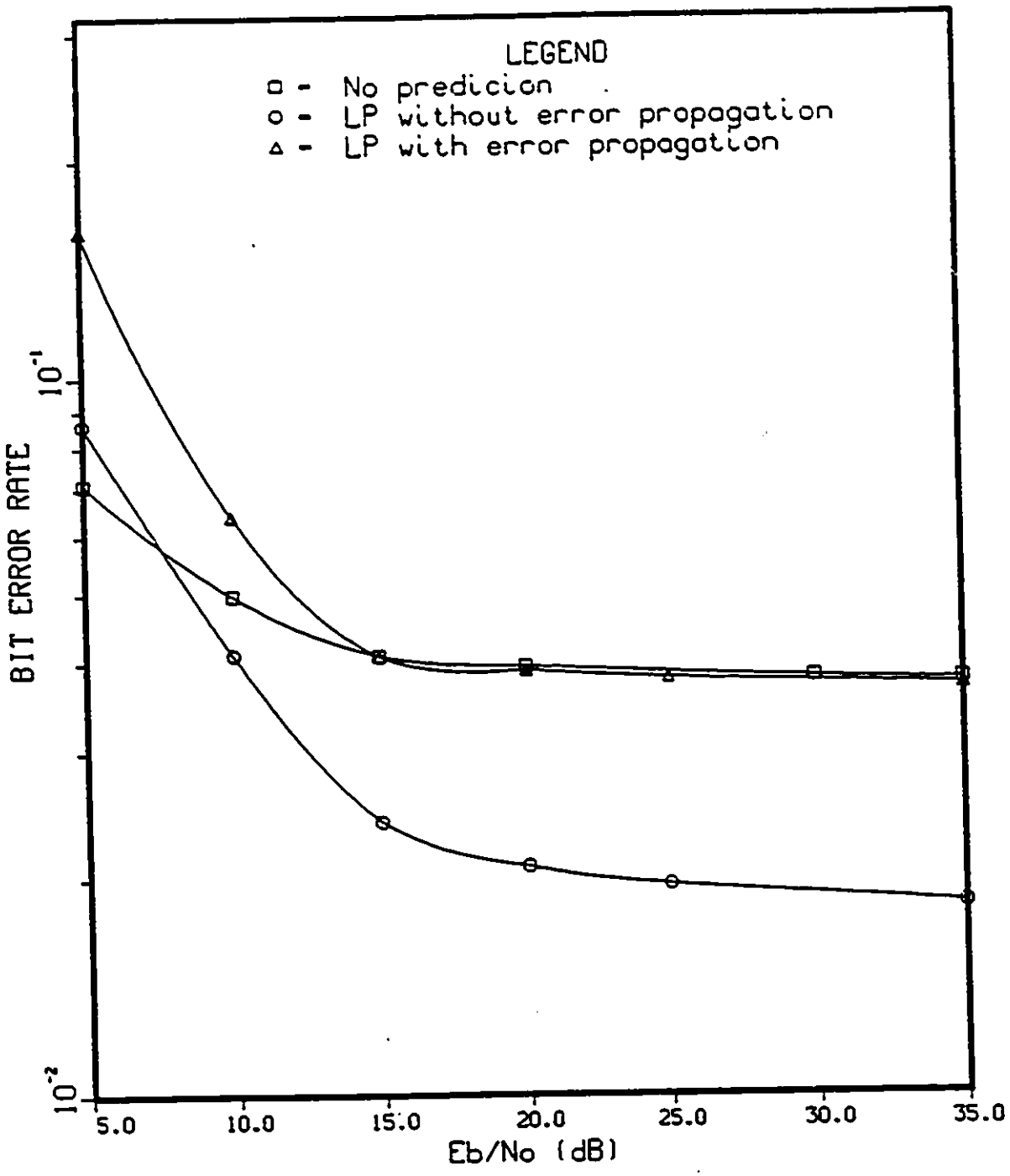

Figure 5.2: BER performance of BPSK with linear prediction over Rician channel with K =5 dB and a predictor optimized at a SNR of 10 dB.

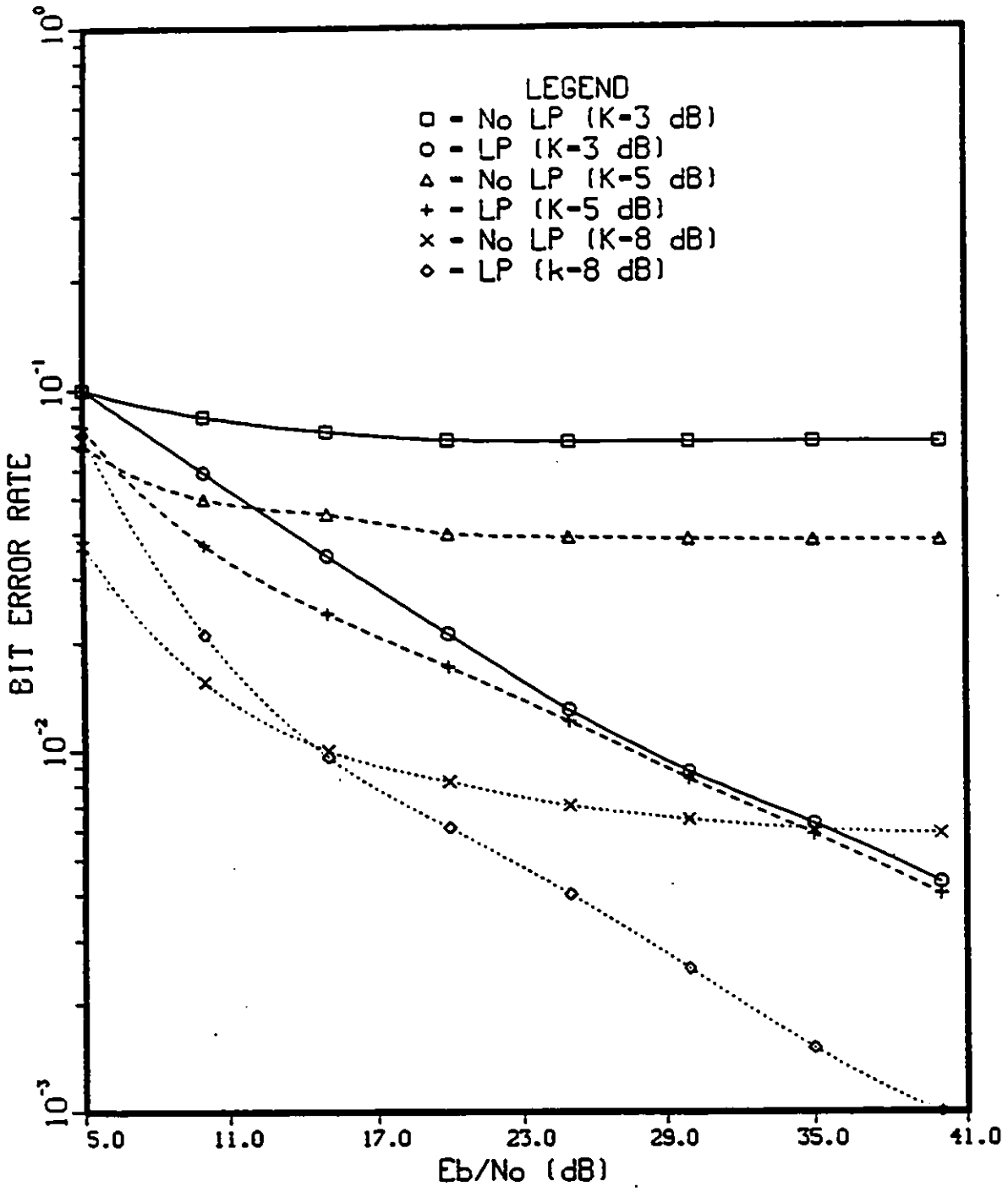

Figure 5.3: BER performance of BPSK with linear prediction over Rician channel with differenr K−factor and a predictor optimized at each SNR.

5.6.2 Coded System Performance with Linear Prediction

Results of the previous simulation show that error propagation is a significant problem of the proposed fading prediction technique over Rician channel. One way to overcome this problem is to use this prediction technique in conjunction with an coding/interleaving scheme.

Our objective in this simulation is to show that coding/interleaving is an effective method to solve the problem of the BER performance degradation due to error propagation. For this reason a simple (15,9) RS code was chosen and an interleaving degree of 16 was taken.

The RS encoder transform each symbol information sequence into a n-symbol encoded sequence. Let's assume that the RS encoder outputs the following codeword:

$$\bar{A}\,\bar{B}\,\bar{C}\,\bar{D}\,\bar{E}\,...\,\bar{P}$$

where $\bar{A}$ represents the first codeword, $\bar{B}$, the second codeword and so on. Prior to transmission the codewords are written into a $D \times n$ matrix column by column, one codeword in each of the D columns. The symbols are transmitted over the channel row by row. The matrix for (15,9) RS code and $D = 16$ could be formulated as :

$$\begin{pmatrix} A_1 & B_1 & . & . & . & P_1 \\ A_2 & B_2 & . & . & . & P_2 \\ . & . & & & & . \\ . & . & & & & . \\ . & . & & & & . \\ A_{60} & B_{60} & . & . & . & P_{60} \end{pmatrix} \tag{5.27}$$

where $A_1, A_2, ..., A_{60}$ represent the code bits of the codeword $\bar{A}$. It is assumed that $\bar{A}$ is a known codeword (i.e., preamble).

First to decode $\bar{B}$ the following steps are necessary:

1) $\bar{A}$ is used to predict fading estimates $s_1, s_2, ..., s_{60}$ corresponding to the code bits

$A_1, A_2, ..., A_{60}$

2) Using the knowledge of $s_1, s_2, ... s_{60}$ we decide on $B_1, B_2, ..., B_{60}$

3) $B_1, B_2, ..., B_{60}$ are fed into a RS decoder to produce the estimate codeword $\bar{B}'$.

As a second step $\bar{A}$ and $\bar{B}'$ are used to predict and decode the codeword $\bar{C}$. Two values of past fading plus noise estimates are available. If a second order prediction is considered, only $\bar{B}'$ and $\bar{C}'$ are used to predict and decode the codeword $\bar{D}$ and $\bar{C}'$ and $\bar{D}'$ are used to predict and decode the codeword $\bar{E}$ and so on. However with a third order prediction, $\bar{A}$, $\bar{B}'$ and $\bar{C}'$ are used to predict and decode the codeword $\bar{D}$ and $\bar{B}'$, $\bar{C}'$ and $\bar{D}'$ are used to predict and decode the codeword $\bar{E}$, etc.

The BER performance of a (15,9) RS code with BPSK signal transmission employing the proposed fading prediction is illustrated in Figure 5.4. This figure correspond to a Rician channel ($K = 5$ dB) with a third order prediction, and a predictor optimized at a SNR of 10 dB.

As it can be seen from this figure, there is a significant improvement in performance which results in high error floor reductions. Furthermore we note that the effects of error propagation were small in this simulation and as the SNR increases the performance of this technique with and without error propagation tend to be similar, which prove that the proposed fading prediction technique used in conjunction with RS code is an effective technique and prove the BER performance considerably.

5.7 Conclusions

A novel receiver structure, which dramatically reduces the level of error floors and improves the performance of land mobile satellite communication systems has been introduced and analyzed. The essence of the proposed detection technique is based on predicting the fading process and designing the receiver accordingly. BER

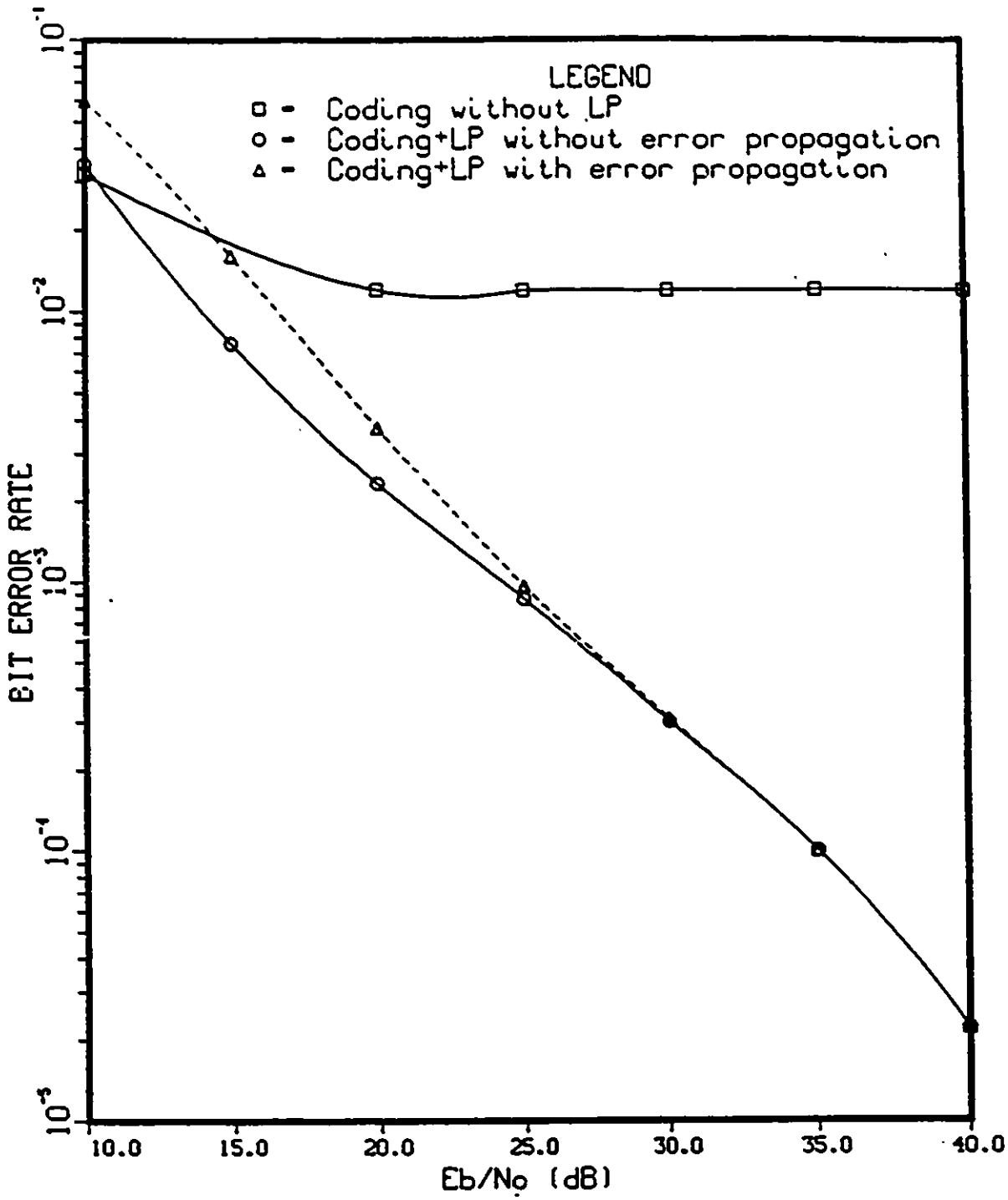

Figure 5.4: BER performance of linear prediction in conjunction with (15,9)RS code over Rician channel with K =5 dB.

performance evaluation results have indicated that :

- By employing a fading prediction in an uncoded system, an important improvement on the BER performance were obtained. But in this case we found that the effect of the error propagation was significant.

- The fading prediction technique is especially powerful when the channel exhibits deep fading.

- To overcome the problem of the degradation of the BER performance due to error propagation, a proposed technique which employs a fading prediction in conjunction with RS codes was investigated. Results show that the proposed technique greatly reduces the performance degradation caused by the fading channel. For example, for the 3rd order predictor and at $\frac{E_b}{N_o} = 30$ dB a BER improvement of about two orders the magnitude was obtained. Furthermore with this technique the effects of error propagation was almost negligible which improve the effectiveness of this technique over such fading channels.

Chapter 6

Conclusions and Recommendations

6.1 Conclusions

In this thesis we have applied forward error correction coding (FEC) to compensate for the degradation caused by fading and shadowing.

1) The initial stages of the work was to characterize the land mobile satellite channel, and develop a simulation model which could be useful in estimating the performance of communications systems with various modulation and coding schemes.

A computer-based module has been developed using BOSS to generate the fading and shadowing process. The cumulative density function of the amplitude and phase of the received signal envelope has been deduced and it is found that our results conform with Loo's results.

2) The bit error rate (BER) performance curves for binary phase shift keying and the second order statistics described in Chapter 2 and 3 show that some kind of multipath compensation technique is required to improve the error performance. In this thesis we have applied FEC to compensate the effect of fading. RS codes as non binary block codes with multiple burst-error correcting capability have been studied

and a characterization of these codes for a class of land mobile satellite communication channels has been given. Simulation results indicate the following:

- Shadowing has a significant effect in the system performance. The BER performance of BPSK over the lognormal shadowed Rician channel indicates that, at $P_e = 10^{-3}$ the fade margin goes from 6.5 dB to 21 dB for light and heavy shadowing, which indicates a significant degradation on the error performance when the channel exhibits heavy shadowing. Therefore, in the design of modulation, coding and access methods especially for small terminal, shadowing effects should be taken into consideration.

- The coding gain increases with the blocklengths and the increase of this coding gain becomes less at large blocklengths.

- The coding gain is larger in the case of fading and shadowing than occurs for the AWGN channel.

- As the shadowing becomes more pronounced the coding gain increases.

- The coding gain increases with an increase in the fading bandwidth, this increase could be explained by the fact that as bandwidth decreases, channel memory increases and the channel has a bursty error nature. We found approximately a 2 dB difference on the performance between $BT = 1\%$ and $BT = 5\%$ at BER $= 10^{-3}$

- The second order statistics of the received signal envelope show that the length of the burst of errors increases as the shadowing becomes more pronounced, therefore one has to consider this when designing the coding scheme. For heavy

shadowing with 2% BT, an effective coding/interleaving scheme should overcome bursts of 100 erroneous bits. For example RS code with blocklengths of 15 are not effective over such fading channel since their correcting capability is not significant. High degree of interleaving ($D > 17$) should be applied if this code has to be used. But interleaving with high degree is not preferred since it introduces delay to the system, and the delay is an important factor to be considered where the propagation delay is large and additional delay is not tolerable.

- We found that the longer the code, the better performance we wil have and less degree of interleaving is required. But with a long code the decoding delay will be considerable and the receiver wil be more complex, therefore one may trade-off between the blocklength and the interleaving degree.
  (31,17) RS code with interleaving degree of 6 could be a good choice. An improvement of 1.7 dB for $BT = 1\%$ and 2.45 dB for $BT = 5\%$ was found for this code with interleaving degree of 6 at BER = 10^{-3}.

- In addition to interleaving we found that erasure information improve the performance of the decoder significantly. An additionaly coding gain of 1.9 dB is achieved with error-erasure decoding at BER of 10^{-3}.

3) A new receiver struture which uses fading prediction for BPSK signal over LMSAT has been presented. This technique was found to be superior to conventional BPSK scheme. For the uncoded system it is found that degradation from error propagation was the major problem of the proposed fading technique over LMSAT channel. For this reason an effective fading prediction technique in conjunction with RS codes was introduced and analyzed. Results shows that the proposed technique greatly

reduces the performance degradation caused by the fading channel. For example, for the 3rd order predictor and at $\frac{E_b}{N_o} = 30dB$ a BER improvement of about two orders the magnitude was obtained. Furthermore with this technique the effects of error propagation was almost negligible which improve the effectiveness of this technique over such fading channels.

6.2 Suggestions for Further Research

There are many interesting techniques which could be investigated for the MSAT communications system which could not be pursued in the context of this thesis.

- A concatenated coding scheme could be very interesting for providing reliable data over mobile satellite channels. The outer code could be a RS code which provides error detection as well as error correction capabilities and the inner code could be a trellis code which is bandwidth efficient and provide good performance by itself.

- A combined FEC and automatic repeat request (ARQ) could be an interesting techniques to investigate over the MSAT channel. Compared to ARQ schemes with pure error detection hybrid ARQ schemes with error correction could be superior and are able to work at lower link power.

- In this thesis the proposed fading/prediction technique is applied only to BPSK signal and RS codes. A more general receiver which employs more than one sample per receiver symbol and deals with higher level modulation and coding techniques (i.e., QPSK, TC-8PSK) could be investigated.

Appendix A

BOSS Modules

All BOSS Modules have been used to evaluate the error performance for the uncoded and coded system are given in this appendix. Figure A.1 represents the system model used in our simulation to evaluate the performance of BPSK in an AWGN. This figure was given in Chapter 4, but it is repeated here that the reader can better follow this appendix.

RANDOM DATA module in Figure A.1 represents the data source which generates a binary sequence. The symbol generated at any time is independent of all previous symbols, and both elements of the symbol alphabet are equally likely.

WHITE NOISE GIVEN SNR-&-BW module is used to generate complex white Gaussian noise samples with zero mean and variance adjusted to provide the desired signal to noise ratio over the specified single sided bandwidth.

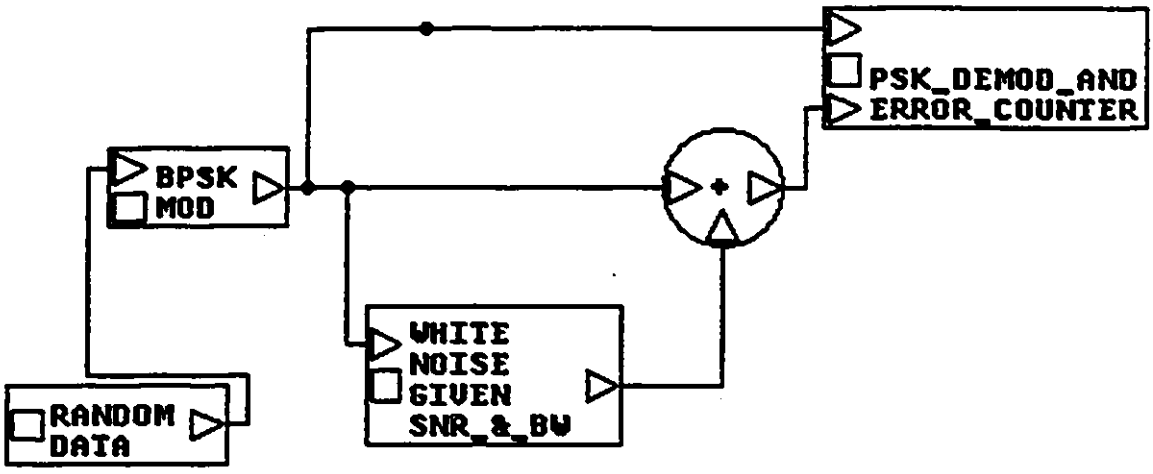

Figure A.1: System model for BPSK in an AWGN channel

PSK-DEMOD-AND ERROR-CQUNTER module does matched filter detection of the received waveform, then delays the transmitted waveform and counts the number of times the transmitted and received bits do not agree. The transmitted waveform should be uncorrupted, that is, it should be ideal PSK. The time delay to the input of this module is needed so that the matched filter can know when to sample, this can be determined by making a small test simulation, then correlating the transmitted waveform with the waveform at the input to this module. An expansion of this module is given in Figure A.2.

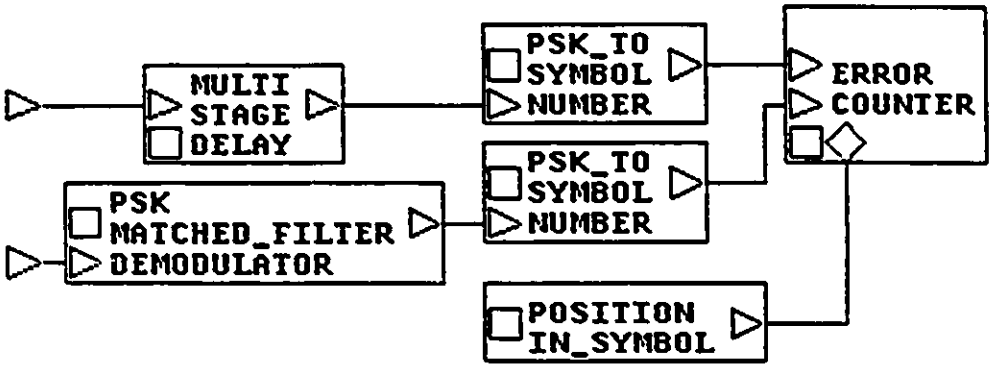

Figure A.2: Expansion of PSK-DEMOD-AND-ERROR COUNTER module

MULTISTAGE DELAY module in Figure A.2 represents the time delay of the transmitted waveform.

PSK-TO-SYMBOL NUMBER module inputs a complex number, and quantizes its phase to the nearest constellation point, then outputs the symbol number which corresponds to this phase. Where an angle equal to the first constellation point is numbered zero, and the next angle in the constellation (in a counterclock wise sense) is numbered one, etc up to the PSK order -1. The constellation is defined by specifying the phase of the first angle in the constellation in degrees, and specifying the number of points in the constellation.

ERROR COUNTER module counts the number of times its two inputs are unequal, and then prints this number divided by the number of tries after every block of count tries. The block of count tries is called "print estimate modulo " which is a parameter of the module. If this number is 100, then the estimate gets printed every 100 tries.

PSK MATCHED-FILTR DEMODULATOR module is a matched filter demodulator for PSK signal. It integrates over each symbol interval, and then quantizes the output to the nearest PSK constellation point. In order to know when to sample the integrate and dump this module must know the time delay between time equal zero and the begining of the first symbol start at the input to this module. This parameter is made as global parameter for the module described above (PSK-DEMOD-AND-ERROR-COUNTER). An expansion of this module is given in Figure A.3.

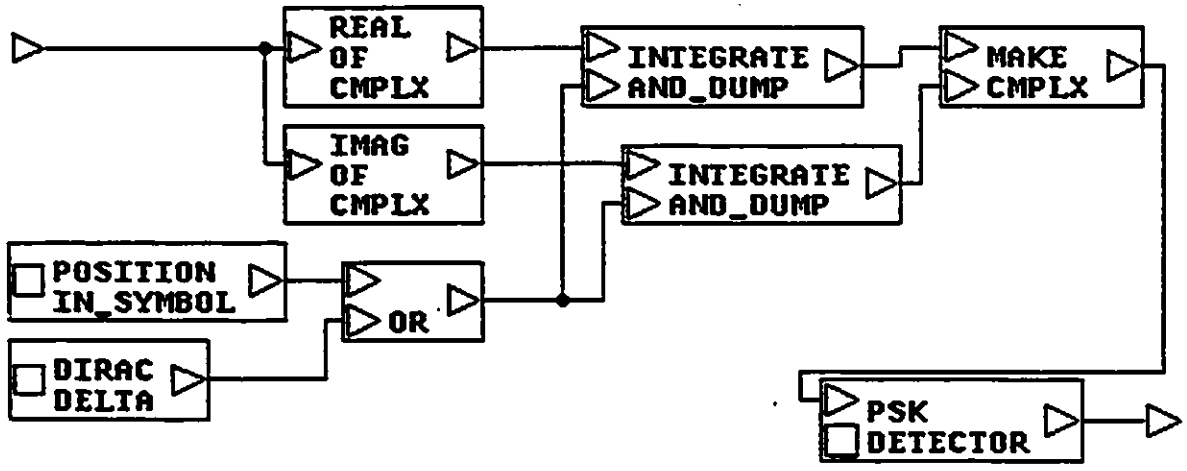

Figure A.3: Expansion of PSK MATCHED-FILTER DEMODULATOR module

INTEGRATE AND-DUMP module in Figure A.3 does a trapezoidal approximation integral as long as the dump reset signal is "False", the sample at which this input goes "True", the integrator output is the integral up to that sample. This doesn't include the DT of the current sample. At the sample after this, the output is the integral up to the reset sample were zero. The integral between resets starts with the sample of the previous reset, does a trapezoidal integration up to the sample before the next reset, and then outputs at the reset the value of this integral with the sample before the reset held for its DT. In this way, the integrals in separate reset intervals are uncorrelated. For example, if a ramp were being integrated, then the trapezoidal approximation would exactly fit to the actual function, except that the fit used for the integration would be flat across the last DT (rather than ramping on up to the sample of the reset). The sample before the terminating reset is held (rather than using the actual signal sample at the reset) in order to make the integration in separate intervals uncorrelated.

PSK DETECTOR module is used to produce ideal PSK signal from rotated, noisy PSK. It quantizes to the nearest PSK constellation point. The output is determined form the input at the sample times, and is held between samples times. The output is zero until the specified time delay has passed. An expansion of this module is given in Figure A.4.

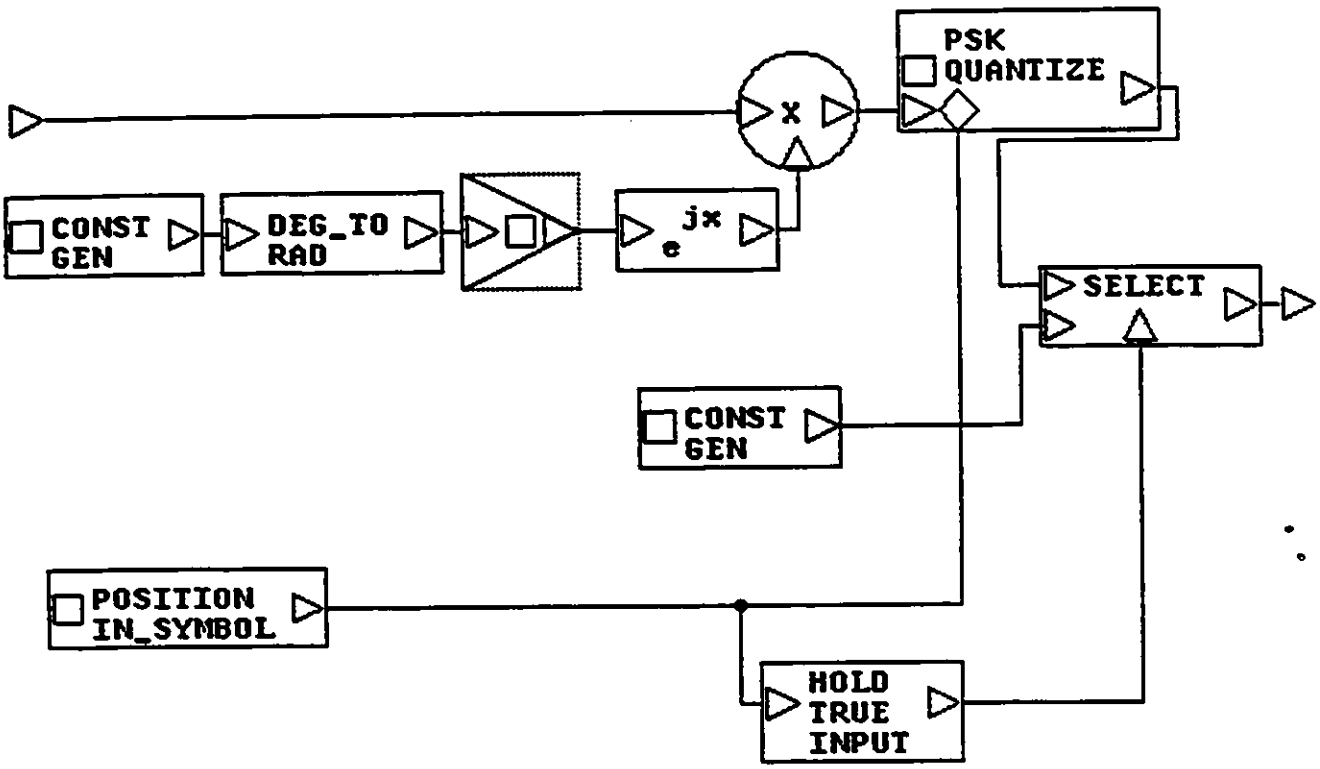

Figure A.4: Expansion of PSK-DETECTOR module

In what follows Figure A.5 represents the system model for BPSK in an AWGN, fading and shadowing channel. Figure A.6 represents the system model for coded sytem in an AWGN. Finally Figure A.7 represents the system model for coded system in an AWGN, fading and shadowing channel.

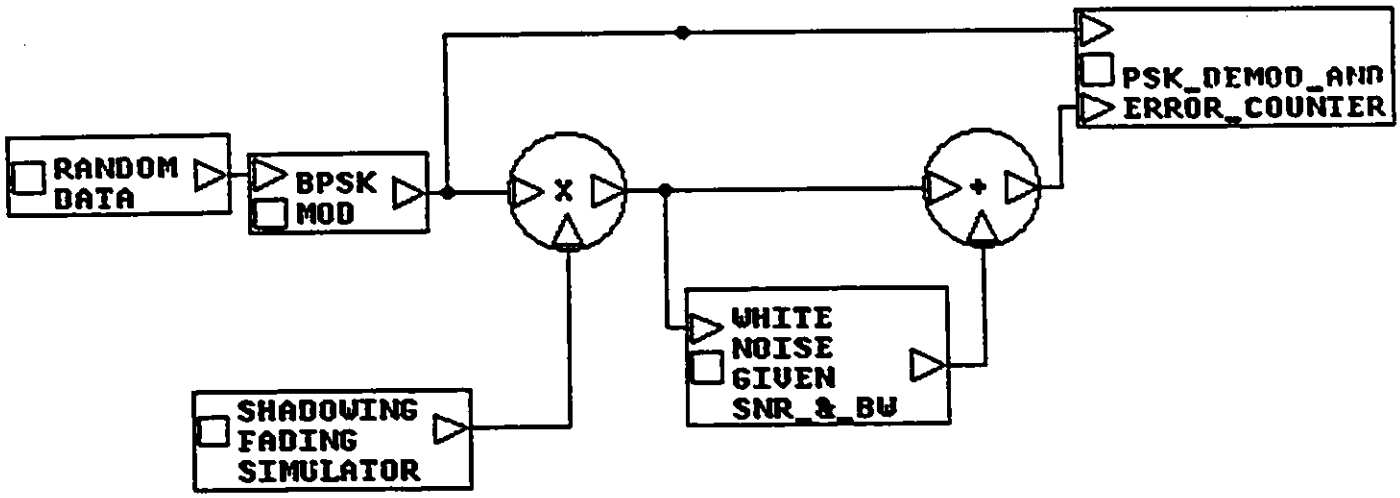

Figure A.5: System model for BPSK over AWGN and lognormal shadowed Rician fading channel

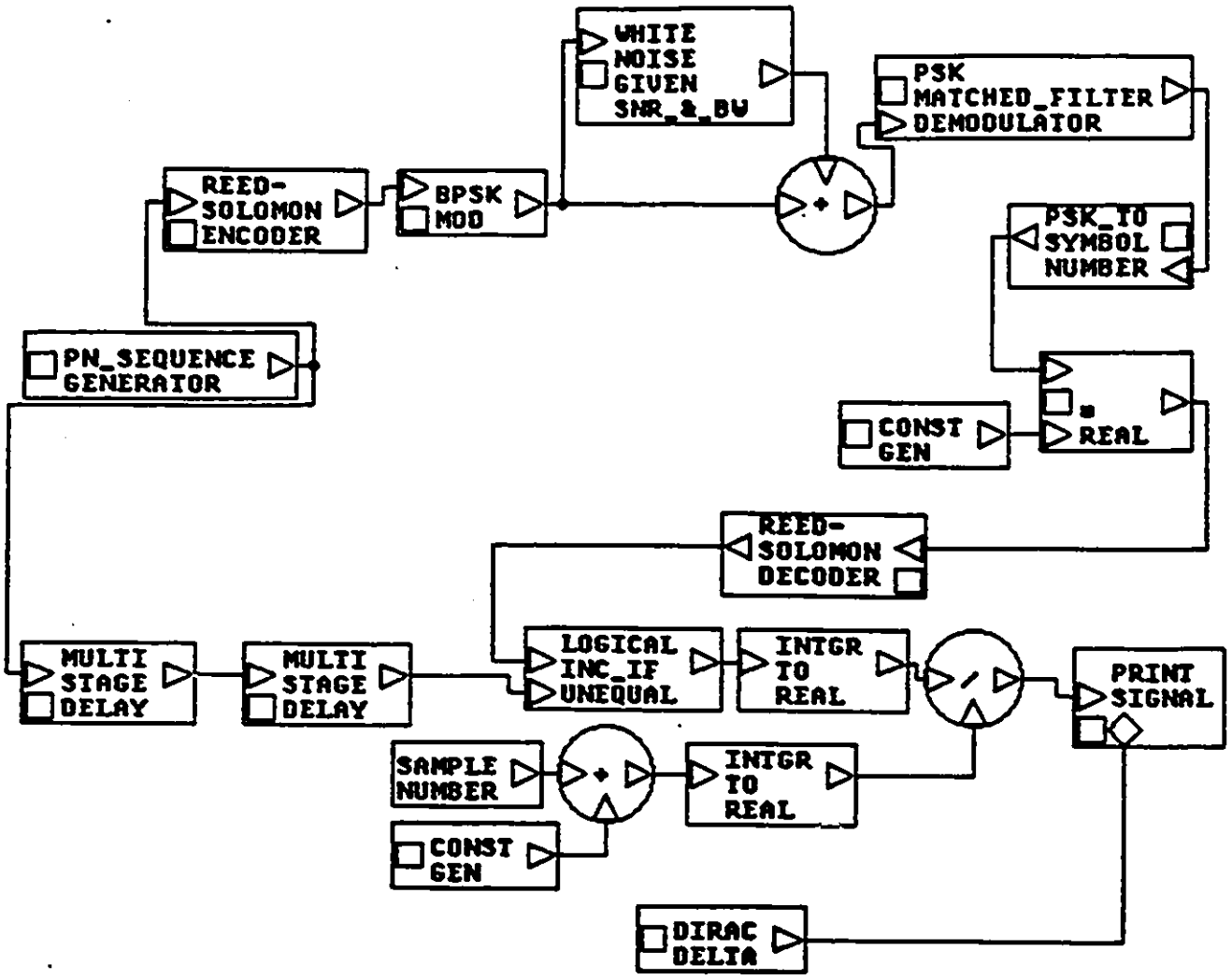

Figure A.6: System model used to determine the performance of RS codes in an AWGN channel.

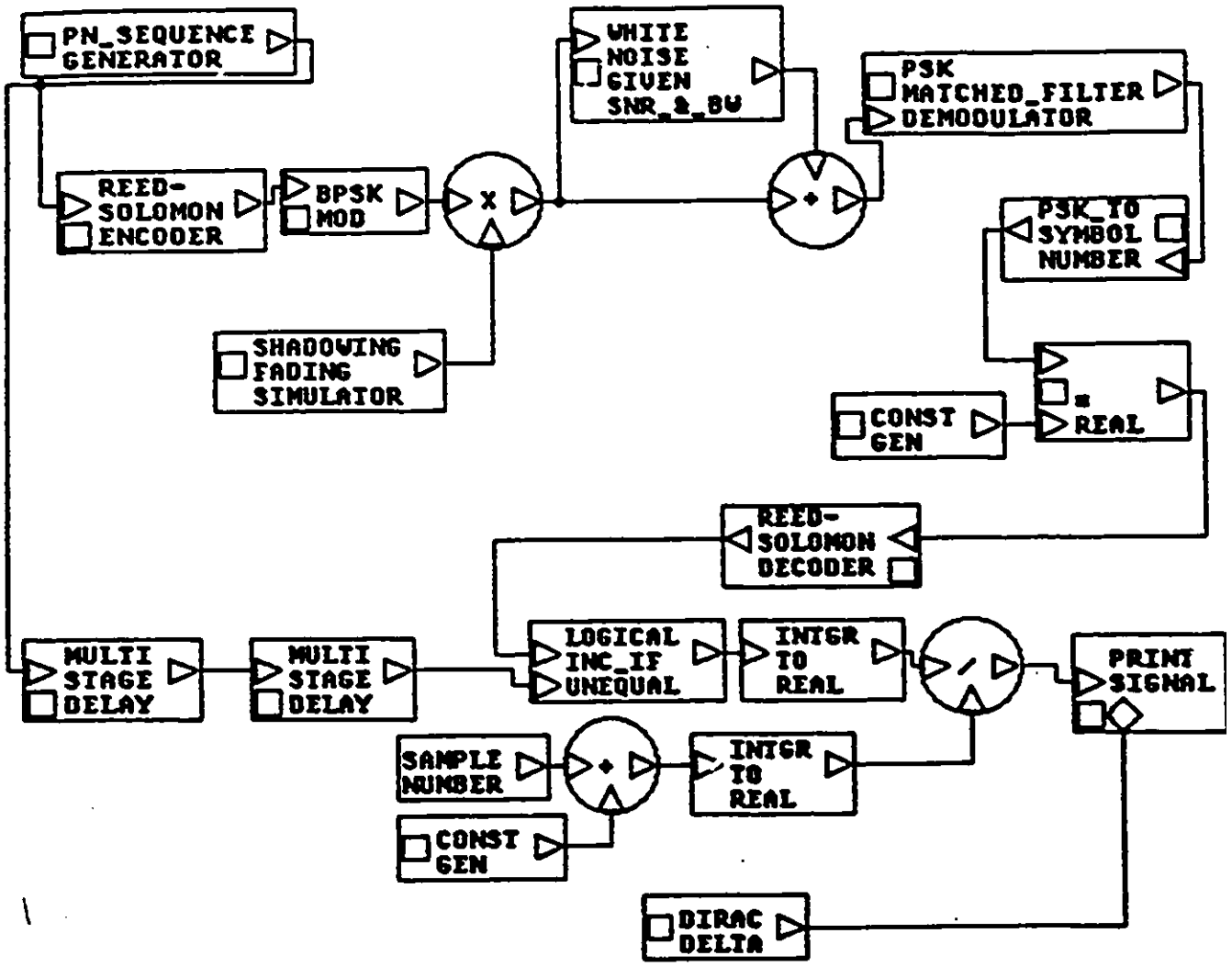

Figure A.7: System model used to determine the performance of RS codes over a fading and shadowing channel.

Appendix B

RS codes and interleaver

In this appendix, we give some of the background information relevant to our study on RS codes, erasure decoding and interleaving. The analysis closely follows Lin & Costello [52], Clark & Cain [53], etc.

B.1 Reed-Solomon codes

In addition to the binary codes, there are nonbinary codes. In fact if p is a prime number and q is any power of p, there are codes with symbols from the Galois field, GF(q). These code are called q-ary codes. The most important subclass of q-ary BCH codes is the Reed-Solomon codes.

A t-error-correcting Reed-Solomon code with symbols from GF(q) has the following parameters:

blocklength	$n = q - 1$
Number of parity-check digits	$n - k = 2t$
Minimum distance	$d_{min} = 2t + 1$

We see that the length of the code is one less than the size of code symbols and the minimum distance is one greater than the number of parity-check digits.

In what follows we consider RS codes with code symbols from the Galois field, GF(2^m) (i.e., $q = 2^m$). Let α be a primitive element in GF(2^m). The generator polynomial of a primitive t-error-correcting RS code of length $2^m - 1$ is :

$$\begin{aligned} \mathrm{g}(X) &= (X+\alpha)(X+\alpha^2)...(X+\alpha^{2t}) \\ &= g_0 + g_1 X + g_2 X^2 + ... + g_{2t-1} X^{2t-1} + X^{2t}. \end{aligned} \tag{B.1}$$

Clearly, g(X) has $\alpha, \alpha^2, ..., \alpha^{2t}$ as all its roots and has coefficients from GF(2^m).

B.1.1 Encoding of RS Code

The code generated by g(X) is an $(n, n-2t)$ cyclic code with code which consists of those polynomials of degree $n-1$ or less with coefficients from GF(2^m) that are multiples of g(X). Encoding of this code is similar to the binary case, let

$$\mathrm{a}(X) = a_0 + a_1 X + a_2 X^2 + ... + a_{k-1} X^{k-1} \tag{B.2}$$

be the message to be encoded where $k = n - 2t$. In systematic form, the 2t parity-check digits are the coefficients of the remainder

$$\mathrm{b}(X) = b_0 + b_1 X + b_2 X^2 + ... + b_{2t-1} X^{2t-1} \tag{B.3}$$

resulting from dividing the message polynomial X^{2t} a(X) by the generator polynomial g(X).

Encoding consists of three steps,

(1) multiply the message polynomial a(X) by X^{2t}

(2) divide X^{2t} a(X) by g(X) to obtain the remainder b(X)

(3) form the code word b(X) + X^{2T} a(X).

All these three steps can be accomplished with a division circuit as shown in Figure B.1.

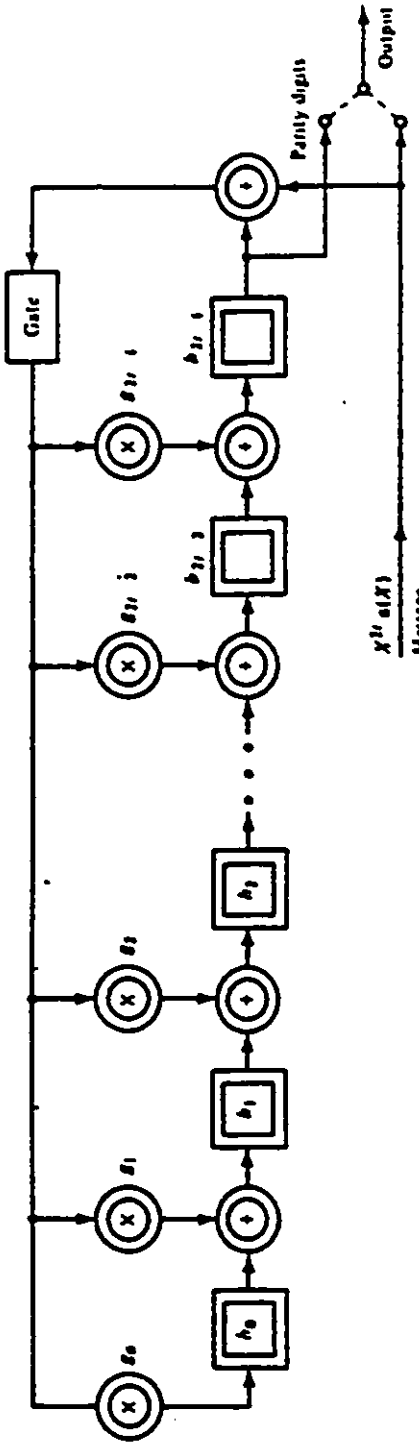

Figure B.1: Encoding cicuit for RS codes [52].

The encoding operation is carried out as follows:

Step1 : With the gate turned on, the k information digits $a_0, a_1, ..., a_{k-1}$ are shifted into the circuit and simultaneously into the communication channel. Shifting the message a(X) into the circuit from the front end is equivalent to premultiplying a(X) by X^{2t}. As soon as the complete message has entered the circuit, the $2t$ digits in the register form the remainder and thus they are the parity-check digits.

Step2 : Break the feedback connection by turning off the gate.

Step3 : Shift the parity-check digits out and send them into the channel. These $n-k$ parity-check digits $b_0, b_1, ..., b_{2t-1}$, together with the k information digits, form a complete code word.

B.1.2 Decoding of RS Codes

Suppose that a code word $\mathrm{v}(X) = v_0 + v_1X + v_2X^2 + ... + v_{n-1}X^{n-1}$ is transmitted and the transmission errors result in the following received vector:

$$\mathrm{r}(X) = r_0 + r_1X + r_2X^2 + ... + r_{n-1}X^{n-1} \tag{B.4}$$

Let e(X) be the error pattern. Then

$$\mathrm{r}(X) = \mathrm{v}(X) + \mathrm{e}(X) \tag{B.5}$$

where

$$\mathrm{e}(X) = e_0 + e_1X + ... + e_{n-1}X^{n-1} \tag{B.6}$$

where $e_i = r_i - v_i$ is a symbol from GF(2^m). Suppose that the error pattern e(X) contains ν errors (non zero component) at location $X^{j_1}, X^{j_2}, ..., X^{j_\nu}$, where $0 \leq j_1 < j_2 < j_\nu \leq n-1$. Then

$$\mathrm{e}(X) = e_{j_1}X^{j_1} + e_{j_2}X^{j_2} + ... + e_{j_\nu}X^{j_\nu} \tag{B.7}$$

hence to determine $\mathbf{e}(X)$, we need to know the error locations X^{j_l}'s and the error values e_{j_l}'s.

As usual, the first step of decoding a code is to compute the syndrome from the received vector $\mathbf{r}(X)$. For decoding a t-error-correcting RS codes the syndrome is a 2t-tuple

$$\mathbf{S} = (S_1, S_2, ..., S_{2t}) = \mathbf{r}.\mathbf{H}^T \tag{B.8}$$

where $\mathbf{H}$ is the parity-check matrix. The ith component of the syndrome is given by $S_i = r(\alpha^i)$. The syndrome component S_i can also be computed by dividing $\mathbf{r}(X)$ by $X + \alpha^i$. The division results in the equality

$$\mathbf{r}(X) = c_i(X)(X + \alpha^i) + b_i \tag{B.9}$$

where the remainder b_i is a constant in GF(2^m). Substituting α^i in both sides of (B.9) we have $S_i = b_i$. This computation can be accomplished with a simple division circuit.

Since α^i are roots of each code polynomial, $\mathbf{v}(\alpha^i) = 0$ then we obtain the following relationship between the syndrome components and the error pattern:

$$S_i = \mathbf{e}(\alpha^i) \tag{B.10}$$

For convenience, let $\beta_l = \alpha^{j_l}$ for $1 \leq l \leq \nu$. We call these elements the error location numbers since they tell us the locations of the errors. The 2t syndrome components are obtained by substituting α^i into (B.7) thus, we have

$$
\begin{aligned}
S_1 &= e_{j_1}\beta_1 + e_{j_2}\beta_2 + ... + e_{j_\nu}\beta_\nu \\
S_2 &= e_{j_1}\beta_1{}^2 + e_{j_2}\beta_2{}^2 + ... + e_{j_\nu}\beta_\nu{}^2 \\
&\vdots \\
S_{2t} &= e_{j_1}\beta_1{}^{2t} + e_{j_2}\beta_2{}^{2t} + ... + e_{j_\nu}\beta_\nu{}^{2t}
\end{aligned}
$$

Any method for solving these equations is a decoding algorithm for the RS codes. These 2t equations are symmetric functions in $\beta_1, \beta_2, ..., \beta_\nu$. Now we define the following polynomial

$$\sigma(X) = (1+\beta_1 X)(1+\beta_2 X)...(1+\beta_\nu X) \quad \text{(B.11)}$$

$$= 1 + \sigma_1 X + \sigma_2 X^2 + ... + \sigma_\nu X^\nu \quad \text{(B.12)}$$

The roots of $\sigma(X)$ are $\beta_1{}^{-1}, \beta_2{}^{-1}, ..., \beta_\nu{}^{-1}$, which are the inverses of the error location numbers. For this reason, $\sigma(X)$ is called the error location polynomial.

At this point it will be appropriate to outline the error-correcting procedure for RS codes. The procedure consists of four major steps:

Step1 : Compute the syndrome $S = (S_1, S_2, ..., S_{2t})$ from the received polynomial $\mathrm{r}(X)$.

Step2 : Determine the error-location polynomial $\sigma(X)$ from the syndrome components $S_1, S_2, ..., S_{2t}$.

Step3 : Determine the error location numbers $\beta_1, \beta_2, ..., \beta_\nu$ by finding the roots of $\sigma(X)$.

Step4 : Determine the error value at each location and correct the errors in $\mathrm{r}(X)$.

Many decoding algorithm are available to carry out these steps. Berlekamp's iterative algorithm is the most useful algorithm for decoding RS codes.

The decoding computation for a RS code is best explained by an example. Consider a double-error-correcting RS code with symbols from GF(2^4). The generator polynomial of this code is

$$\begin{aligned} g(X) &= (X+\alpha)(X+\alpha^2)(X+\alpha^3)(X+\alpha^4) \\ &= X^4+\alpha^{13}X^3+\alpha^6X^2+\alpha^3X+\alpha^{10}. \end{aligned}$$

Let the all-zero vector be the transmitted code vector and the received vector is

$$r(X) = \alpha^{12}X+\alpha^8X^3 \tag{B.13}$$

Step1 : The syndrome components are computed as follows

$$\begin{array}{llll} S_1 & = r(\alpha) & = \alpha^{13}+\alpha^{11} & = \alpha^4 \\ S_2 & = r(\alpha^2) & = \alpha^{14}+\alpha^{14} & = 0 \\ S_3 & = r(\alpha^3) & = 1+\alpha^2 & = \alpha^8 \\ S_4 & = r(\alpha^4) & = \alpha+\alpha^5 & = \alpha^2 \end{array}$$

Step2 : To find the error-location polynomial $\sigma(X)$, we fill out the Table 6.5 given in Lin and Costello book [52].

μ	$\sigma^\mu(X)$	d_μ	l_μ	$\mu - l_\mu$	
-1	1	1	0	-1	
0	1	α^4	0	0	
1	$1+\alpha^4X$	α^8	1	0	take $\rho=-1$
2	1	α^8	0	2	take $\rho=0$
3	$1+X+\alpha^4X^2$	1	2	1	take $\rho=1$
4	$1+\alpha^9X+\alpha^4X^2$	-	2	2	take $\rho=2$

In what follows we give the major computation we have to do to complete this Table.

(1) Since $d_0=\alpha^4$ then $\sigma^1(X)=\sigma^0(X)+d_0d_\rho^{-1}X^{-\rho}\sigma^\rho(X)$

with $\rho=-1$ we have $\sigma^1(X)=1+\alpha^4X$

(2) $d_1=S_2+\sigma_1^1S_1=\alpha^8$ therefore $\sigma^2(X)=\sigma^1(X)+d_1d_0^{-1}X\sigma^0(X)=1+\alpha^4X+$

$\alpha^4 X + 1 = 1$

(3) $d_2 = S_3 = \alpha^8$ therefore $\sigma^3(X) = \sigma^2(X) + d_2 d_1^{-1} X\sigma^1(X) = 1 + X + \alpha^4 X^2$

(4) $d_3 = S_4 + S_3 + \alpha^4 S_2 = \alpha^2 + \alpha^8 = 1$ therefore

$\sigma^4(X) = \sigma^3(X) + d_3 d_2^{-1} X\sigma^2(X) = 1 + \alpha^9 X + \alpha^4 X^2$

Thus $\sigma(X) = 1 + \alpha^9 X + \alpha^4 X^2$

By substituting the all elements of GF(2^4) into $\sigma(X)$ we find that only $\sigma(\alpha^{12}) = 0$ and $\sigma(\alpha^{14}) = 0$; α^{12} and α^{14} are the roots of $\sigma(X)$. The reciprocals of these roots are α and α^3 which are the error location numbers of the error pattern $\mathbf{e}(X)$, thus the errors occur at position X and X^3. The last step is to find the error value.

Let

$$Z(X) = 1 + (S_1 + \sigma_1)X + (S_2 + \sigma_1 S_1 + \sigma_2)X^2 + ... + (S_\nu + \sigma_1 S_{\nu-1} + \sigma_2 S_{\nu-2} + ... + \sigma_\nu)X^\nu. \tag{B.14}$$

then the error value at location $\beta_l = \alpha^{j_l}$ is given by

$$e_{j_l} = \frac{Z(\beta_l^{-1})}{\prod_{i=1}^{\nu}(1 + \beta_i \beta_l^{-1})} \tag{B.15}$$

in our example $Z(X) = 1 + \alpha^{14}X + \alpha^{11}X^2$ therefore we find $e_1 = \alpha^{12}$ and $e_3 = \alpha^8$ thus given:

$$\mathbf{e}(X) = \alpha^{12}X + \alpha^8 X^3 \tag{B.16}$$

which is exactly the difference between the received vector and the transmitted vector. The decoding is completed by taking $\mathbf{r}(X) - \mathbf{e}(X)$

B.1.3 Error/Erasure-Decoding

If the code is defined over the field GF(q), then the demodulator is assumed to have the normal q outputs plus a $(q+1)$th output corresponding to an erasure. The erasure output is assumed to contain absolutely no information about which of the q possible symbols was exactly transmitted.

If a code has minimum distance d and a received word contains e erasures, then the e erased positions can be ignored in the decoding process. However, even ignoring these positions, all code words will differ in at least $d - e$ of the remaining positions allowing correction of up to

$$t_m = \lfloor \frac{d-e-1}{2} \rfloor \tag{B.17}$$

channel errors in addition to the erasures. Thus, all combinations of t channel errors and e erasures are correctable providing that

$$2t + e \leq d - 1 \tag{B.18}$$

d is the minimum distance of the code which for maximum-distance code is determined by the number of parity symbols in a code word

$$d - 1 = n - k \tag{B.19}$$

B.2 Interleaver/Deinterleaver

Most of the well known codes that have been devised for increasing the reliability in the transmission of information are effective when the errors caused by the channel are statistically independent. This is the case for the AWGN channel. However, there are channels that exhibit bursty error characteristics. One example is the class of the channels characterized by multipath and fading. Signal fading due to time-variant multipath propagation often causes the signal to fall below the noise level, thus resulting in a large number of errors. An effective method for dealing with burst error channels is to interleave the coded data in such a way that the bursty channel is transformed into a channel having independent errors.

The most common type of interleaver is a block interleaver, in which, for example, symbols are laid down in the rows of a $D.n$ matrix, and read out from the columns.

In what follows a simple type of interleaver is described [45]. Schematically , as illustrated in Figure B.2, symbols to be interleaved are arranged in blocks of n (by a serial/parallel conversion, if necessary). The ith symbol in each block is delayed by $(i-1)nD'$ time units through a $(i-1)D'$ stage shift register clocked once every n symbol times, where $D' = \frac{D}{n}$. (A time unit thus corresponds to the transmission of block of n symbols). Output bits may be serialized for channel transmission. At the receiver, groups of n symbols are reblocked, and the ith symbol in each block is delayed by $(n-i)nD'$ time units through an $(n-1)D'$ stage shift register. We call this a $D.n$ interleaver. Correspondingly there exists a similar but inverse $D.n$ deinterleaver, also illustrated in Figure B.2. The combination has the following properties.

(1) All symbols receive a total delay of $(n-1)D$ symbol times or $(n-1)mDT \approx nDmT$ second (where m is the number of bits per code symbol and T is the data bit duration) plus the channel delay.

(2) The interleaver storage requirements is $(n-1)D$ symbols or $(n-1)mD \approx nmD$ bits.

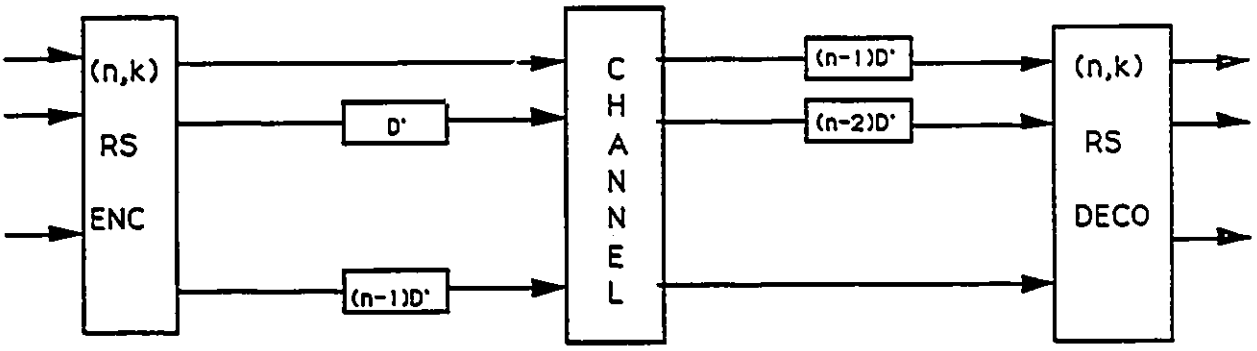

Figure B.2: Use of an (n, k) RS codes with $D \times n$ interleaver.

Appendix C

Simulation Information

In our simulation a sequence length of 100 times the inverse of the BER was considered. In this appendix a brief explanation about the choice of this value is given. It has been stated [55] that the binary error mean could be approximated by

$$P_e = \frac{N_e}{L} \tag{C.1}$$

where N_e is the total number of errors and L is the length of the binary sequence generated. It is obvious that P_e is a random variable with a mean and variance depending on the choice of L. Table C.1 shows how P_e varies with the sequence length.

The percent error of the approximation given in (C.1) was found to be approximately [55]:

$$\begin{aligned} E(\%) &= \frac{100}{P_e}\left[\frac{N_e}{L} - \frac{N_e}{L-1} + \frac{1}{L-1}\right] \\ &= \frac{100}{P_e}\left[\frac{L-N_e}{L(L-1)}\right] \end{aligned} \tag{C.2}$$

In Table C.2 different percent errors of the approximation are given for different error probabilities.

Although $E(\%)$ is actually a random variable estimated from a sample as is P_e, it is considered in Table C.2 on an individual sample basis. It has been shown [55] that

Sequence length L	Number of errors N_e	Average error rate P_e
1024	13	0.012695
10240	166	0.016211
20480	322	0.015723
30720	477	0.015527
40960	613	0.014966
51200	765	0.014941
60416	926	0.015327
70665	1095	0.015498
80896	1252	0.015477
91136	1428	0.015669
101376	1575	0.015536
102400	1592	0.015547
111616	1732	0.015517
121856	1915	0.015715
132096	2067	0.015648
142336	2223	0.015618
152576	2373	0.015553
Total average error rate : 0.015363		

Table C.1: Average error rate statistics from simulation.

Percent error $E(\%)$		
Sequence length (L)	$P_e = 10^{-2}$	$P_e = 10^{-3}$
10 000	0.99	9.99
100 000	0.099	0.99
1 000 000	9.9×10^{-3}	0.099

Table C.2: Error probability approximation.

usual sample size requirements for estimating P_e also serve to maintain $E(\%) < 1\%$ on a sample by sample basis. Therefore, we can deduce from Table C.2 that a good approxiamtion of P_e is achieved whenever the sequence length, L, is greater than 100 times the inverse of P_e.

It has been reported [56] that a reliable simulation of an error-correcting code should produce a bit error probability estimator ($\hat{P}_e$ = total erroneously decoded information bits/total decoded information bits) within the interval $[0.8P_e, 1.2P_e]$ with 95% confidence. To produce estimators with this degree of reliability requires the simulated encoding, transmission, reception, and decoding of at least $70/P_e$ information bits for each code. For a system having a $P_e = 10^{-4}$, this requires the simulation of 7×10^5 bit information sequence.

Also it has been shown [57] that the estimation of the BER with a normalized estimation error less than 1/3, requires a Monte-Carlo simulation with a sample size of the order of $10/P_e$. A normalized estimation error of 1/3 corresponds to a 95% confidence interval of $[\frac{1}{3}P_e, 1\frac{2}{3}P_e]$. With a typical BER of, say, 10^{-6}, direct Monte-Carlo simulation requires 10^7 samples per simulation run.

Finally we can say that our choice is very reliable and yields a good approximation of the BER.

Bibliography

[1] C. Loo, "A Statistical Model for a Land Mobile Satellite Link", ICC'84, also in Science, Systems, and Services for Communication, P. Dewilde and C.A.May, editors, IEEE/Elsevier science publishers, North-Holland, 1984.

[2] C. Loo, "Measurements and Models of a Mobile-Satellite Link with Applications", Proc GLOBECOM'85, New Orleans, LA. Dec. 2-5, 1985.

[3] C. Loo, "A Statistical Model for a Land Mobile Satellite Link", IEEE Trans on Vehicular Technology, vol. VT-34, pp. 122-127, Aug 1985.

[4] C. Loo, E. E. Matt, J. S. Butterworth and M. Dufour, "Measurements and Modelling of Land-Mobile Satellite Signal Statistics", 1986 Vehicular Technology Conference, Dallas, Texas, May 20-22, 1986.

[5] C. Loo, "Measurements and Models of a Land Mobile Satellite Channel and their Applications to MSK signals", IEEE Trans on Vehicular Technology, Vol. VT-35, No. 3. pp 114-121. Aug 1987.

[6] K. A. Norton, L. E. Vogler, W.V. Mansfield, and P. J. Short, " The probability distribution of the amplitude of a constant vector plus a Rayleigh-distibuted vector", Proc of the IRE, pp 1354-1361, October 1955.

[7] Erich Lutz and Ernst Plochinger, " Generating Rice Processes with given spectral propreties", IEEE Trans on Vehicular Technology, Vol. VT-34, No.4, pp 178-181, November 1985.

[8] W. C. Jakes, Ed, "Microwave mobile communication" New York : Wiley 1974.

[9] William C. Y. Lee, "Mobile Communications Engineering", New York, Mc Graw-Hill, 1982.

[10] Faramarz Davarian, "Fade Margin Calculation for Channel Impaired by Rician Fading", IEEE Trans on Vehicular Technology, Vol. VT-34, No. 1, pp 41-44, February 1985.

[11] LLoyd J. Mason, "Error probability evaluation for systems employing differential detection in a Rician fast fading environment and gaussian noise", IEEE Trans on Commun, Vol. Com-35, No.1, Jan 1987.

[12] P.Beckmann, "Probability in communication engineering", New York, Harcourt, Brace and World, Inc. 1967.

[13] D.R.Hummels and F.W.Ratcliffe, "Calculation of error probability for MSK and OQPSK system operating in a fading multipath environment", IEEE Trans on Vehicular Technology, pp 112-120, Aug 1981.

[14] Faramaz Davarian, "Channel Simulation to Facilate Mobile Satellite Communications Research", IEEE Trans on Commun, VOL. COM-35, NO.1, Jan 1987.

[15] Daniel Cygan, "Analytical Evaluation of Average Bit Error Rate For The Land Mobile Satellite Channel", International Journal of Satellite Communications. Vol. 7, pp 99-102, 1989.

[16] Tor Aulin, " Characteristics of a Digital Mobile Radio Channel", IEEE Trans on Vehicular Technology, Vol. VT-30, N0. 2, pp 45-53, May 1981.

[17] K. A. Norton, P. L. Rice, H. B. Janes and A. P. Barsis, "The Rate of Fading in Propagation through a Turbulent Atmosphere", Proc of the IRE, pp 1341-1353, October 1955.

[18] John S. Butterworth, " Satellite Communications Experiment for the Ontario Air Ambulance Service" Communications Canada, Communication Research Center.

[19] Athanasios Papoulis, "Probability, Random Variables, and Stochastic Processes" New York : McGraw-Hill, 1984.

[20] Richard C.French, " The Effect Of Fading and Shadowing on Channel Reuse in Mobile Radio", IEEE Trans on Vehicular Technology, Vol. VT-28, No.3, Aug 1979.

[21] Y. Miyagaki, N. Morinaga and T. Namikawa, "Double Symbol Error Rate of M-ary DPSK in A Satellite Aircraft Multipath Channel. ", IEEE Trans on Commu, Vol.Com-31, No.12, December 1983.

[22] Robert Matyas, "Effect of Noisy Phase References on Coherent Detection of FFSK signals", IEEE Trans on Commun, Vol.Com-26, No.6, June 1978.

[23] J.H.Lodge, M.L.Moher and S.N.Crozier, "A Comparison Of Data Modulation Techniques for Land Mobile Satellite Channels", IEEE Trans on Vehicular Technology, Vol.VT-36, No.1, February 1987.

[24] Theodore Brenig, "Data Transmission For Mobile Radio", IEEE Trans on Vehicular Technology, Vol, VT-27, No.3, Aug 1978.

[25] J.H.Lodge and Daniel Boudreau, "The implementation and Performance of Narrowband Modulation Techniques for Mobile Satellite Applications", ICC 1986.

[26] B. T. Tan and T. T. Tjhung, "On Binary DPSK Error Rates Due To Noise and Intersymbol Interference.", IEEE trans on commun, Vol, Com-31, No.3, March 1983.

[27] H. W. Arnold and W. F. Bodtmann, "The Performance Of FSK In Frequency Selective Rayleigh Fading", IEEE trans on Commun, Vol, Com-31, No.4, April 1983.

[28] Y. Miyagaki, N. Morinaga and T. Namikawa, " Error Probability Characteristics for CPSK signal Through m-Distributed Fading Channel", IEEE Trans on Commun, Vol. Com-26, No.1, January 1978.

[29] R. Muammar and S. C. Gupta, "Diversity Improvement in Frequency- Hopping Multilevel FSK Systems Under The Influence Of Rayleigh Fading and Lognormal Shadowing", IEEE Trans on Commun, Vol.Com-31, No.2, February 1983.

[30] Erich Lutz, "Code and Interleaver Design For Data Transmission Over Fading Channel", Institute of Communications Technology DFVLR (German Aerospace Research Establishment), GLOBCOM 1984.

[31] P. J. Mclane, P. H. Wittke and P.K.-M. Ho, "A Study on Combined Channel Coding and Modulation For Mobile Satellite Communications", DSS Contract OST85-00197, March 26, 1986.

[32] Shou Y.Mui and James W.Modestino, "Performance of DPSK with Convolutinal Encoding on Time-varying Fading Channel", IEEE Trans on Commun, Vol.Com-25, No.10, October 1977.

[33] Shou Y.Mui and James W.Modestino, "Convolutional Code Performance in The Rician Fading Channel" IEEE Trans on Commun, Vol.Com-24. No.6, June 1976.

[34] Stephen G.Wilson, Robert W.Sotton and Edgar H.Schroeder, " Differential Phase-Shift Keeying Performance on L-Band Aeronautical satellite Channel: Test Result and a Coding Evaluation", IEEE Trans on Commun, March 1976.

[35] Joachim Hagenauer and Erich Lutz, "Forward Error Correction Coding for Fading Compensation in Mobile Satellite Channel", IEEE Journal on Selected Areas in communications, Vol.Sac-5, No.2, February 1987.

[36] Jean-Yves Chouinard, Marc Grégoire, Michel Lecours, Gilles Y. Delisle, "Simulation d'un Canal de Transmission Radio Mobile Numérique.", Département de génie Electrique, Université Laval, Québec.

[37] Joachim Hagenauer, Frank Dolainsky, Erich Lutz, Wolfgang Papke and Robert Schweikert, "The Maritime Satellite Communication Channel-Channel Model, Performance of Modulation and Coding", IEEE Journal on Selected Areas in Communications, Vol. Sac-5. No.4, May 1987.

[38] A. C. M.Lee and P. J. Mclane, " Convolutionally Interleaved PSK and DPSK Trellis Codes for Shadowed, Fast Fading Mobile satellite Channels", IEEE Trans on Vehicular Technology, Vol 39,No.1, February 1990.

[39] Michael L. Moher and J. H. Lodge, "Performance of Concatenated Reed Solomon Trellis-Coded Modulation over Rician Fading Channels", Department of Communications, Communications Research Center.

[40] Zelma McC. Huntoon and Arnold M. Michelson. "On The Computation of the Probability Of Post-Decoding Error Events For Block Codes", IEEE Trans on Information Theory, May 1977.

[41] W. Sandrin, H. Chen, W. Hagmann, K. Mackenthun and S. Rhodes, "Aeronautical Satellite Data Link Study", COMSAT Technical Review Vol 15 No.1., Spring 1985.

[42] S. O. Rice, "Mathematical Analysis of Random Noise", Bell Syst.Tech.J. Vol 27, pp 109-117, January 1948.

[43] C. Loo, "Digital transmission through a land mobile satellite channel", IEEE Trans on Commun, Vol 38, No 5, May 1990.

[44] T. Shiokowa, Y. Karasawa, and M. Yamada, "Compact antenna systems for Inmersat standard B ship earth station", in Proc. IEE Conf. Satellite system for mobile communications, navigation, london, England, June 1983.

[45] G. David Forney, "Burst-correcting codes for the classic bursty channel", IEEE Tans on Commun, Vol. Com-19, No. 5, pp 772-780, October 1971.

[46] J. L. Ramsey, " Realisation of optimum interleavers.", IEEE Trans on Information Theory, Vol. IT-16, No. 3, pp 338-345, May 1970.

[47] M. K. Simon and C. C. Wang, "Differential detection of Gaussian MSK in a mobile radio environment", IEEE Trans on Vehicular Technology, Vol. VT-33, pp 307-320, Nov.1984.

[48] K. S. Chung, "Generalized tamed frequency modulation and its application for mobile radio communications", IEEE Trans on Vehicular Technology, Vol. VT-33, pp 103-113, Aug 1984.

[49] J. P. McGeehan and A. J. Bateman, "Phase-Locked transparent tone-in-band (TTIB): A new spectrum configuration particulary suited to the transmission of data SSB mobile radio networks", IEEE Trans on Commun, Vol. Com-32, pp 81-87, Jan 1984.

[50] F. Davarian, "High performance digital communications in mobile channel" in Proc. IEEE Vehicular Technology Conference, pp 114-118, 1984.

[51] M. Yokoyama, "BPSK system with sounder to combat Rayleigh fading in mobile radio communication", IEEE Trans on Vehicular Technology, Vol VT-34, pp 35-40, Feb 1985.

[52] S. Lin and D. J. Costello, "Error control coding fundamentals and apllications" Prentice-Hall, Inc. Englewood cliffs, New Jersey, 1983.

[53] George C.Clark, Jr., and J. Bibb Cain, "Error-Correction Coding for Digital Communications", Plenum Press, New York, 1981.

[54] John G. Proakis, " Digital Communications", McGraw-Hill Book Company, Second edition, 1989.

[55] P. Mcmanamon, " HF Markov Chain Model and Measured Error Averaged", IEEE Trans on Commun. Technol., VOL.COM-18, pp 201-208, june 1970.

[56] M. A. Herro and J. M. Nowack, " Simulated Viterbi Decoding using importance sampling", IEE Proceedings. Vol. 135, No 2, April 1988.

[57] K. S. Shanmugam and P. Balaban, "A modified Monte-Carlo simulation technique for the evaluation of error rate in digital communication systems", IEEE Trans on commun, Com-28, pp 1916-1924, November 1980.

[58] C. Loo "Digital Transmission Through a Land Mobile Satellite Channel", IEEE Trans on Commun, Vol 38, No 5, pp 693-698, May 1990.